ELECTRONIC STRUCTURE OF LIQUID AND AMORPHOUS IRON

by

Shyamal Kumar Bose

B.Sc., Patna University, India, 1971

M.Sc., Patna University, India, 1974

M.Sc., Dalhousie University, Canada, 1977

THESIS SUBMITTED IN PARTIAL FULFILLMENT OF

THE REQUIREMENTS FOR THE DEGREE OF

DOCTOR OF PHILOSOPHY

in the Department

of

Physics

SIMON FRASER UNIVERSITY

March 1983

APPROVAL

Name: Shyamal Kumar Bose

Degree: Doctor of Philosophy

Title of thesis: ELECTRONIC STRUCTURE OF LIQUID AND AMORPHOUS IRON

Examining Committee:

Chairman: B.P. Clayman

L.E. Fallentine
Senior Supervisor

M. Plischke

E.D. Crozier

B. Moos

R. Haydock
External Examiner
Professor, Department of Physics
University of Oregon, Eugene, Oregon

Date Approved: 29 March, 1983

PARTIAL COPYRIGHT LICENSE

I hereby grant to Simon Fraser University the right to lend my thesis, project or extended essay (the title of which is shown below) to users of the Simon Fraser University Library, and to make partial or single copies only for such users or in response to a request from the library of any other university, or other educational institution, on its own behalf or for one of its users. I further agree that permission for multiple copying of this work for scholarly purposes may be granted by me or the Dean of Graduate Studies. It is understood that copying or publication of this work for financial gain shall not be allowed without my written permission.

Title of Thesis/Project/Extended Essay

ELECTRONIC STRUCTURE OF LIQUID AND AMORPHOUS IRON

Author: _____
(signature)

SHYAMAL KUMAR BOSE
(name)

April,21,'83
(date)

ABSTRACT

The electronic structure of liquid and amorphous iron is calculated by applying the linear combination of atomic orbitals method to clusters representing these systems, generated by the Monte Carlo technique. Tight-binding matrices representing the one-electron Hamiltonian for these clusters have been obtained by two different schemes that produce the band structure appropriate to the crystalline phases. A comparative study of these two schemes as well as two different methods of calculating the local density of electronic states, namely, the recursion method and the equation of motion technique, is presented. Both methods achieve similar results. However, the recursion method is found to be considerably faster.

The essential change in the electronic density of states(DOS) introduced by disorder seems to be a gradual smoothing as one goes from the crystal to the amorphous and then to the liquid phase. The double peaked structure of the DOS in bcc iron is found to survive in the amorphous but not in the liquid state. The difference in the band widths for the solid , liquid and amorphous clusters is found to be inappreciable.

In calculating the electrical resistivity of transition metals from the Boltzmann equation it is necessary to make an assumption about which electronic states are the current carriers. To shed some light on this problem, we have formed Bloch-like running states with wave vectors K from all the d or the s states in the clusters and calculated the electronic DOS

projected onto these states. For the s states in the liquid and the amorphous clusters such projected DOS curves show a peaked structure. The peak positions change with K values, indicating dispersion relations and hence propagating characters for these states. For the d states, the projected DOS curve for each K shows a sharp peak as long as K is small. For higher values of K these peaks become broad. No appreciable change in the peak position is observed on changing the K value.

A comparison of these results with various experimental observations and other theoretical works is also presented.

ACKNOWLEDGEMENT

I am sincerely thankful to Dr. L. E. Ballentine for helping me and having borne with me through various stages of this work. Without his constant guidance this work would not have been possible. I am also grateful to him for a careful reading of the manuscript and for pointing out, on several occasions, flaws and weaknesses in the presentation of ideas. I have benefited greatly from discussions with Dr. M. Plischke and Dr. E. D. Crozier and I wish to thank them for providing me with many valuable comments and suggestions. Interesting discussions with Dr. J. Hammerberg are also gratefully acknowledged.

Lastly I acknowledge with delight the help I received from Mr. Shiva Chinniah who drew the band structure diagram(Fig.7) for me.

TABLE OF CONTENTS

LIST OF TABLES

LIST OF FIGURES

I. CHAPTER (1)

INTRODUCTION

In a system with an essential lack of periodicity, the most important factor in determining the behaviour of the electron is its immediate neighbourhood. This concept has greatly influenced the study of the electronic states in condensed matter in the recent past. Though the concept dates as far back as the fifties when Friedel[1] used it to explain several electronic properties of dilute alloys, the importance of this concept has been realised only during the last decade in connection with the study of the elementary excitations in disordered systems. Unlike an extended crystalline solid, its amorphous counterpart, solid or liquid, is devoid of any obvious symmetry. Hence the theoretical machinery based on the ideas of translational and point group symmetries, which proved immensely successful in the study of crystalline solids, was of little help in the study of aperiodic systems. This necessitated an alternative formalism, an altogether different way of perceiving the behaviour of the electron. The importance of the local environment was soon realised and the concept of the local density of states, introduced by Friedel, was much appreciated. Various methods were proposed and developed to calculate this local density of states(LDS), which is the total density of states modulated by

the probability of the electron being at a certain point in space. In a compound it discloses the relative weights of various bands on different atoms. At the surface of a solid, it reveals the effect of the surface potential as well as the decrease in the number of neighbours and shows remarkable deviation from the bulk density of states. In a magnetic material, the difference between the up and the down spin local density of states describes the distribution of magnetic moments. Thus in an aperiodic system, the local density of states forms an important object of study. The density of states(DOS) appropriate to the bulk system is obtained by simply averaging over such local densities.

In this work we undertake the calculation and study of this quantity in liquid and amorphous iron. Being a member of the transition metal series, iron provides an interesting and nontrivial case of study. It is nontrivial in that it represents a system with strong scattering potentials and cannot be, therefore, treated within the premises of the nearly free electron(NFE) model. It is a system for which realistic calculation of the electronic DOS has been lacking,* though the need for such calculations has been expressed from time to time. Quite often calculations of electronic properties in liquid transition metals have been based, for lack of realistic data,

---

*Tight-binding calculations on computer generated models of liquid and amorphous iron have been performed by Fujiwara and Fujiwara and Tanabe. However, these calculations neglect hybridisation effects and use somewhat artificial transfer matrix elements in the Hamiltonian (see chap.8).

on speculations about the nature of the DOS in these systems. Such intuitive speculations may often yield correct results. However, verification of these results with reliable data on the DOS is certainly desirable. Below we present a brief review of the electronic DOS calculations that have been carried out so far for liquid and amorphous transition metals, specially iron. Detailed exposition to the subject of liquid metals in general has been provided by Ballentine[2] and Shimoji.[3]

In principle all information regarding the electronic properties of a liquid can be obtained from a knowledge of the eigenstates of the electron. However, it is impossible to calculate these for all possible arrangements of the ions in the liquid state. Also, the wavefunctions contain so much irrelevant detail that it is not at all useful to work with them directly. An alternative formalism is based on studying the Green's[4] function. However, in structurally disordered systems such as liquid and amorphous metals, it is necessary to calculate the average of the Green's function over the ensemble of all possible configurations of the ions. This ensemble averaging requires a knowledge of the multi-ion distribution functions. Since the only experimentally accessible distribution function is the pair distribution function, the multi-ion distribution functions are usually approximated by the sums and products of the latter. In simple liquid metals, where the scattering by the ionic potentials is weak, triplet and higher order correlation effects can be altogether ignored (as in the theory of Edwards[4]).

However, in systems with strong scattering potentials, like transition metals, short range correlations are important and hence special care is required while approximating the higher order correlation functions.

Thus most attempts made so far to study the electronic structure of liquid transition metals have concerned themselves with finding a reasonable approximate average of the entire perturbation series for the one electron Green's function. Among them are the quasicrystalline approximation (QCA) due to Lax,[5] Ziman[6] and Cyrot-Lackmann,[7] the self-consistent QCA due to Gyorffy,[8] Watabe[9] and Korringa and Mills[10] and various self-consistent single-site approximations due to Schwartz and Ehrenreich,[11] Ishida and Yonezawa[12] and Movaghar et al[13] ψ. A multiple scattering theory based on a single site approximation was proposed by Anderson and McMillan.[15] In their model, each ion of the liquid was isolated within its Wigner-Seitz sphere, which was supposed to be embedded in a medium with a uniform complex energy-dependent potential. Paralleling the arguments leading to the coherent potential approximation (CPA),[16] the effective medium potential was determined by requiring that there be no further scattering in the forward direction of an electron incident on the isolated ion. Using a muffin-tin potential model, this scheme was tested for liquid iron. The DOS in their calculation showed a double-peaked structure. However, a computational error in their work as well as the inadequacy of the single-site

---

ψA review of these multiple scattering theories based on various approximations has been provided by Ballentine[2] and Watabe.[14]

approximation used by them was pointed out by several workers.[17-19]

Once the numerical error was corrected the DOS curve showed a single-peaked structure, but with an unusually narrow d-band width. Schwartz and Ehrenreich[11] proposed a different single site approximation using the reaction operator formalism of DeDycker and Phariseau,[20] and carried out a numerical calculation for liquid Cu. The DOS curve in their calculation showed a double-peaked structure similar to that obtained by Anderson and McMillan for liquid iron. Chang et al[18] showed that there are some defects in the numerical calculations of Schwartz and Ehrenreich and made some modified calculations of the DOS, which still showed a double-peaked structure, though with considerable difference in the peak heights. Schwartz and Ehrenreich also proposed higher order expressions for scattering and reaction operators, in which the correlations of ionic positions are explicitly taken into account. However, no numerical calculation has been done so far using these higher order equations. Calculations for liquid iron and copper, using a scheme similar to Anderson and McMillan's (but different approximations regarding the effective medium), have been performed by John and Keller[21] and Blaudeck and Lenk.[22]

Keller and Jones[23] and Keller et al[24] have used the cluster method of Klima, McGill and Ziman,[25] which applies Lloyd's[26] expression for the integrated density of states to clusters of N atoms. Effects of multiple scattering between clusters are neglected. The determinant involving the reaction matrix in

Lloyd's expression for the integrated density of states is evaluated for a finite cluster of N atoms and averaged over various possible clusters. However, it is difficult to decide what type of clusters to consider to represent the structure of a particular liquid transition metal. Keller and Jones[23] suggested that the only structural features that are important for the DOS in liquid transition metals are the co-ordination number and the nearest neighbour distance. House and Smith[27] showed that although such an approximation is valid for copper, it is not adequate for iron.

Some of the theories or approximations mentioned above were developed with a view to establishing in the theory of liquid metals a counterpart of the coherent potential approximation(CPA)[16] for substitutionally disordered alloys. It was proved,[28,29] however, that the most straight forward and satisfactory generalisation of the CPA to liquid metals is the effective medium approximation(EMA) of Roth.[30] Recently it has been shown how several of these theories(e.g., Schwartz-Ehrenreich,[11] Gyorffy,[8] Korringa and Mills,[10] Ishida-Yonezawa[12] and the EMA of Roth) can be derived from a single abstract multiple scattering approach and that EMA is the only theory completely consistent with the assumption needed to derive all these theories from the multiple scattering approach.[31] Some of these theories have also been known to suffer from the problem of nonanalyticity of the Green's function. Asano and Yonezawa[32] have calculated the DOS in liquid Ni by

applying the KKR theory of Green's function under several of these approximations. It is found that QCA[5] gives reasonable d-band width and works well outside the resonance region, but it gives a negative DOS near the resonance level, where the analyticity of the Green's function breaks down. The Ishida-Yonezawa theory works satisfactorily over the energy region near the resonance level, but at higher energy, where the electrons are nearly free, the analyticity breaks down. The results calculated by EMA, however, show a reasonable behaviour over the whole energy region. Thus the EMA of Roth appears as a theory capable of describing the behaviour of a strongly scattering disordered system. However, quite understandably, it is still an approximation and is unable to fully take into account the detailed atomic description that really characterises particular liquid and amorphous systems.

The approach that can actually take into account the detailed atomic structure of orientationally disordered systems is the tight-binding method applied to finite cluster models of these systems. Khanna and Cyrot-Lackmann[33] have applied this method to computer generated model of liquid Ni. Similar calculations for liquid and amorphous Co have been performed by Khanna et al.[34] Fujiwara[35] and Fujiwara and Tanabe[36] have performed similar calculations for liquid and amorphous iron. However, their calculations include only the d-electron states. The d-bands in iron are known to strongly hybridise with the s-band and hence the effect of this hybridisation should be noticable

in the density of states. A recent calculation by Fujiwara,[37] based on the Linear Muffin-Tin Orbitals method, where the secular equation assumes a form similar to the tight-binding one, reveals that the hybridisation appreciably modifies the DOS in the whole energy range. This is also expected of liquid iron. Hence we have decided to apply the tight-binding method to liquid and amorphous iron by taking the hybridisation into account. Tight-binding Hamiltonians defined on computer generated realistic models of these systems and represented in a basis of suitable s and d orbitals are used to compute the DOS. The density of states that we are interested in, as mentioned in the beginning of this section, is primarily the local density of states, and the tight-binding approach seems to be a natural language to express this quatity.

II. CHAPTER (2)

SIMULATION OF LIQUID AND AMORPHOUS IRON

Early attempts to describe the liquid or the amorphous structure were based on the lattice gas or the microcrystallite models. In the lattice gas model, the liquid or the amorphous solid was supposed to consist of atoms that occupied well-defined lattice sites with preassigned probabilities, whereas the proponents of the micro(para)crystallite models viewed the system as consisting of small microcrystallites with wholly or partially coherent boundaries, where a coherent boundary simply means a surface with a regular shape. Such models were often inadequate to describe the desired liquid or amorphous structure, as reflected by the discrepancies in the measured and calculated structure factors and radial distribution functions. A review on this subject has been provided by Cargill[38] (see also Phillips, 1980,Ref.39). From a theoretical point of view these models are not satisfactory for amorphous and liquid metals, since they do not describe the topological disorder that distinguishes these systems from a substitutionally disordered solid or a solid with substantial number of holes, dislocations, defects etc.

2.1 THE DRPHS MODEL

The first satisfactory attempt to simulate the topological disorder in liquid and amorphous metals was made by Bernal, when he chose to represent these systems by dense random packing of hard spheres(DRPHS). Such structures are arrangements of rigid spheres which are dense in the sense that they contain no internal holes large enough to accomodate another sphere, but are random in that there are only weak correlations between positions of spheres separated by five or more sphere diameters. They do not apparently contain any recognizable regions of crystalline-like order. Bernal and Finney[40-42] have studied these structures experimentally by filling rubber bladders with ball bearings, and squeezing and kneading these bladders to prevent nucleation of periodic arrays at the container surfaces. Finney[42] measured the co-ordinates of the centres of several thousand spheres packed in a rubber balloon and obtained the radial distribution function with much better resolution than those previously available. The packing fraction (fractional volume occupied by the spheres) was found to be 0.6366 ± 0.0004 compared with 0.7405 for close-packed crystalline structure.

Subsequently computer algorithms were developed by Bennett[43] and Adams and Matheson[44] to create the DRPHS structures. Both used an initial seed, i.e., an initial input of co-ordinates of centres of spheres in a small cluster, to which new spheres were added by following a certain criterion. Bennett used a seed consisting of three spheres forming an equilateral triangle.

Adams and Matheson began with a cluster of ten spheres placed randomly around and in contact with another sphere. The criterion for adding spheres to these initial clusters consisted of enumerating all possible sites for which an added sphere would be in hard contact with three spheres already in the cluster but would not overlap with any of them. The site nearest to the centre of the cluster was selected from this list and a sphere was added there. The list of possible sites was then updated, adding those created by the last sphere and removing those blocked by it. The structures thus obtained by both Bennett, and Adams and Matheson were roughly spherical in shape. The packing fraction decreased with increasing radius. Adams and Matheson reported a packing fraction of 0.628 for an assembly of 3900 spheres. Bennett found that the packing fraction varied almost linearly with inverse of radius and obtained an extrapolated value of 0.61 for the packing fraction for infinite radius. The actual measured value of the packing fraction for his cluster of 3999 spheres was 0.625 ± 0.005. The radial distribution functions of these clusters obtained by Bennett, and Adams and Matheson were very similar. Both yielded a co-ordination number (obtained by integrating upto the first minimum following the first maximum) between 11 and 12. The co-ordination number in the ball bearing model of Finney was 12.

Sadoc et al[45] generated a DRPHS cluster of 1000 spheres using a different criterion for adding new spheres to the seed. New spheres were added to an initial seed of three spheres

arranged in an equilateral triangle, at the site adjacent to spheres with the smallest number of neighbours. The radial distribution function for this cluster showed significant difference from those obtained by Bennett and Adams and Matheson in terms of the positions and relative heights of the secondary peaks. No packing fraction was reported by Sadoc et al.

Ichikawa[46] introduced a parameter K in Bennett's algorithm to control the short range tetrahedral perfection. In this algorithm one starts with a small seed, and three spheres within distances less than Kd (where d is the hard sphere diameter and $(1 \leqslant K \leqslant 2)$ prepare a possible site for a new sphere in hard contact with these three spheres as long as it does not overlap with any other existing spheres. After calculating the co-ordinates of all pockets, a new sphere is placed at the pocket nearest to the centre of the system. It can be seen that K=1 requires the perfect tetrahedral configuration for the nearest neighbour arrangement. It is observed that the structure with smaller K has high tetrahedral perfection and leads to a high local density. However, smaller K values require the structure to be much more porous with a smaller overall packing fraction.

Even with Ichikawa's modification of Bennett's algorithm, the DRPHS models often fail to produce the particular features of the radial distribution functions observed in real amorphous and liquid metals, though the agreement for the amorphous metals is somewhat better than that for the liquid. It is suggested

that the hard sphere potential is not realistic and one must consider softer interatomic potentials. Heimendahl[47] has relaxed the Bennett's model[43] using Lennard-Jones and Morse potentials and obtained radial distribution functions in closer agreement with that of glassy metals. Similar results have been reported by Barker et al[48] who relaxed the Bernal[42] structure using Lennard-Jones potential. The relaxation procedure consists in starting with a given cluster and moving the atoms in the cluster sequentially until a minimum in the potential energy of the cluster in the neighbourhood of the initial configuration is obtained. Yamamoto et al[49] have obtained good agreement for the radial distribution function in amorphous iron by relaxing the Bennett structure modified by Ichikawa's parameter (K=1.2), according to the interatomic potentials suggested for bcc iron.

It is perhaps worth mentioning that our initial attempt to simulate a cluster representing amorphous iron was based on Ichikawa's method of modifying the Bennett cluster with a suitable value of K. However, no value of K in the specified range ($1 \leq K \leq 2$) could yield a satisfactory radial distribution function. Hence we were faced with the problem of either relaxing the cluster or resorting to some alternate technique. In the following we discuss these alternate schemes. It should be noted that relaxing a DRPHS cluster often generates satisfactory models of amorphous metals. However, the method is not suitable for creating clusters to represent liquid metals which show significant difference in the radial distribution

function from their amorphous ccunterparts.

2.2 ALTERNATIVE SCHEMES: MOLECULAR DYNAMICS AND MONTE CARLO METHODS

Alternatives to the DRPHS models are provided by Monte Carlo [50-53] and Molecular dynamics methods.[54-57] These methods have been found to yield better models for the liquid than the relaxed DRPHS models. In the molecular dynamics method the co-ordinates of each atom in the cluster are allowed to move under the resultant force derived from suitably chosen interatomic potential. The positicn and momentum co-ordinates of the particles at any time are stored and their evolution in a small interval of time is described by solving the Newtonian equations of motion. In the equilibrium state the distribution of velocities is Maxwellian, and hence the temperature of the system of N particles should be

$$T = M \sum_{i=1}^{N} v_i^2 / 3KN \qquad (2.1)$$

in which Vi is the velocity of the i-th particle with mass M and K is the Boltzmann constant. All the velocities are, therefore, limited within a specified allowable range, consistent with eqn. (2.1). Surface effects arising from the boundaries of the cluster are taken care of by imposing the periodic boundary condition, and various equilibrium properties of the cluster are calculated from the time averages.

Contrary to the deterministic approach followed in the molecular dynamics method, Monte Carlo technique is based on a stochastic or probabilistic approach. In this method only those configurations of the atoms, which have a significant statistical weight, are considered. One starts with an initial configuration specified by the position co-ordinates of the particles in a basic cell. A sequence of configurations of the system is then generated by a process of random walk on a Markov chain. The transition probability at every step is chosen so that the limiting frequency of each configuration, as the length of the Markov chain goes to infinity, becomes proportional to the Boltzmann factor $\exp(-E/KT)$, where E is the energy associated with the configuration, K is the Boltzmann constant and T is the temperature of the system on the absolute scale. This is achieved as follows. Each particle, chosen at random or by succession, is moved by small steps of random sizes within preassigned limits. After each move, the change in the energy of the system, DE, is calculated. A suitable interatomic potential is used for this purpose. If $DE < 0$, i.e., the move would bring the system to a state of lower energy, then the move is allowed and the particle is put in its new position. If $DE > 0$, then the move is allowed with a probability $\exp(-DE/KT)$. To achieve this result, a random number ξ is chosen between 0 and 1. If $\exp(-DE/kT)$ is greater than ξ, then the particle is moved to its new position. Otherwise the move is rejected. If the move is rejected, the old configuration is counted as having occurred

again in the computation of averages.

Using the Markov chain of configurations constructed in this way, one obtains the average of any function of configuration simply by averaging over all members of the chain. The result is equivalent to averaging over a canonical ensemble as the limiting frequency of each configuration is proportional to the Boltzmann factor exp(-E/kT). That the above procedure of selecting the configurations does lead to a limiting frequency distribution proportional to exp(-E/kT) has been shown by Metropolis et al.[50] One could also do a calculation by choosing configurations at random, and then assigning weights to them. While such a procedure should give the same result as the above method, if both are carried out for a sufficiently large number of configurations, it has the disadvantage that a large amount of time would be wasted on relatively improbable configurations. The Markov chain method is an example of "importance sampling" and gains efficiency by concentrating on the more probable configurations.

We have employed the Monte Carlo technique to generate clusters with 365 atoms representing liquid and amorphous iron. The method followed is essentially the same as described above. We used the interatomic potential as given by Johnson.[58] This potential is derived by fitting its first and second derivatives at the nearest and next nearest neighbour separations in bcc iron to the elastic modulii. The potential is cut off at a point between the second and the third nearest neighbours. The

original form suggested by Johnson consists of three third order polynomials for three different regions of the interatomic distance. For computational efficiency we have reparameterised the potential $U(r)$ using a single expression for all distances upto the cutoff point, which consists of even powers of r only:

$$U(r) = A_0 + A_1/r^4 + A_2/r^6 + A_3/r^8 + A_4/r^{12}, \quad r \leq 3.3\,A^\circ$$

$$= 0, \quad r > 3.3\,A^\circ \qquad (2.2)$$

with $A_0 = 0.07$, $A_1 = -20.65$, $A_2 = 174.7868$,

$A_3 = -445.37$, $A_4 = 1000.00$.

The constants ($A_0 - A_4$) were chosen to reproduce the Johnson potential accurately between the nearest and next nearest neighbours. We start with cubic cluster of 365 atoms supposed to represent liquid La. This cluster was obtained by Ballentine[59] for calculations of electronic structure in liquid La. Appropriate change in the volume of the cluster was made to obtain the correct density of liquid iron at 1550°C. Each atom was moved by succession and the resulting configuration was accepted or rejected according to the criterion described above. Periodic boundary condition was imposed to keep the particles confined within the given volume. This cubic volume was supposed to be surrounded by periodic replicas of itself to avoid surface effects. The following criteria were used to determine the

reaching of the equilibrium:

a) the fluctuations in energy had no longer any systematic component,

b) the pair distribution function reached a stable limit,

c) slices of the cluster examined graphically revealed no particular lines along which the atoms tended to lie.

Starting from our initial liquid La configuration, about six hundred and fifty iterations, at a success rate of fifty per cent, were needed to obtain a pair distribution function of the type shown in Fig. (1). This is close to the experimentally determined pair distribution function,[60] though it represents somewhat more short range order than the liquid.

The cluster representing the amorphous iron was generated from the liquid cluster by carrying out the Monte Carlo procedure at a much lower temperature (100 ^{o}C). Appropriate change in the volume of the cluster was made to represent the density of amorphous iron. Starting from the liquid cluster, about four hundred iterations were needed to generate a cluster with the pair distribution function as shown in Fig. (2), which is in reasonable agreement with the experimentally determined distribution.[61]

Small clusters with 125 atoms representing liquid and amorphous iron were also obtained by the technique discussed above. In this case the starting configuration was chosen to be a simple cubic one. About the same number of iterations as quoted above were needed to achieve equilibrium. The pair

distribution function obtained for these clusters are displayed in Figs.(3) and (4).

FIGURE CAPTIONS

FIG.1. Pair distribution function for liquid Fe near the melting point, according to experiment (Ref.60)(smooth curve) and as simulated in a cluster of 365 atoms (histogram).

FIG.2. Pair distribution function for amorphous Fe, according to experiment (Ref.61)(smooth curve) and as simulated in a cluster of 365 atoms (histogram).

FIG.3. Pair distribution function for liquid Fe near the melting point, according to experiment (Ref.60)(smooth curve) and as simulated in a cluster of 125 atoms (histogram).

FIG.4. Pair distribution function for amorphous Fe, according to experiment (Ref.61)(smooth curve) and as simulated in a cluster of 125 atoms (histogram).

FIG.(1)

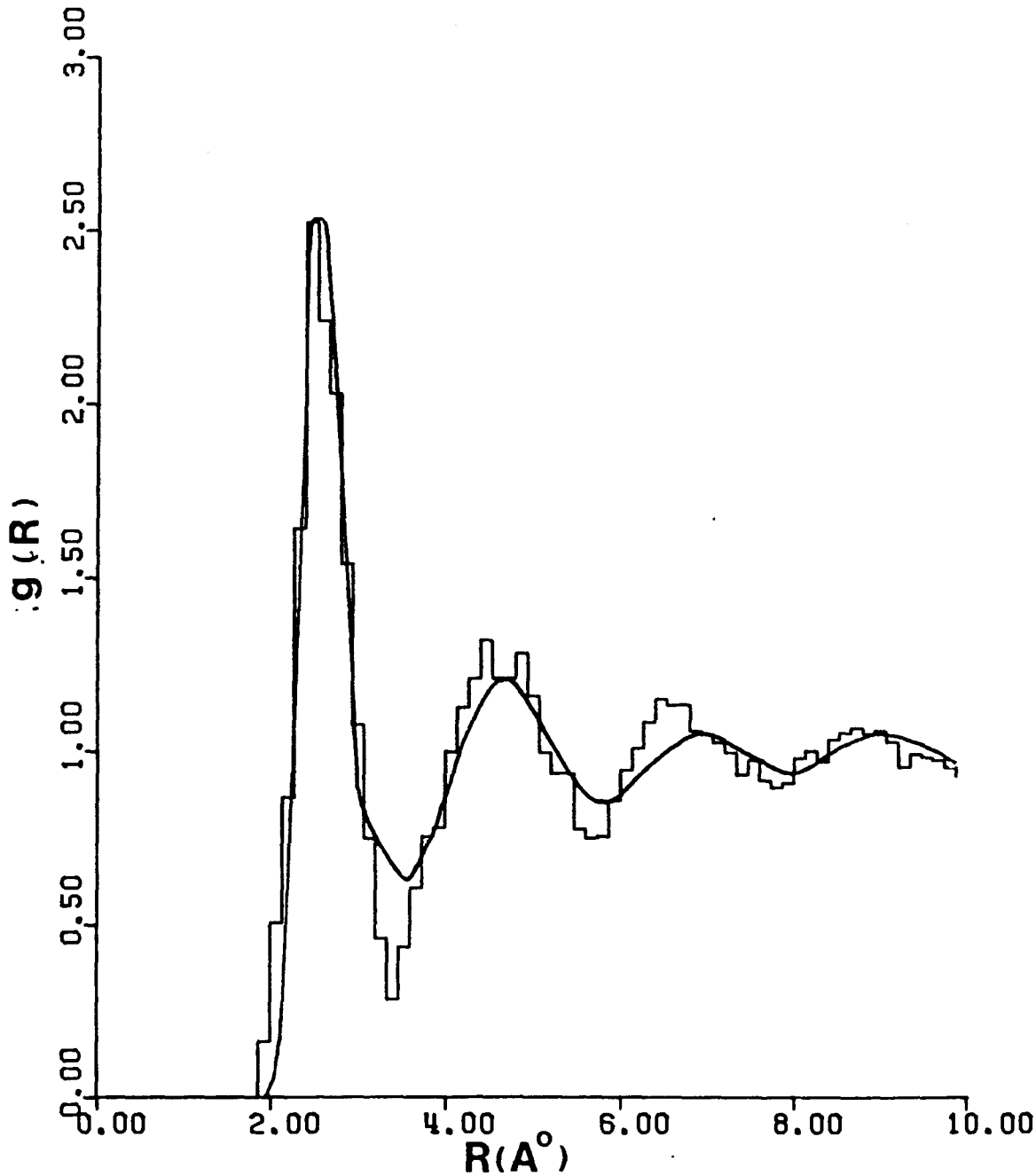

FIG. (2)

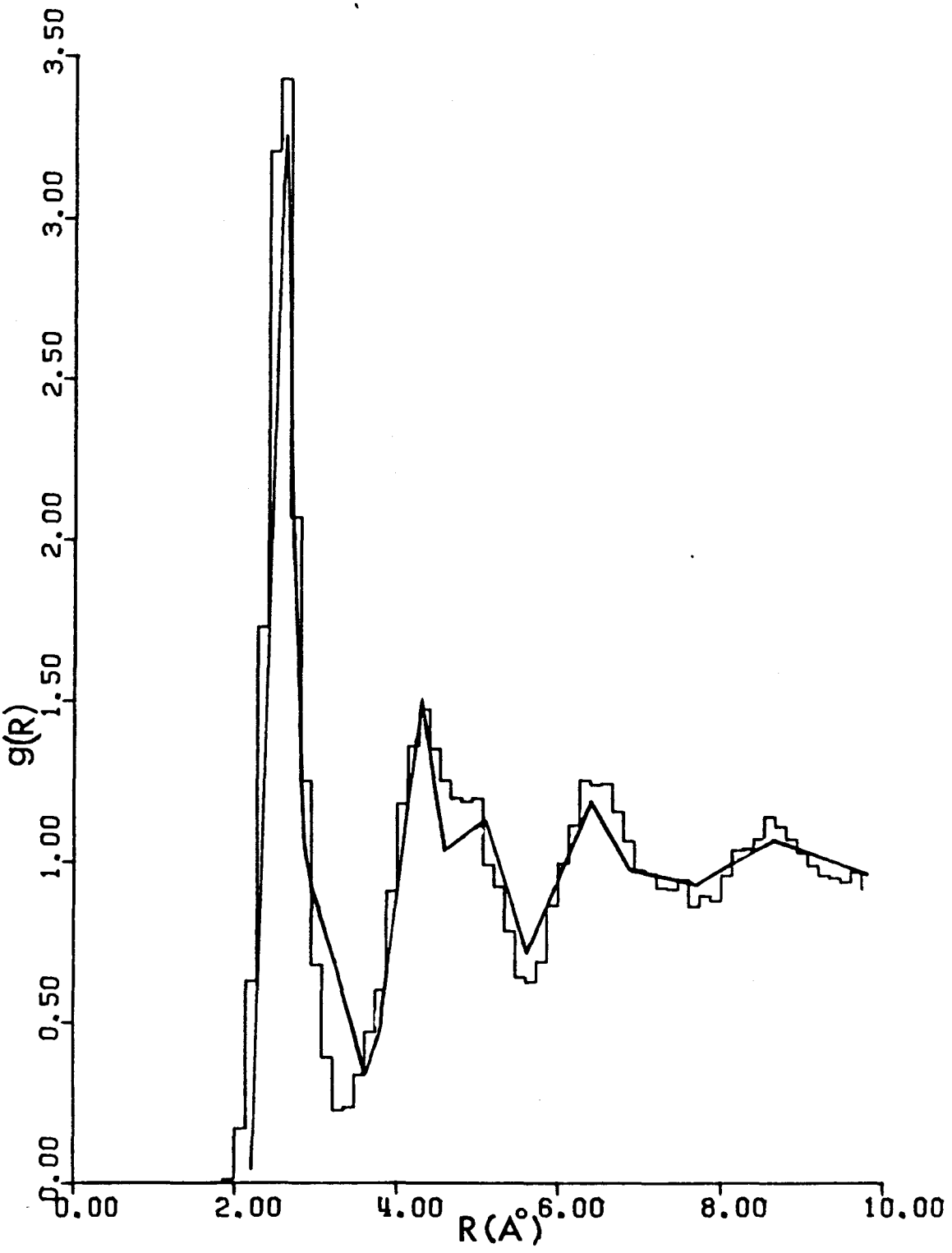

FIG. (3)

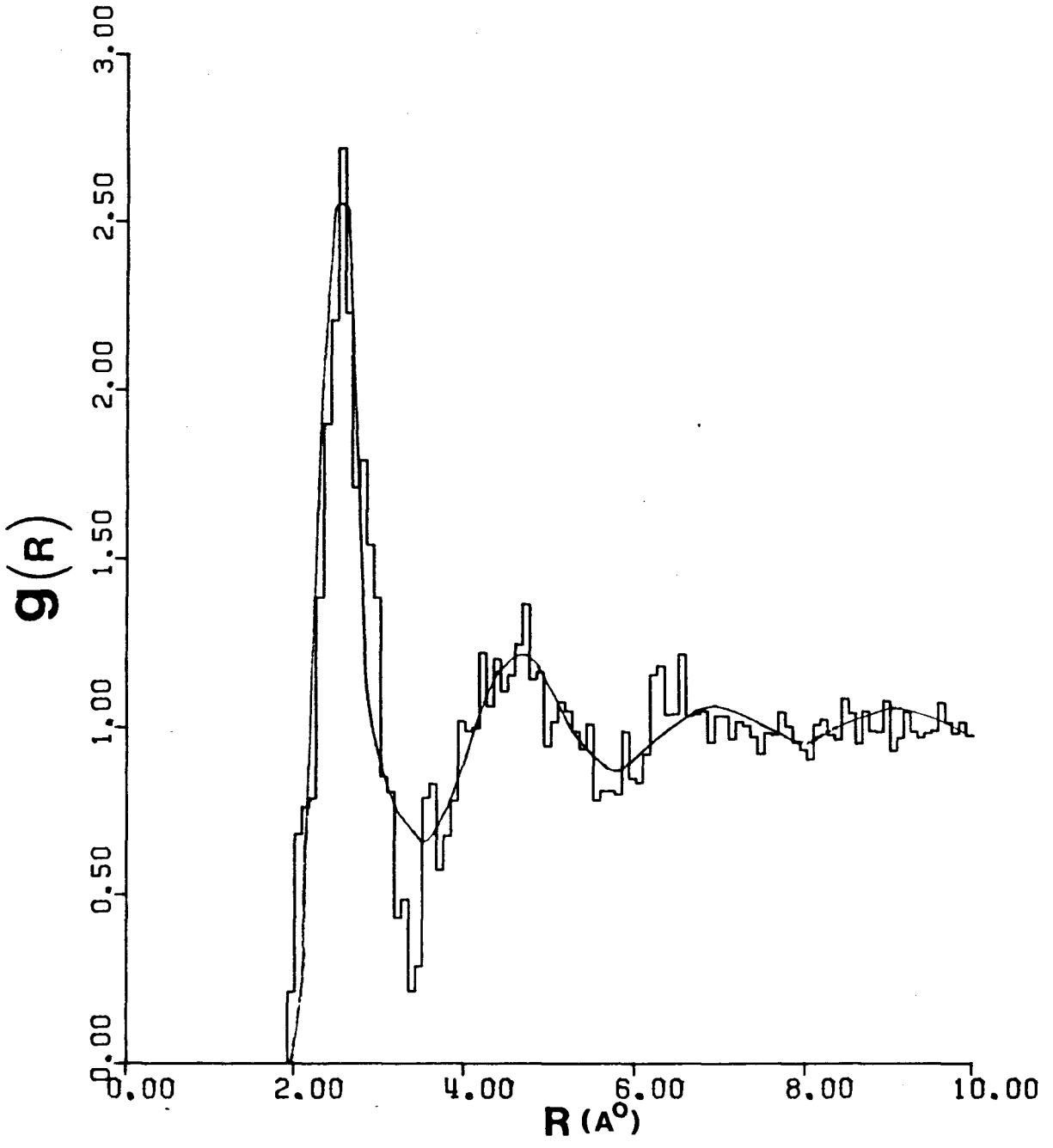

FIG.(4)

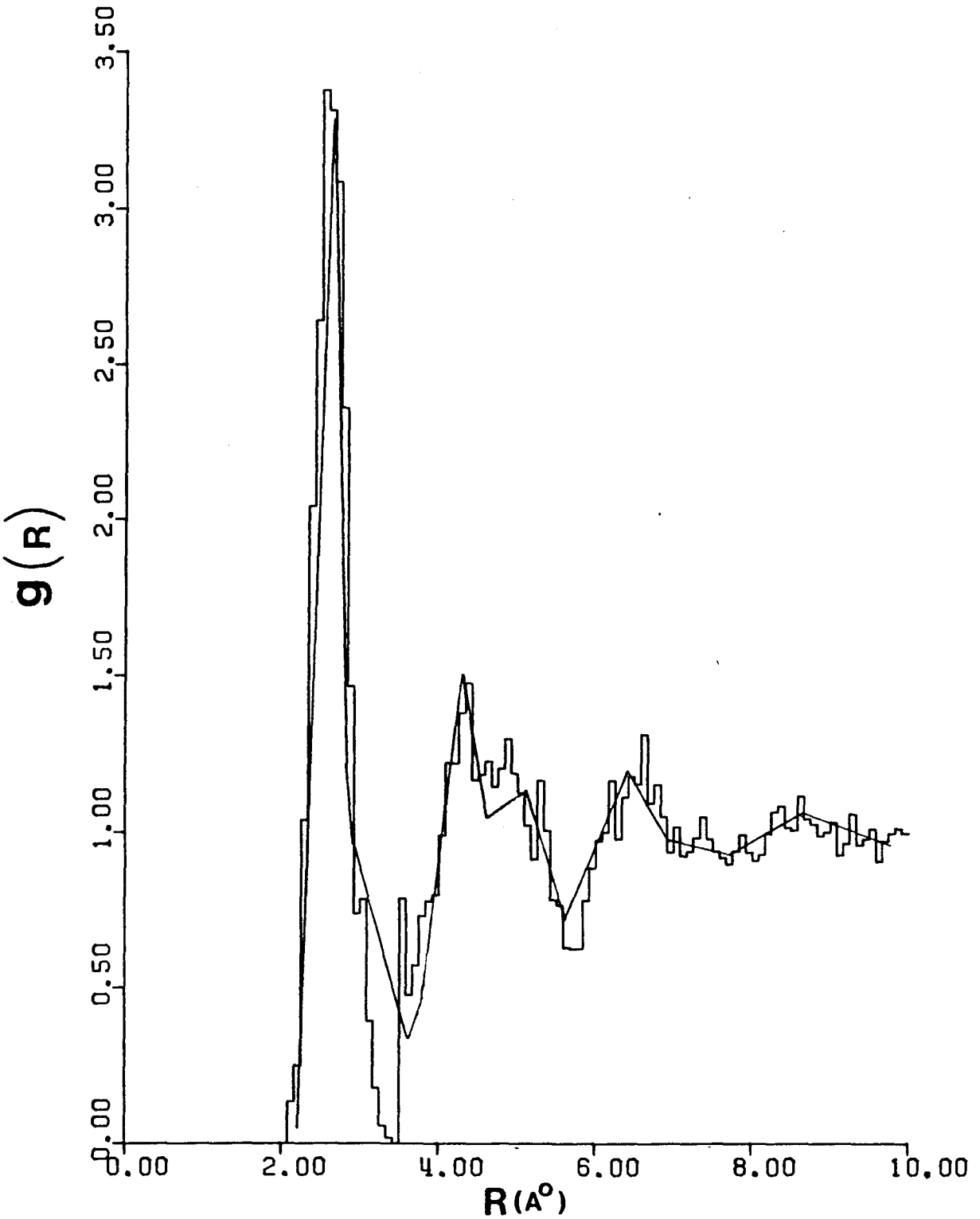

III. CHAPTER (3)

3. LCAO METHOD

The basic requisite for a tight-binding calculation of the electronic structure of a system, periodic or otherwise, is a set of orbitals localised about the atomic sites. The method was introduced to crystal calculations by Bloch,[62] when he used a basis of atomic orbitals $\{|\phi_\alpha\rangle\}$ to express the one-electron wavefunctions Ψ_i:

$$|\Psi_i\rangle = \sum_\alpha C_{i\alpha} |\phi_\alpha\rangle , \tag{3.1}$$

where the subscript α refers to the site as well as the orbital type. The Schrödinger eqn. for the electron with the Hamiltonian H,

$$H|\Psi_i\rangle = \varepsilon_i |\Psi_i\rangle , \tag{3.2}$$

or,

$$\sum_\alpha H C_{i\alpha} |\phi_\alpha\rangle = \varepsilon_i \sum_\alpha C_{i\alpha} |\phi_\alpha\rangle \tag{3.3}$$

can be transformed, by taking the inner product with a basis vector $|\phi_\beta\rangle$, to a matrix eqn.

$$\sum_{\alpha} (H_{\beta\alpha} - \varepsilon_i S_{\beta\alpha}) C_{i\alpha} = 0 . \qquad (3.4)$$

Here $H_{\alpha\beta}$'s represent the matrix elements of the Hamiltonian in the given basis, i.e.,

$$H_{\alpha\beta} = \langle \phi_\alpha | H | \phi_\beta \rangle \qquad (3.5)$$

and $S_{\alpha\beta}$'s represent the elements of the overlap matrix:

$$S_{\alpha\beta} = \langle \phi_\alpha | \phi_\beta \rangle . \qquad (3.6)$$

The eigen values ε_i of the eqn. (3.3) can be obtained by solving the secular eqn.

$$\det [H_{\alpha\beta} - \varepsilon_i S_{\alpha\beta}] = 0, \qquad (3.7)$$

or equivalently

$$\det [(S^{-1}H)_{\alpha\beta} - \varepsilon_i \delta_{\alpha\beta}] = 0 \qquad (3.8)$$

$(S^{-1})_{\alpha\beta}$ represent the elements of the inverse of the overlap matrix $[S_{\alpha\beta}]$. $[S^{-1}H]_{\alpha\beta}$ can be given the following interpretation. Suppose the Hamiltonian H acting on the basis state $|\phi_\alpha\rangle$ produces a state that we approximate or in some cases write exactly as a linear combination of the basis states, i.e.,

$$H|\phi_\alpha\rangle = \sum_{\beta} D_{\beta\alpha} |\phi_\beta\rangle . \qquad (3.9)$$

Using the expression

$$I = \sum_{\alpha\beta} |\phi_\alpha\rangle (S^{-1})_{\alpha\beta} \langle\phi_\beta|$$

(see Appendix (A-1))

for the identity operator

$$H|\phi_\alpha\rangle = \sum_{\gamma\beta} |\phi_\gamma\rangle (S^{-1})_{\gamma\beta} \langle\phi_\beta|H|\phi_\alpha\rangle$$

$$= \sum_{\gamma} (S^{-1}H)_{\gamma\alpha} |\phi_\gamma\rangle = \sum_{\gamma} D_{\gamma\alpha} |\phi_\gamma\rangle .$$

Thus the matrices D and $S^{-1}H$ are identical. In what follows we will refer to D as the Hamiltonian matrix and note that the elements of this matrix are different from the matrix elements of the Hamiltonian $H_{\alpha\beta}$. This distinction vanishes if the basis $\{|\phi_\alpha\rangle\}$ is orthogonal.

This method of solving the one-electron Schrödinger equation has come to be known as the Linear Combination of Atomic Orbitals (LCAO) method. However, the set $\{|\phi_\alpha\rangle\}$ need not be confined to atomic orbitals and subsequent tight-binding calculations have often been based on various different basis sets. The problem of nonorthogonality associated with the atomic orbitals has been tackled by using orthogonalised Löwdin orbitals,[63] thus giving rise to the name LCOAO. Calculations based on a basis of bond orbitals have been termed the LCBO method. For crystalline solids Wannier functions as well as

various other unitary transformations of Bloch functions, molecular orbitals have been used. However, these orthogonalised orbitals are more extended than atomic orbitals, having oscillatory tails and are thus sensitive to their environment. In other words, these orbitals form basis sets that are non-transferable from one situation to another. There is a direct conflict between the requirements that basis orbitals be transferable and at the same time, be orthogonal in each new situation. The transferability of the basis set from one situation to another is a highly desirable property, not only because of the obvious ease it provides for new calculations, but also because it is appealing to the intuitive "chemical building block" picture of solids and molecules. Atomic orbitals, having no oscillatory tails, are transferable or at least approximately transferable. However, there are some basic problems associated with the use of atomic orbitals. Expansion (3.1) is apparently only an approximation in a variational method unless we have a complete set of basis functions in the representation. Inclusion of more and more states do not necessarily help convergence of eqn. (3.2) and the method breaks down completely if one attempts to include the continuum of unbound states without which the representation (3.1) is incomplete.

The important advancement in the theory in this regard came relatively recently with the work of Adams,[64] Gilbert[65] and Anderson,[66] who showed for the first time how to write a defining

equation for a localised atomiclike basis so that the influence of the distant environment occurs only as a weak perturbation. It was thus demonstrated that the LCAO expression (3.1) need not be considered simply as a variational expansion in which by adding more and more arbitrary functions one hopes to converge on an accurate answer, but that sets of basis functions may be defined in such a way that the expansion in local orbitals is exact, and these localised basis functions are atomiclike and therefore approximately transferable from one situation to another. Below we briefly discuss how to obtain such a localised basis set. We will concentrate on the work of Anderson, which is of direct relevance to our work.

3.1 THE ANDERSON-BULLETT SCHEME

Let us consider an isolated band of some N atom system with the one-electron Hamiltonian H. By an isolated band we simply mean a group of closely spaced energy levels that is separated from any other such groups of energy values for the system. The energy eigenvalues in the band are given by the eigenvalues of the equation

$$H|\psi_i\rangle = \varepsilon_i|\psi_i\rangle \quad . \tag{3.10}$$

Let P be the projection operator onto the band subspace, i.e.,

$$P = \sum_{i=1}^{Nn} |\psi_i\rangle\langle\psi_i| \quad , \tag{3.11}$$

where we have assumed that there are Nn number of energy levels

in the band (n levels per atom). P is a hermitian operator satisfying

$$P^2 = P. \tag{3.12}$$

Furthermore P commutes with H :

$$PH = HP. \tag{3.13}$$

The basic idea of the localised orbital (LO) theories developed by Adams,[64] Gilbert,[65] and Anderson[66] is to represent exactly the eigenfunctions in the band as linear combinations of atomiclike LOs $\phi_{a,\alpha}$, localised about the atom 'a'. The subscript denotes the type of the orbital and runs over the total number of orbitals, n, per atom. The first condition that is imposed on these LOs is that they must span the band subspace of the functions Ψ_i, i.e.,

$$P|\phi_{a,\alpha}\rangle = |\phi_{a,\alpha}\rangle. \tag{3.14}$$

Using the identities (3.13) and (3.12), eqn. (3.14) can be written as

$$H|\phi_{a,\alpha}\rangle - PHP|\phi_{a,\alpha}\rangle = 0. \tag{3.15}$$

This equation merely represents the constraint that the LOs belong to the subspace represented by P. To define the $\phi_{a,\alpha}$'s uniquely, we need to specify another condition. For this we divide the total Hamiltonian into two parts

$$H = H_a + U_a, \tag{3.16}$$

where H_a refers to the atom 'a' and U_a refers to the 'rest of the system'. Following Adams,[64,66] we demand that the LOs satisfy the equation

$$P H_a P \,|\phi_{a,\alpha}\rangle = \varepsilon_{a,\alpha}\,|\phi_{a,\alpha}\rangle. \qquad (3.17)$$

In a single band consisting of Nn energy values, there are Nn nontrivial functions that satisfy this equation. Of these, we take the lowest n as the functions $\phi_{a,\alpha}$. These functions are localised about the atom 'a'. Eqns. (3.15) and (3.17) are the defining equations for the LOs. These can be combined into a single equation:

$$H\,|\phi_{a,\alpha}\rangle - P\,(H - H_a)\,P|\phi_{a,\alpha}\rangle = \varepsilon_{a,\alpha}\,|\phi_{a,\alpha}\rangle, \qquad (3.18)$$

or,

$$H\,|\phi_{a,\alpha}\rangle - P\,U_a\,P|\phi_{a,\alpha}\rangle = \varepsilon_{a,\alpha}\,|\phi_{a,\alpha}\rangle. \qquad (3.19)$$

This equation can also be written as

$$H_a\,|\phi_{a,\alpha}\rangle + (U_a - P U_a P)\,|\phi_{a,\alpha}\rangle = \varepsilon_{a,\alpha}\,|\phi_{a,\alpha}\rangle. \qquad (3.20)$$

This latter form demonstrates why the effect of the 'neighbouring atoms' or the 'rest of the system' may actually be small and the functions $\phi_{a,\alpha}$ only weakly distorted from the eigenfunctions of the operator H_a. The perturbation from the surrounding atoms is weakened by projecting out the part that acts within the band.

To solve eqn. (3.20), the projection operator P has to be expressed in the nonorthogonal basis:

$$P = \sum_{a,b=1}^{N} \sum_{\alpha,\beta=1}^{n} |\phi_{a,\alpha}\rangle (S^{-1})_{a\alpha,b\beta} \langle\phi_{b,\beta}| . \qquad (3.21)$$

(see Appendix (A-1))

This is a rather complicated function of the Localised orbitals and several approximate treatments, such as keeping only terms of the first order in overlaps of the expansion of S^{-1}, have been suggested.[68,69] One can thus start with the eigenfunctions of H_a and solve eqn. (3.18) by successive iterations until self-consistency is achieved. If the residual interaction term $U_a - PU_aP$ is small, then the self-consistent solutions $\phi_{a,\alpha}$ are expected to be close to the initial approximations.

Using the pseudopotential ideas of Austin, Heine and Sham,[67] Anderson[66] developed a simplified version of the above theories, justifying and suggesting semiempirical approaches such as the extended Hückel parameterisation schemes in case of organic molecules. Following Anderson, let us formally represent the total Hamiltonian as

$$H = T + \sum_{a=1}^{N} V_a \quad , \qquad (3.22)$$

where T is the kinetic energy operator and V_a is the effective potential from atom 'a'. Such a representation is always possible in principle, since it is perfectly within our power to choose V_b for $b \neq a$ to be the difference, whatever it may be,

from the potential V_a due to the presence of 'b'. With such a division of the total potential, the pseudopotential equation defining the localised orbitals in the theory of Anderson can be derived from the general form (3.19) by setting

$$U_a = \sum_{b \neq a} P_b V_b \quad , \quad P_b = \sum_{\beta=1}^{n} |\phi_{b,\beta}\rangle \langle \phi_{b,\beta}| \quad . \tag{3.23}$$

We note that this choice of U_a implies

$$H_a = H - U_a = (T + V_a) + \sum_{b \neq a} (V_b - P_b V_b) \quad . \tag{3.24}$$

Eqn. (3.19) thus assumes the form

$$\left[(T + V_a) + \sum_{b \neq a} (V_b - P_b V_b)\right] |\phi_{a,\alpha}\rangle = \varepsilon_{a,\alpha} |\phi_{a,\alpha}\rangle \quad , \tag{3.25}$$

or,

$$\left[(T + V_a) + \sum_{\beta=1}^{n} \sum_{b \neq a} (V_b - |\phi_{b,\beta}\rangle \langle \phi_{b,\beta}| V_b)\right] |\phi_{a,\alpha}\rangle = \varepsilon_{a,\alpha} |\phi_{a,\alpha}\rangle \quad . \tag{3.26}$$

The form of V_a is yet unspecified. However, it is desirable that the eigenfunctions of $T + V_a$ be fairly localised. The self-consistent solutions to eqn. (3.26), which are expected to be only weakly perturbed from these functions, will then be localised about the atom 'a'. Hence, one can choose V_a to be the atomic potential centered about the atom 'a',

$$V_a = V_a^{(0)} \quad . \tag{3.27}$$

However, since the total potential seen by the electron cannot be obtained by simply summing over atomic potentials, the

potential V_b for $b \neq a$ will then have a form

$$V_b = V_b^{(0)} + \delta V_x \qquad (3.28)$$

where $V_b^{(0)}$ is the free atom potential centered about the atom 'b', and δV_x can be looked upon as a correction term. The form of δV_x used in our calculation will be specified in the next section. The important point is that such a division of the total potential can be achieved in turn for each atom 'a', to solve for the corresponding $\phi_{a,\alpha}$ in (3.26). Once a particular V_a is set equal to $V_a^{(0)}$, the potentials V_b ($b \neq a$) will then be given by the form (3.28) to be consistent with the actual potential seen by the electron in the presence of all the atoms in the vicinity of 'a'.

With this division of the potential, the eigenfunction of T + V_a are the unperturbed atomic orbitals,

$$(T + V_a)\,|\phi_{a,\alpha}^{(0)}\rangle = (T + V_a^{(0)})\,|\phi_{a,\alpha}^{(0)}\rangle = \varepsilon_{a,\alpha}^{(0)}\,|\phi_{a,\alpha}^{(0)}\rangle .$$

Thus one can start with the atomic orbitals $\phi_{a,\alpha}^{(0)}$ as the initial approximation to the localised orbitals and solve eqn. (3.26) iteratively till self-consistency is achieved.

To compute the eigenvalues of the Hamiltoian H, eqn. (3.26) can be put into a more convenient form

$$H\,|\phi_{a,\alpha}\rangle = \sum_{\beta=1}^{n} \sum_{\substack{b=1 \\ b\neq a}}^{N} |\phi_{b,\beta}\rangle \langle \phi_{b,\beta}|V_b|\phi_{a,\alpha}\rangle + \varepsilon_{a,\alpha}\,|\phi_{a,\alpha}\rangle$$

or,
$$H\,|\phi_{a,\alpha}\rangle = \sum_{b=1}^{N} \sum_{\beta=1}^{n} D_{b\beta,a\alpha}\,|\phi_{b\beta}\rangle , \qquad (3.29)$$

where,

$$D_{a\alpha,a\beta} = \varepsilon_{a,\alpha}\,\delta_{\alpha\beta} \qquad (3.30)$$

and

$$D_{b\beta,a\alpha} = \langle \phi_{b,\beta} | V_b | \phi_{a,\alpha} \rangle \;, \; b \neq a \qquad (3.31)$$

Recalling eqns. (3.8) and (3.9), we see that the Anderson scheme helps us find the matrix elements $(S^{-1}H)_{a\alpha,b\beta}$ directly and the secular equation that has to be solved to obtain the eigenvalues in the band is

$$\det\left[D_{a\alpha,b\beta} - \varepsilon_i\, \delta_{a\alpha,b\beta} \right] = 0 \,. \qquad (3.32)$$

Thus the overlap matrix $(S_{a\alpha,b\beta})$ does not appear explicitly in the secular equation, although the basis orbitals $\phi_{a,\alpha}$ are not mutually orthogonal. The price paid is that the matrix D is in general nonhermitian. It is hermitian if and only if the hermitian matrices S and H commute.

As a test of the validity of this scheme, Anderson considered the π-orbitals in benzene. The purpose was to offer a justification for the Hückel type parameterisation scheme in organic molecules,[70,71] where inspite of large overlap between the atomic orbitals on neighbouring sites (the basis functions), the secular equation which is found to work very well is of the type

$$\det\left[(H_{eff})_{\alpha\beta} - \varepsilon\, \delta_{\alpha\beta} \right] = 0$$

Anderson found that for the π-orbitals in benzene, the matrix elements (3.31) calculated with the unperturbed atomic orbitals

$\phi^{(0)}_{a,\alpha}$ were very close to those obtained with the iterated solutions $\phi_{a,\alpha}$. This result, apart from providing a proper understanding as to why the simple minded Huckel model works so, offers a practical scheme for calculating the energy values in a band. One can simply start with atomic orbitals and potential (with exchange and correlation properly included), calculate the matrix elements $D_{\alpha\beta}$ as defined and obtain reasonably good results for the eigenvalues ε_i by solving eqn. (3.32). Bullett has applied this method to calculate the band structure for Se and Te as well as the electronic DOS in their amorphous phases.[72] He has also applied this method to the calculation of band structure in the Chevrel phases, where other methods are difficult to apply due to the large number of atoms per unit cell.[73] We will thus call this version of the LCAO method the Anderson-Bullett scheme and apply it to the computation of the energy eigenvalues in iron. We suppose that the basis set to represent the s-d bands in iron can be obtained from the atomic s and d wavefunctions and calculate the matrix elements

$$D_{\alpha\beta} = \langle \phi_\alpha | V_\alpha | \phi_\beta \rangle \; ; \qquad \alpha \neq \beta \qquad (3.33)$$

which can then be used to solve the secular equation (3.32). In (3.33) the subscripts a,α for the orbitals have been condensed to α and we have used V_α for V_a.

3.2 EXCHANGE AND CORRELATION EFFECTS

Although the total potential seen by an electron can always be formally written as a sum of contributions centered on each atom, it is clear that this, if only because of exchange and correlation effects , is far from the sum of atomic potentials. In particular, the atomic potential at large radii goes as 1/r, while the electron actually sees neutral atoms at all distant sites. The potential V_β in (3.33), therefore, should combine atomic potential with modifications caused by exchange and correlation effects. The actual exchange potential is nonlocal and extremely difficult to handle from the computational point of view. Hence some local approximation to the exchange potential is necessary. An approximation that is frequently made replaces the Hartree-Fock exchange term by a local potential dependent only on the local charge density (of parallel spin electrons, in case spin is included). The form suggested by Slater[74] is

$$V_x^S(\vec{r}) = -3e^2 \left\{ 3\rho(\vec{r})/8\pi \right\}^{1/3}, \qquad (3.34)$$

where $\rho(\vec{r})$ is the electron charge density. However, the density functional formalism of Hohenberg, Kohn and Sham[75] supports the original derivation of Dirac,[76] who obtained a value only 2/3 of that given by (3.34). Most often, therefore, one assumes an effective Dirac-Slater exchange potential($X\alpha$ approximation) containing a disposable parameter α,

$$V_x(\vec{r}) = \alpha V_x^S(\vec{r}) \qquad (3.35)$$

and adjusts α (in the range $2/3 \leq \alpha \leq 1$) so that the effective Hamiltonian reproduces in some optimum way the energy levels of isolated atoms in the system.[77] In some calculations the parameter α is taken to be a function of the charge density.[78] Further corrections such as correlation potentials[79] and gradient terms[80] are sometimes added to (3.35).

We have calculated the 4s and 3d atomic orbitals and the potential in Fe using the Herman-Skillman[81] program and the Slater exchange potential. Since the Slater exchange potential is proportional to one-third power of the electron density, the additional potential due to an atom 'b' placed at a distance R from an atom 'a' at the origin is $V_b^{(0)} + \delta V_x$, where $V_b^{(0)}$ is the atomic potential centered at atom 'b' and δV_x is the correction due to the nonadditivity of the atomic potentials :

$$\delta V_x = C\left\{\left[\rho_a(\vec{r})+\rho_a(\vec{r}-\vec{R})\right]^{1/3} - \left[\rho_a(\vec{r})\right]^{1/3} - \left[\rho_a(\vec{r}-\vec{R})\right]^{1/3}\right\}, \quad (3.36)$$

where $\rho_a(\vec{r})$ is the atomic charge density, and the constant C is given by

$$C = -\frac{3}{2}e^2\left(\frac{3}{\pi}\right)^{1/3} \qquad (\text{using } \alpha = 1 \text{ in } (3.35)).$$

The transfer matrix elements (3.33) are computed as

$$D_{\beta\alpha} = \langle\phi_\beta|V_\beta^{(0)}|\phi_\alpha\rangle + \langle\phi_\beta|\delta V_x|\phi_\alpha\rangle, \quad (3.37)$$

where $V_\beta^{(0)}$ is the free atom potential on the same center as β. The two terms in (3.37) partially cancel each other, reducing the magnitude of the overlap.

The term $\delta V_x(\vec{r})$ is centered about a point somewhat midway between the sites $0, \vec{R}$. Thus the second term in (3.25) does not have the form of a two-center integral and is difficult to compute. However, it is found to be slowly varying in the region of overlap of nearest and next nearest neighbour orbitals and thus may be approximated by a constant. To calculate the matrix elements $D_{\beta\alpha}$ we follow a method suggested by Ballentine.[59] From a plot (see Fig.5) of $\delta V_x(\vec{r})$ for the nearest and the next nearest neighbour separations, we first guess the limits within which δV_x may be varied. This is then treated as a parameter in our subsequent band structure calculation and varied within reasonable limits to yield the correct s band width ($H_{15} - \Gamma_1$) in bcc iron. Our reference band structure is the one computed by Callaway and Wang (CW),[82] who have carried out a self-consistent tight-binding calculation for the majority and the minority spin states in ferromagnetic bcc iron using three different spin-dependent exchange potentials. For our paramagnetic model, we have used, as reference, their band structure for the majority spin states obtained with the von Barth and Hedin[78] exchange-correlation potential. We have adjusted the difference between the s and the d atomic levels to yield the correct separation between the s and d bands at the zone center and the constant δV_x in (3.37) to yield the correct s band width. The band structure, thus obtained, is displayed in Fig. (6). The band structure near the Fermi level, which consists of predominantly d bands, is reproduced reasonably well. Since the basis set used

by CW is much larger than ours, we do not expect to reproduce exactly their results away from the Fermi level. The important difference between the band structure in Fig.(6) and the band structure of CW (Fig.(7)) is the size of the hybridisation gap, which is substantially less in the former. However, the above scheme provides a convenient way to obtain parameters which can be transferred to the disordered phases for the purpose of electronic structure calculation. These parameters are also found to reproduce reasonably well the band structure in fcc iron as obtained by the APW calculations of Wood.[83] Hence, in our susequent electronic structure calculation for the disordered phases we decide to use these parameters to generate the tight-binding Hamiltonian matrices for various clusters.

3.3 EMPIRICAL LCAO SCHEME

Since the hybridisation gap produced by the LCAO method (Anderson-Bullett scheme) described above falls short of the expected value (as obtained in the calculation of Callaway and Wang), we also use an ad hoc parameterisation scheme in an attempt to fit the CW band structure more closely. We refer to this as the empirical LCAO scheme as we directly parameterise the matrix elements of the Hamiltonian, $H_{\alpha\beta}(\vec{R})$, without specifying the basis functions.

The symmetry of a matrix element of the Hamiltonian, $H_{lm,l'm'}(\vec{R})$, is the same as the symmetry of the overlap integral between two functions,

$$\int \xi_{lm}(\vec{r})\, \xi_{l'm'}(\vec{r}-\vec{R})\, d^3r \qquad (3.38)$$

We therefore introduce two functions, depending upon certain parameters,

$$\xi_0(\vec{r}) = \left(e^{-\alpha_1 r} + A e^{-\alpha_2 r}\right) Y_0^0(\hat{r}), \qquad (3.39)$$

$$\xi_{2m}(\vec{r}) = r^2 e^{-\alpha_3 r} Y_2^m(\hat{r}), \quad m=-2,-1,0,1,2, \qquad (3.40)$$

and set

$$H_{ss}(\vec{R}) = C_1 \int \xi_0(\vec{r})\, \xi_0(\vec{r}-\vec{R})\, d^3r, \qquad (3.41)$$

$$H_{sd}(\vec{R}) = H_{ds}(\vec{R}) = C_2 \int \xi_{2m}(\vec{r})\, \xi_0(\vec{r}-\vec{R})\, d^3r, \qquad (3.42)$$

$$H_{dd}(\vec{R}) = C_3 \int \xi_{2m}(\vec{r})\, \xi_{2m}(\vec{r}-\vec{R})\, d^3r. \qquad (3.43)$$

Eqns.3.41 to 3.43 involve seven constants, namely, $\alpha_1, \alpha_2, \alpha_3$, A, C_1, C_2, C_3. These constants are treated as parameters in the band structure calculation. In addition, the on-site energies of the s and the d basis functions, $H_{ss}(0)$ and $H_{dd}(0)$, are also treated as parameters. The Slater functions ξ's are to be viewed as mathematical entities that provide a convenient means of parameterising the matrix elements $H_{\alpha\beta}(\vec{R})$ and should not be confused with the basis functions. In other words, we

pretend that using eqns. (3.41-3.43) we have obtained the matrix elements of the Hamiltonian in a localised basis consisting of functions with s and d symmetries, although we do not know what these basis functions are.

Our parameterisation scheme† generates a symmetric Hamiltonian. Therefore in calculating the band structure we assume that the basis of this representation is orthogonal and solve the secular eqn.

$$\det \left[H_{\alpha\beta} - \varepsilon \delta_{\alpha\beta} \right] = 0 . \qquad (3.44)$$

The nine parameters mentioned above are varied to obtain a least square fit to the majority spin state band structure of CW. In the least square fitting, bands near the Fermi level are given greater weightage than those far above or below this level. The band structure, thus obtained, is shown in Fig. (8). We note that the size of the hybridisation gap has increased from the band structure in Fig. (6). It is still less than that in the band structure of CW (Fig. 7). However, it is of the same magnitude as in a previous calculation by Tawil and Callaway.[84]

---

†The values of the parameters used in this scheme and the Anderson-Bullett scheme discussed in section (3.1) are listed in Appendix (A-3).

FIGURE CAPTIONS

FIG.5. Contours of $\delta V_x(\vec{r})\ 10^3$(Ryd.). $\delta V_x(\vec{r})$ is the nonadditive part of the potential of two atoms. One atom is shown on the +X axis, the other being at the same distance from the origin along the -X axis.

FIG.6. Band structure for bcc Fe along certain symmetry directions, obtained by employing the Anderson-Bullett scheme (section 3.1).

FIG.7. Band structure for bcc Fe along certain symmetry directions, as obtained in the calculations of Callaway and Wang(1977) (Ref.82).

FIG.8. Band structure for bcc Fe along certain symmetry directions, obtained by employing the empirical LCAO scheme (section 3.3).

FIG.(5)

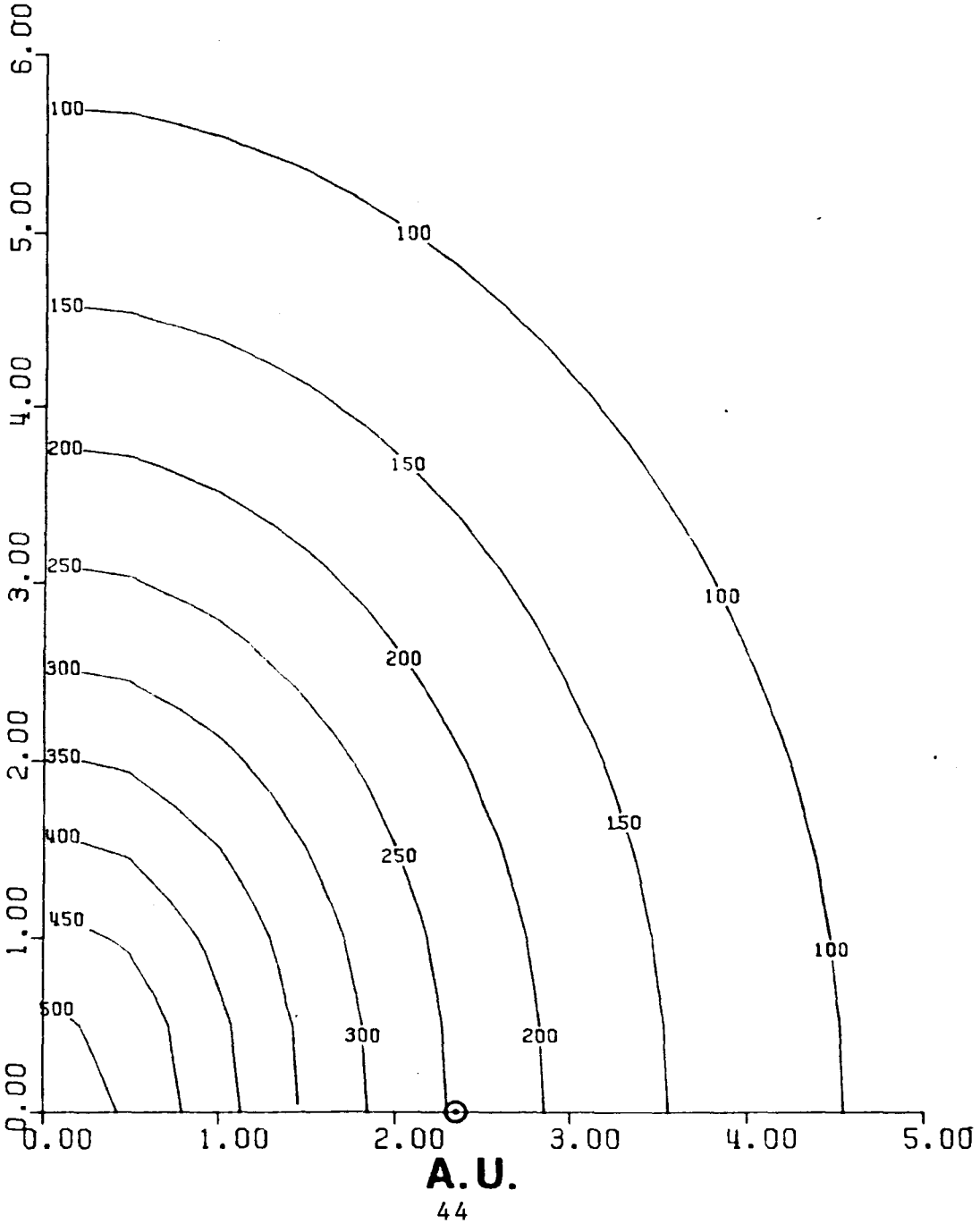
6.00
5.00
4.00
3.00
2.00
1.00
0.00
100
150
200
250
300
350
400
450
500
0.00
1.00
2.00
3.00
4.00
5.00
A.U.

FIG. (6)

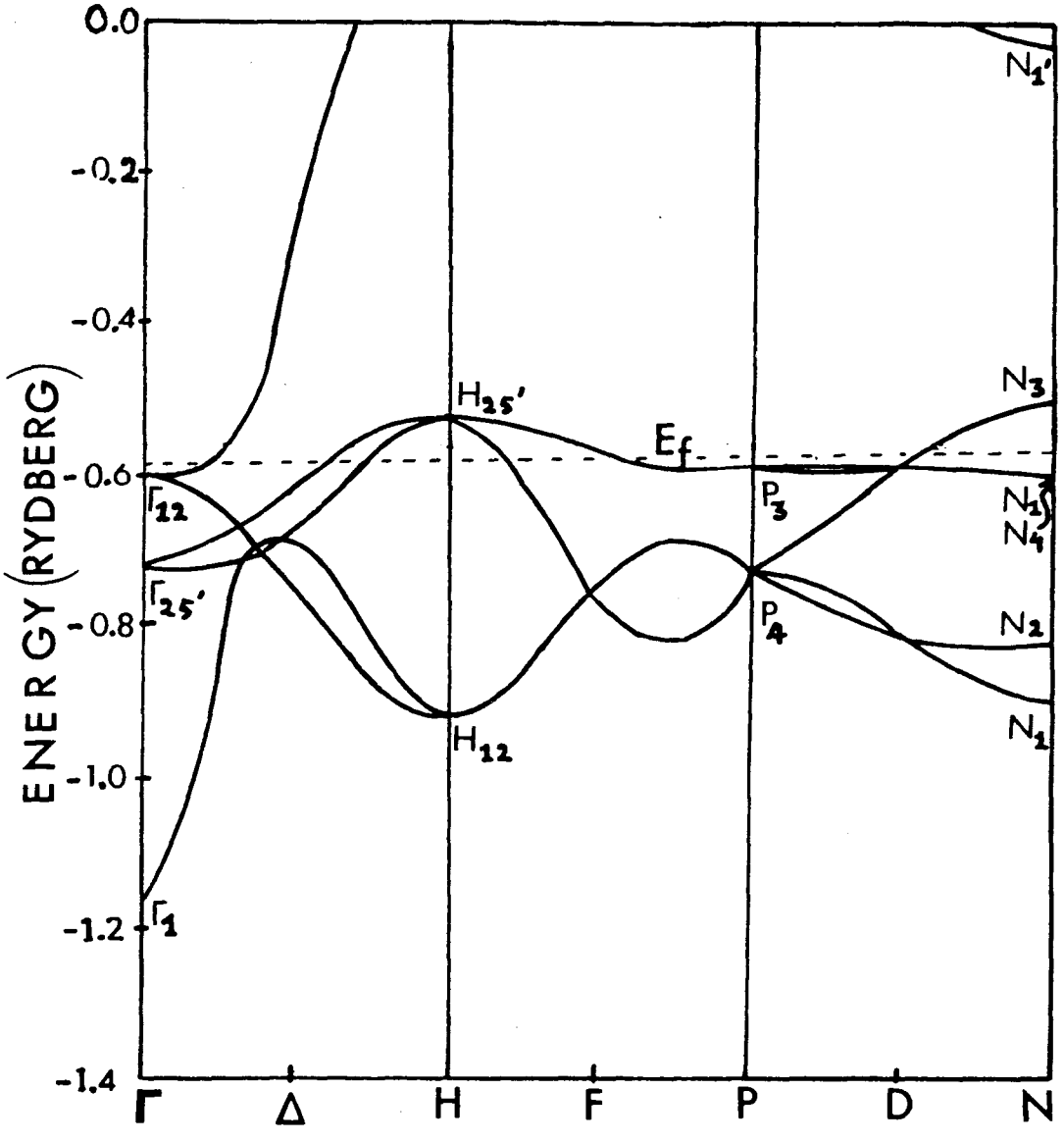
0.0
-0.2
-0.4
-0.6
-0.8
-1.0
-1.2
-1.4
ENERGY (RYDBERG)
Γ
Δ
H
F
P
D
N
Γ12
Γ25'
Γ1
H25'
H12
Ef
P3
P4
N1'
N3
N1
N4
N2
N1

FIG. (7)

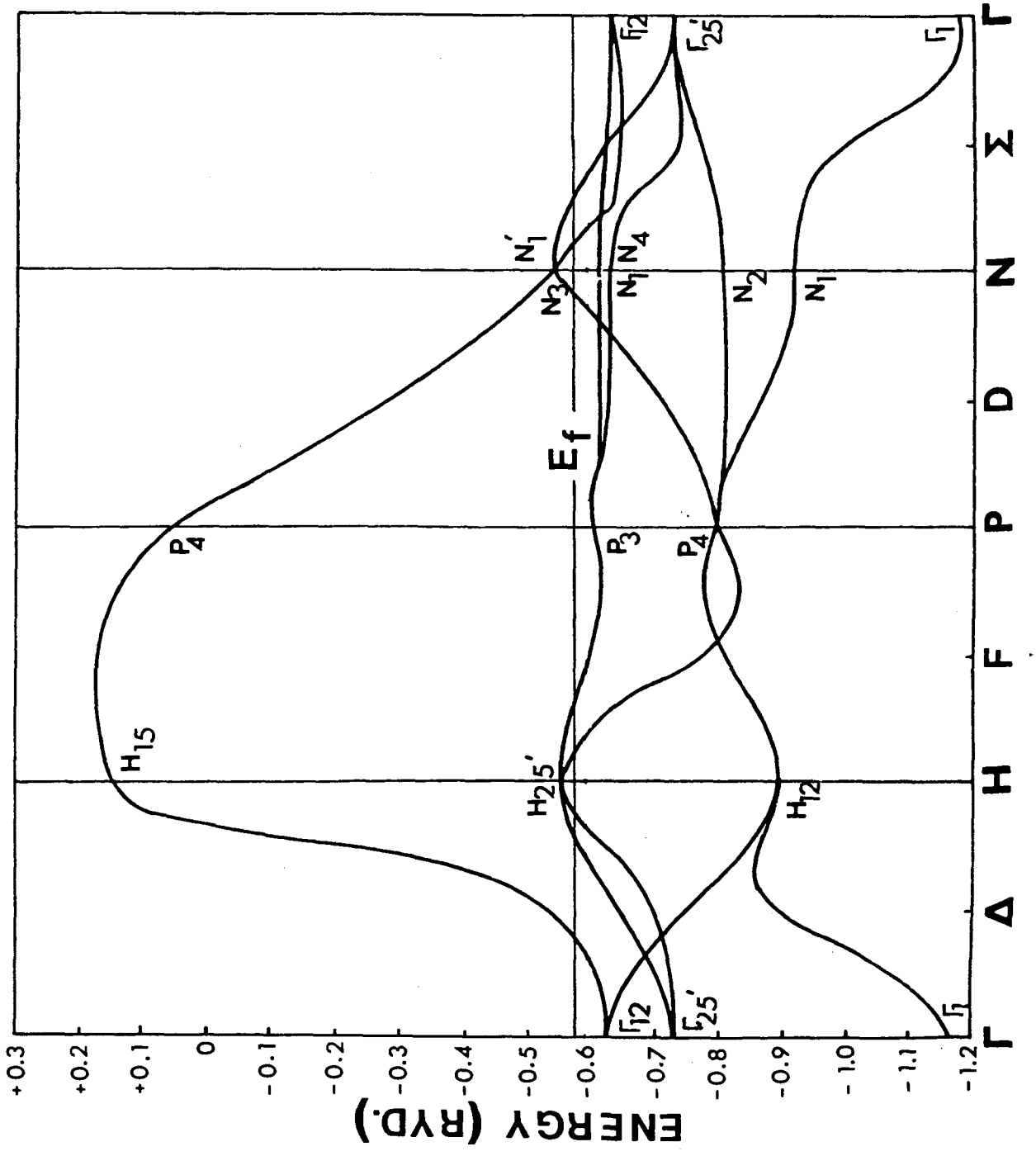
ENERGY (RYD.)
+0.3
+0.2
+0.1
0
-0.1
-0.2
-0.3
-0.4
-0.5
-0.6
-0.7
-0.8
-0.9
-1.0
-1.1
-1.2
Γ Δ H F P D N Σ Γ
E_f
H_{15}
P_4
$H_{25'}$
H_{12}
P_3
P_4
N_3
N_1'
N_1 N_4
N_2
N_1
Γ_{12}
$\Gamma_{25'}$
Γ_1
Γ_{12}
$\Gamma_{25'}$
Γ_1

FIG. (8)

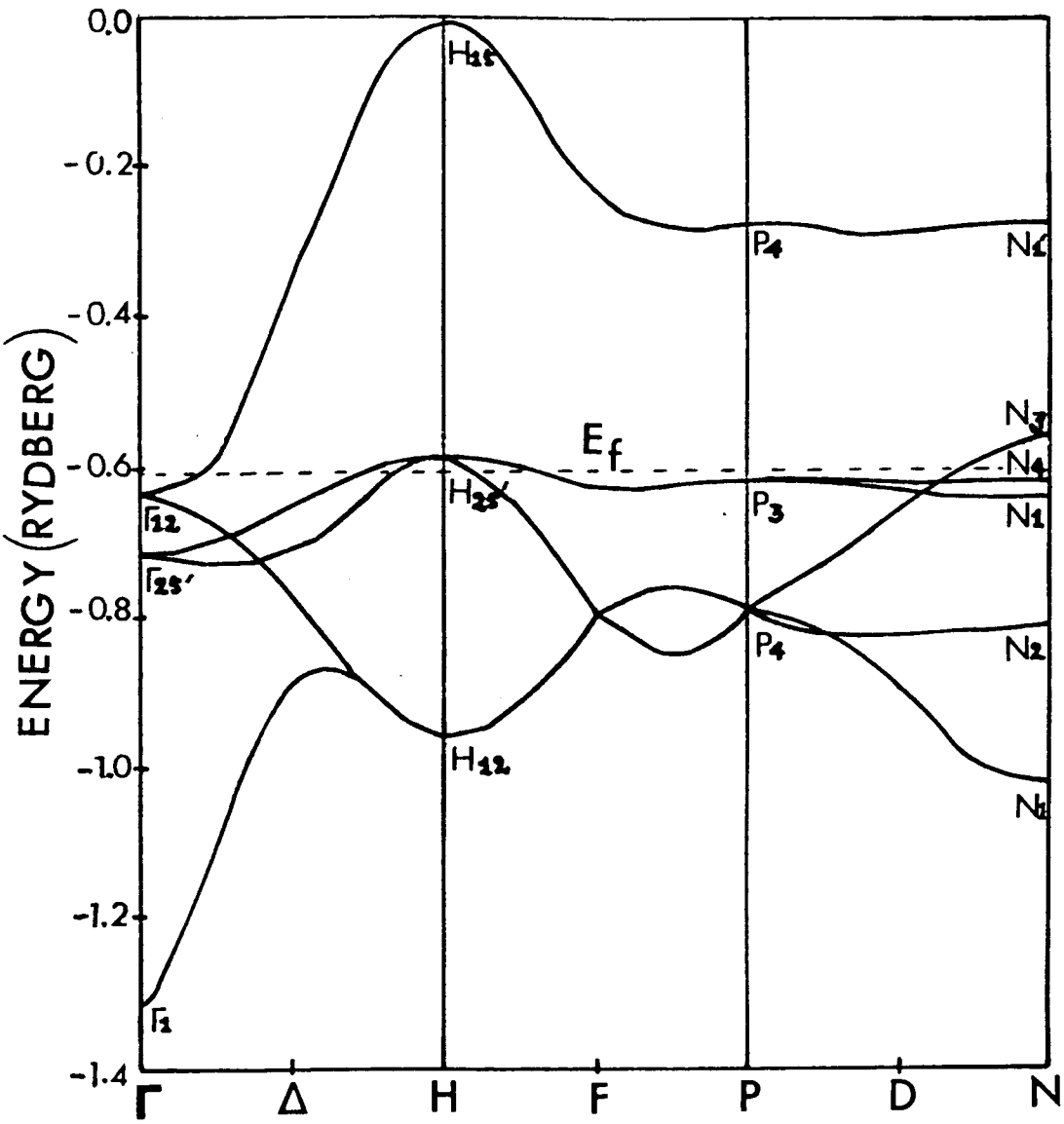
0.0
-0.2
-0.4
-0.6
-0.8
-1.0
-1.2
-1.4
ENERGY (RYDBERG)
Γ
Δ
H
F
P
D
N
E_f
H_{15}
$H_{25'}$
H_{12}
Γ_{12}
$\Gamma_{25'}$
Γ_1
P_4
P_3
P_4
N_3
N_4
N_1
N_2

3.4 EVALUATION OF THE TWO-CENTER INTEGRALS

In our calculations involving the LCAO schemes discussed in sections (3.1) and (3.3) all wavefunctions and potentials are expressed in the form of Slater type functions

$$f^{n}_{l,m}(\alpha,\vec{r}) = e^{-\alpha r}\, r^{n+l-1}\, Y^{m}_{l}(\hat{r}) \qquad (3.45)$$

Thus the transfer matrix elements ($D_{\alpha\beta}$) and ($H_{\alpha\beta}$) are written as linear combinations of two center integrals involving Slater type functions. Overlap integrals of two such functions centered on different atoms have been evaluated by several workers by employing various techniques.[85-93] However, these results are scattered throughout the literature in various notations and often expressed in an inconvenient co-ordinate system. For this reason we have chosen to generate all the overlap integrals in a systematic fashion that is convenient for computation. The method, which is due to L. E. Ballentine, has been discussed briefly in a recent publication.[59]

Suppose

$$I(\vec{R}) = \int f_1(\vec{r})\, f_2(\vec{r}-\vec{R})\, d^3r,$$

where

$$f_1(\vec{r}) = f^{n_1}_{l_1 m_1}(\alpha_1,\vec{r}) \quad \text{etc.}$$

Then

$$F\{I(\vec{R})\} = (2\pi)^{3/2} F\{f_1(\vec{r})\} F\{f_2(\vec{r})\},$$

where $F\{\cdots\}$ denotes the Fourier transform of the function inside the brackets, e.g.,

$$F\{f_1(\vec{r})\} = F_1(\vec{k}) = (2\pi)^{-3/2} \int e^{i\vec{k}\cdot\vec{r}} f_1(\vec{r})\, d^3r$$

$$= (2\pi)^{-3/2} \int e^{i\vec{k}\cdot\vec{r}}\, e^{-\alpha_1 r}\, r^{l_1+n_1-1}\, Y_{l_1}^{m_1}(\hat{r})\, d^3r. \qquad (3.47)$$

Fourier transform of Slater type functions can be calculated analytically. Expanding $e^{i\vec{k}\cdot\vec{r}}$ in spherical harmonics about the vectors $\hat{k}$ and $\hat{r}$, the angular and radial parts of the integral in (3.22) can be carried out separately to yield

$$F_1(\vec{k}) = Y_{l_1}^{m_1}(\hat{k})\; X_{l_1 n_1}^{\alpha_1}(k)$$

where

$$X_{l_1 n_1}^{\alpha_1}(k) = i^{l_1} k^{-1/2} (\alpha_1^2 + k^2)^{-(l_1+n_1+3/2)/2} \cdot \Gamma(2l_1+n_1+2)$$

$$\cdot P^{-(l_1+1/2)}_{(l_1+n_1+1/2)}\left(\alpha_1 (\alpha_1^2+k^2)^{-1/2}\right).$$

We have used [94]

$$\int_0^\infty e^{-\alpha x} J_\nu(\beta x)\, x^{\mu-1}\, dx = (\alpha^2+\beta^2)^{-\mu/2}\, \Gamma(\nu+\mu)$$

$$P^{-\nu}_{\mu-1}\left(\alpha(\alpha^2+\beta^2)^{-1/2}\right) \;;\; \alpha, \beta, \mathrm{Re}(\nu+\mu) > 0$$

$J_\nu(z)$ is the Bessel Function of the first kind of order ν and related to spherical Bessel function by

$$j_\ell(z) = \sqrt{\pi/2z}\; J_{\ell+1/2}(z),$$

and $P_\nu^\mu(z)$ is the associated Legendre function of the first kind. Thus

$$F\left\{I(\vec{R})\right\} = (2\pi)^{3/2} Y_{\ell_1}^{m_1}(\hat{k})\, Y_{\ell_2}^{m_2}(\hat{k})\, X_{\ell_1 n_1}^{\alpha_1}(k)\, X_{\ell_2 n_2}^{\alpha_2}(k)$$

Writing

$$e^{-i\vec{K}.\vec{R}} = 4\pi \sum_{L,M} (-i)^L Y_L^M(\hat{R})\, Y_L^{M*}(\hat{k})\, j_\ell(kR),$$

we obtain

$$I(\vec{R}) = 4\pi \sum_{L,M} C_{\ell_1 L \ell_2}^{m_1 M m_2}\, Y_L^M(\hat{R})\, S_{\ell_1 \ell_2}^{L n_1 n_2}(\alpha_1, \alpha_2, R), \quad (3.48)$$

where $C_{\ell_1 L \ell_2}^{m_1 M m_2}$ are the Gaunt Co-efficients:

$$C_{\ell_1 L \ell_2}^{m_1 M m_2} = \int Y_{\ell_1}^{m_1}(\hat{k})\, Y_L^{M*}(\hat{k})\, Y_{\ell_2}^{m_2}(\hat{k})\, d\Omega_K,$$

and $S_{\ell_1 \ell_2}^{L n_1 n_2}(\alpha_1, \alpha_2, R)$ are integrals of the type:

$$S_{\ell_1 \ell_2}^{L n_1 n_2}(\alpha_1, \alpha_2, R) = (-i)^L \int j_L(kR)\, X_1\, X_2\, k^2\, dk, \quad (3.49)$$

with

$$X_1 = X^{\alpha_1}_{\ell_1, n_1}(k) \quad \text{etc.}$$

These integrals can be done by contour integration by applying the residue theorem and hence $I(\vec{R})$ can be obtained from (3.48). The integrals (3.49) can be done relatively easily for $n_1 = n_2 = 0$ and the rest can be generated by differentiation w.r.t. α's, i.e.,

$$S^{L\, n_1, n_2}_{\ell_1\, \ell_2} = \left(-\partial/\partial\alpha_1\right)^{n_1} \left(-\partial/\partial\alpha_2\right)^{n_2} S^{L\, 0\, 0}_{\ell_1, \ell_2} \quad . \qquad (3.50)$$

The spherical harmonics

$$Y^m_\ell(\theta, \phi) = |\ell, m\rangle$$

are complex for $m \neq 0$, with

$$Y^{m\,*}_\ell(\theta, \phi) = (-1)^m Y^{-m}_\ell(\theta, \phi) .$$

However one can introduce normalised real basis functions as follows:

$$|\ell, m^{(+)}\rangle = \frac{1}{\sqrt{2}} \left\{ |\ell, m\rangle + (-1)^m |\ell, -m\rangle \right\} = \sqrt{2}\, R_e\, Y^m_\ell(\theta, \phi),$$

$$|\ell, m^{(-)}\rangle = \frac{1}{\sqrt{2}} \left\{ |\ell, m\rangle - (-1)^m |\ell, -m\rangle \right\} = \sqrt{2}\, J_m\, Y^m_\ell(\theta, \phi),$$

$$m > 0$$

If the overlap between the complex basis functions $|\ell, m\rangle$ are written as I_{m_1, m_2} then the overlap between the real basis functions are related to these by

$$\langle m_1^{(+)} | m_2^{(+)} \rangle = \frac{1}{2}\left\{ I_{m_1,m_2} + (-1)^{m_1+m_2} I_{-m_1,-m_2} + (-1)^{m_1} I_{-m_1,m_2} + (-1)^{m_2} I_{m_1,-m_2} \right\}$$

$$\langle m_1^{(-)} | m_2^{(-)} \rangle = \frac{1}{2}\left\{ I_{m_1,m_2} + (-1)^{m_1+m_2} I_{-m_1,-m_2} - (-1)^{m_1} I_{-m_1,m_2} - (-1)^{m_2} I_{m_1,-m_2} \right\}$$

$$\langle m_1^{(+)} | m_2^{(-)} \rangle = \frac{1}{2i}\left\{ I_{m_1,m_2} - (-1)^{m_1+m_2} I_{-m_1,-m_2} + (-1)^{m_1} I_{-m_1,m_2} - (-1)^{m_2} I_{m_1,-m_2} \right\}$$

$$\langle m_1^{(-)} | m_2^{(+)} \rangle = \frac{-1}{2i}\left\{ I_{m_1,m_2} - (-1)^{m_1+m_2} I_{-m_1,-m_2} - (-1)^{m_1} I_{-m_1,m_2} + (-1)^{m_2} I_{m_1,-m_2} \right\}$$

$$m_1, m_2 > 0$$

If m=0, then $|m^{(+)}\rangle$ and $|m^{(-)}\rangle$ need not be defined, since

$$|m\rangle = |0\rangle = Y_\ell^0(\theta,\phi)$$

is real. The real overlap integrals with m>0 are

$$\langle 0 | m^{(+)} \rangle = \frac{1}{\sqrt{2}}\left\{ I_{0,m} + (-1)^m I_{0,-m} \right\}$$

$$\langle 0 | m^{(-)} \rangle = \frac{1}{i\sqrt{2}}\left\{ I_{0,m} - (-1)^m I_{0,-m} \right\}$$

$$\langle m^{(+)} | 0 \rangle = \frac{1}{\sqrt{2}}\left\{ I_{m,0} + (-1)^m I_{-m,0} \right\}$$

$$\langle m^{(-)} | 0 \rangle = \frac{-1}{i\sqrt{2}}\left\{ I_{m,0} - (-1)^m I_{-m,0} \right\}$$

The remaining case is

$$\langle 0 | 0 \rangle = I_{0,0}$$

The necessary evaluation of the residues at higher order poles

to calculate $S^{L\,oo}_{\ell_1 \ell_2}$, differentiation to generate values for (3.50) for $\eta_1, \eta_2 > 0$ and the use of L'Hospital's rule to obtain the limit $\alpha_1 = \alpha_2$ were conveniently performed by means of a program written in the symbolic computing language FORMAC73. The resulting formulas for $I(\vec{R})$ were expressed in FORTRAN notation and compiled for numerical evaluation.

IV. CHAPTER (4)

4.1 LOCAL DENSITY OF STATES

In a system with one-electron energy levels E_n , the density of electronic states is given by

$$\eta(E) = \sum_n \delta(E - E_n) \quad . \tag{4.1}$$

Correspondingly the number of electron states in the energy range (E, E+dE) is counted as n(E)dE. In case each energy level is occupied by two electrons of opposite spins, we multiply the expression (4.1) by two. The summation in (4.1) should be taken either as a sum or as an integral, depending on whether one is dealing with the discrete or continuous part of the spectrum. For a finite system the spectrum is discrete even for the extended states and $\eta(E)$ is strictly a set of delta functions. For a macroscopic system the energy levels corresponding to states not bound to a particular potential form a continuum and $\eta(E)$ is smeared out into a continuous function of E throughout the band. To calculate $\eta(E)$ one can introduce the spectral operator $\rho(E)$ in terms of the energy eigenstates $|\psi_n\rangle$,

$$\rho(E) = \sum_n |\psi_n\rangle \langle\psi_n| \delta(E - E_n) , \tag{4.2}$$

and obtain the trace of this operator in any convenient representation.

The local density of states(LDS), as introduced by Friedel,[1] is given by the diagonal matrix element of the spectral operator in the position representation:

$$\eta(E,\underline{r}) = \langle \underline{r} | \rho(E) | \underline{r} \rangle = \sum_n |\langle \underline{r} | \psi_n \rangle|^2 \delta(E-E_n) . \quad (4.3)$$

The total density of states can be obtained by integrating this local density over the configuration space of $\underline{r}$. The quantity $\eta(E,\underline{r})$ reveals the effect of the local environment on the electronic structure and hence constitutes an important object of study for systems such as surfaces and interfaces, liquid and amorphous metals, semiconductors and alloys, defects and impurities in solids, molecules, microcrystallites and clusters etc. Even when there is perfect crystal symmetry, one may be interested only in the local environment of an atom and use the local density of states to study the properties like the bonding of the atom with its neighbours etc. The local aspect of $\eta(E,\underline{r})$ is aptly described by the so-called invariance theorem (see section (2) of the article by V. Heine in Ref.95). In approximate terms, the theorem states that as long as $\underline{r}$ is a few wavelengths away from the boundary of a cell surrounding this point, $\eta(E,\underline{r})$ does not change appreciably on changing the condition to be satisfied by the wavefunction and its derivative at the cell boundary. Friedel[1] used this theorem to explain several electronic properties in dilute alloys where, for the cell mentioned above, he considered the region occupied by the solvent, excluding the solute atoms. The theorem explains why

several local electronic properties in dilute alloys change less rapidly than linearly in concentration. It explains the local magnetic moments in such systems, e.g., why the average magnetic moment at an Fe site in an Fe_3Al alloy is remarkably close to that in pure Fe.[95,96] For cluster calculations like ours, it suggests that the LDS at a point more than a few wavelengths away from the boundary should be independent of the boundary conditions. For example, the LDS of the diamond Bethe lattice should be similar to the LDS in the diamond structure[97] or the LDS for a cluster with periodic boundary conditions should be similar to that with free(cluster) boundary conditions etc.[98]

4.2 RELATION TO GREEN'S FUNCTION

Eqn.(4.3) relates the local density to the eigenstates of the whole system. Obviously trying to calculate $\eta(E,\underline{r})$ from the eigenstates is an impractical task as this would mean solving for the E_n's and $|\psi_n\rangle$'s first for the entire system. Individual eigenstates refer to the entire system and may be extremely sensitive to small perturbations in the system, whereas the local quantity $\eta(E,\underline{r})$ lacks such sensitivity if $\underline{r}$ is beyond some distance from the perturbation. Hence calculating $\eta(E,\underline{r})$ from the eigenstates is not a good idea even in principle, unless they are easy to obtain as in a periodic solid. An alternative approach is based on the theory of Green's function. We first introduce the resolvent or the Green operator

$$G(E) = (E-H)^{-1} , \qquad (4.4)$$

where H is the one-electron Hamiltonian for the system. In terms of the eigenstates $|\psi_n\rangle$ we have

$$G(E) = \sum_n |\psi_n\rangle\langle\psi_n| / (E-E_n) , \qquad (4.5)$$

where the summation is to be understood as a sum over the discrete spectrum and an integral over the continuous part. Analogous to the local density of states, we define the local Green's function as the diagonal matrix element of G(E) in the position representation, i.e.,

$$G(E,\underline{r},\underline{r}) = G(E,\underline{r},\underline{r}')|_{\underline{r}=\underline{r}'} ,$$

$$G(E,\underline{r},\underline{r}') = \langle\underline{r}|G(E)|\underline{r}'\rangle = \sum_n \langle\underline{r}|\psi_n\rangle\langle\psi_n|\underline{r}'\rangle/(E-E_n) . \qquad (4.6)$$

One can analytically continue this function to the complex plane and define

$$G(z,\underline{r},\underline{r}') = \sum_n \langle\underline{r}|\psi_n\rangle\langle\psi_n|\underline{r}'\rangle/(z-E_n) . \qquad (4.6a)$$

Since the eigenvalues E_n of a hermitian operator H are real, (4.6a) is regular off the real z-axis. The singularities of G(z) lie on the real z-axis, where it has simple poles at the discrete eigenvalues of H and a branch cut coinciding with the continuous spectrum. Actually, in an infinite disordered system part of the continuous spectrum may belong to localised

eigenstates. This part which belongs to the localised states is called the singularly continuous part. In this region, the line of singularities is formed by a dense distribution of poles, but in a finite energy range only a finite number of these have residues larger than any preset small value.[99] The branch cut on the real z-axis coincides with the spectrum of the extended states only. The singularly continuous part belonging to the localised states is referred to as the natural boundary (this term has been used by Economou[100] and Papatriantafillou et al[101] to distinguish it from the branch cut). For this part of the spectrum $\lim_{\varepsilon \to 0^+} G(E \pm i\varepsilon, \underline{r}, \underline{r}')$ does not exist.[100] In the region of the extended states such limits exist , but are unequal. The difference between these two, i.e., the discontinuity across the branch cut is related to LDS (4.3). This can be easily seen from

$$\begin{aligned}
\tilde{G}(E, \underline{r}, \underline{r}) &= \lim_{\varepsilon \to 0^+} \left[G(E + i\varepsilon, \underline{r}, \underline{r}) - G(E - i\varepsilon, \underline{r}, \underline{r}) \right] \\
&= \lim_{\varepsilon \to 0^+} \sum_n |\langle \underline{r} | \psi_n \rangle|^2 \left[\frac{1}{E + i\varepsilon - E_n} - \frac{1}{E - i\varepsilon - E_n} \right] \\
&= -2\pi i \sum_n |\langle \underline{r} | \psi_n \rangle|^2 \delta(E - E_n),
\end{aligned}$$

where we have used the identity

$$\lim_{y \to 0^+} \frac{1}{x \pm iy} = P.\frac{1}{x} \mp i\pi\delta(x).$$

Thus

$$\eta(E, \underline{r}) = -\frac{1}{2\pi i} \tilde{G}(E, \underline{r}, \underline{r}) = \mp \frac{1}{\pi} \mathrm{Im} \{ G^{\pm}(E, \underline{r}, \underline{r}) \}, \tag{4.7}$$

with

$$G^{+} = \lim_{\varepsilon \to 0^{+}} G(E + i\varepsilon, \underline{r}, \underline{r}) ,$$

and

$$G^{-} = \lim_{\varepsilon \to 0^{+}} G(E - i\varepsilon, \underline{r}, \underline{r}) .$$

Thus in order to obtain the LDS one first obtains the Green's function and then utilises eqn. (4.7). The important point is that the Green's function does not have to be evaluated in the eigenfunction representation and one may choose a representation suitable for the problem at hand. However, in all calculations special care has to be taken to see that

1) $G(z, \underline{r}, \underline{r}')$ is regular off the real axis.

2) $G(z, \underline{r}, \underline{r}')$ satisfies the reality condition, which reflects the hermiticity of the Hamiltonian or that the eigenvalues of H are real,

$$G(z, \underline{r}, \underline{r}')^{*} = \sum_{n} \frac{\langle \underline{r}' | \psi_n \rangle \langle \psi_n | \underline{r} \rangle}{z^{*} - E_n} = G(z^{*}, \underline{r}', \underline{r}) \qquad (4.8)$$

3) The imaginary part of $G(z, \underline{r}, \underline{r}')$ is negative for z in the upper half of the complex plane,

$$\mathrm{Im}\, G(z, \underline{r}, \underline{r}') < 0 \quad , \quad \mathrm{Im}\, z > 0 \qquad (4.9)$$

Utilising condition (2) this yields

$$\mathrm{Im}\, G(z, \underline{r}, \underline{r}') > 0 \quad , \quad \mathrm{Im}\, z < 0 .$$

This ensures that the residue of each eigenvalue in (4.6) is positive. This condition is necessary for the positive definiteness of the LDS. A function satisfying conditions (4.9a) and (4.9b) is called a Herglotz function.

4)
$$G_n(z; r, r') \sim z^{-1} \quad (|z| \to \infty) \qquad (4.10)$$

This is true if the spectrum of H has an upper bound, i.e., the branch cut on the real axis is of finite extent, representing bands of finite width.

Green's function satisfying conditions 1) to 3) are called analytic. The condition (4) is a boundary condition and holds for all Hamiltonians represented in a finite basis.

TIGHT-BINDING FORM

In a tight-binding calculation, the eigenstates $|\psi_n\rangle$ are expanded in a basis of localised states $\{|\phi_\alpha\rangle\}$ centered on each atom in the cluster,

$$|\psi_n\rangle = \sum_\alpha C_{n\alpha} |\phi_\alpha\rangle .$$

One then defines the LDS as the density of states(DOS) projected onto a particular localised state $|\phi_o\rangle$, i.e.,

$$\eta_o(E) = \langle\phi_o|\rho(E)|\phi_o\rangle = \sum_n |\langle\phi_o|\psi_n\rangle|^2 \delta(E-E_n)$$
$$= -\lim_{\epsilon\to 0^+} \frac{1}{\pi} \mathrm{Im}\langle\phi_o|G(E+i\epsilon)|\phi_o\rangle \qquad (4.11)$$

Thus, while $\eta(E,\underline{r})$ refers to LDS per unit volume, $\eta_o(E)$ refers to LDS per orbital $\phi_o(\underline{r})$. LDS per atom can be obtained by summing $\eta_o(E)$ for all orbitals centered on a particular site. The total DOS can be obtained by summing the LDS over all orbitals in the cluster (see Appendix (A-2) for further discussion on this point). However, in a small cluster consisting of a few hundreds of atoms, large number of atoms are on or very close to the surface and may be strongly affected by the surface states. Thus it is only from the LDS near the center of the cluster that one can obtain results characteristic of the bulk material and not from the total DOS of the whole cluster. Since in an amorphous system each atom has a slightly different environment, it is necessary to calculate an average over a few atoms, five to ten usually being more than adequate.

4.3 METHODS OF CALCULATIONS

During the last decade several methods for calculating the LDS from eqn. (4.8) have been proposed and developed. The most important are the recursion method , the moments method, the cluster Bethe lattice method and the equation of motion technique. All these methods have been proven useful when the system lacks translational symmetry and the Bloch theorem is not useful. Nearly ten years of experience has revealed that all these techniques yield similar results, though each method has its characteristic advantages as well as limitations. Below we describe the recursion method and the equation of motion

technique and also present a brief discussion of other methods that have been used so far.

4.31 RECURSION METHOD

The recursion method, introduced by Haydock, Heine and Kelly,[98,102] has become increasingly popular because it provides a simple and probably the fastest algorithm to calculate local electronic properties. Detailed account of this method and various related aspects has been provided by Haydock[95,103] (see also articles by Heine and by Kelly in Ref.95). The method is based on the Lanczos method of tridiagonalising a matrix. The local Green's function acquires a continued fraction representation in terms of the elements of the tridiagonalised Hamiltonian matrix and can be calculated recursively with considerable ease. There are several algorithms that carry out the Lanczos[106] tridiagonalisation procedure. Out of these, the recursion method uses the algorithm which has been shown by Paige[104] to yield extremely good results for the eigenvalues of the tridiagonalised matrix (in terms of convergence to the eigenvalues of the original matrix) and to be numerically stable. Below we discuss first the recursion method for a symmetric Hamiltonian matrix and then describe Haydock and Kelly's[105] extension of the method to the case of nonsymmetric matrices.

4.31(a) SYMMETRIC RECURSION IN ORTHOGONAL BASIS

Let $\{|\phi_\alpha\rangle\}$ represent the localised orthonormal basis used to represent the one-electron Hamiltonian H. The Hamiltonian matrix is hermitian in this representation. The new basis which brings this matrix to a tridiagonal or Jacobi form is obtained by a unitary transformation of the original basis. Members of this new basis are obtained iteratively via a three-term recursion relation which guarantees that each new member interacts only with its preceding and following members. For this reason the new basis is said to provide a chain model for the Hamiltonian.

If we denote the new basis set as $\{|u_n\rangle, n = 0, 1, 2, \ldots\ldots\}$, then the first member of the new basis $|u_0\rangle$, is chosen to be the orbital $|\phi_0\rangle$ whose local density is sought. Let us suppose this vector is normalised. The next member of the new basis, $|u_1\rangle$, is obtained by demanding

$$H|u_0\rangle = a_0|u_0\rangle + b_1|u_1\rangle , \qquad (4.12)$$

where a_0 and b_1 are real numbers. To find a_0 and b_1 in (4.12) we take the inner product of both sides with $|u_0\rangle$:

$$\langle u_0|H|u_0\rangle = a_0\langle u_0|u_0\rangle + b_1\langle u_0|u_1\rangle .$$

Since we want the new basis to be orthogonal, we demand

$$\langle u_0|u_1\rangle = 0,$$

and thus

$$a_0 = \langle u_0 | H | u_0 \rangle ,$$

assuming $|u_0\rangle$ to be normalised. Having determined a_0, we write

$$b_1 |u_1\rangle = H|u_0\rangle - a_0|u_0\rangle ,$$

and take the inner product of this vector with itself giving

$$b_1^2 \langle u_1 | u_1 \rangle = \langle u_0 | (H - a_0)^+ (H - a_0) | u_0 \rangle .$$

We demand

$$\langle u_1 | u_1 \rangle = 1 ,$$

and take b_1 as the positive square root of

$$b_1^2 = \langle u_0 | (H - a_0)^+ (H - a_0) | u_0 \rangle .$$

We now obtain $|u_1\rangle$ as

$$|u_1\rangle = (H - a_0)|u_0\rangle / b_1 .$$

Thus by construction $|u_1\rangle$ is normalised to unity and is orthogonal to $|u_0\rangle$.

To obtain the subsequent vectors in the new basis or the chain, we use a three-term recursion relation

$$H|u_n\rangle = a_n|u_n\rangle + b_{n+1}|u_{n+1}\rangle + b_n|u_{n-1}\rangle \quad , \quad n \geq 1 . \tag{4.13}$$

Consider the case n=1, i.e.,

$$H|u_1\rangle = a_1|u_1\rangle + b_2|u_2\rangle + b_1|u_0\rangle .$$

Taking the inner product of both sides with $|u_1\rangle$ and demanding

$$\langle u_1 | u_2 \rangle = 0 ,$$

we have

$$a_1 = \langle u_1 | H | u_1 \rangle ,$$

since $\langle u_1 | u_0 \rangle$ vanishes by construction. As before, we write

$$b_2^2 = \left[\langle u_1 | (H - a_1)^+ - \langle u_0 | b_1 \right] \left[(H - a_1)|u_1\rangle - b_1|u_0\rangle \right] , \tag{4.14}$$

using $\langle u_2 | u_2 \rangle = 1$

We take b_2 as the positive square root of b_2^2 and write

$$|u_2\rangle = (H - a_1)|u_1\rangle - b_1|u_0\rangle / b_2 \tag{4.15}$$

so that $|u_2\rangle$ is normalised to unity and is orthogonal to $|u_1\rangle$ and $|u_0\rangle$, where the last result follows by using

$$b_1 = \langle u_0 | H | u_1 \rangle ,$$

which follows from using the self-adjointness of H. It is easy to see that

$$b_1 = \langle u_0 | H | u_1 \rangle = \langle u_1 | H | u_0 \rangle . \qquad (4.16)$$

The higher order co-efficients a_n and b_n and the chain states are obtained by following the above prescription. In genaral

$$a_n = \langle u_n | H | u_n \rangle , \qquad (4.17)$$

$$b_{n+1}^2 = \left[\langle u_n | (H - a_n)^+ - \langle u_{n-1} | b_n \right] \left[(H - a_n) | u_n \rangle - b_n | u_{n-1} \rangle \right] , \qquad (4.18)$$

$$| u_{n+1} \rangle = (H - a_n) | u_n \rangle - b_n | u_{n-1} \rangle / b_{n+1} , \qquad (4.19)$$

where b_{n+1} is the positive square root of b_{n+1}^2 . In the basis $\{ | u_n \rangle \}$,

$$\langle u_n | H | u_n \rangle = a_n , \quad \langle u_{n-1} | H | u_n \rangle = \langle u_{n-1} | H | u_n \rangle = b_n ,$$

$$\langle u_n | H | u_m \rangle = 0 \quad , \; |n - m| > 1 ,$$

i.e., the matrix H is tridiagonalised and is symmetric about the line of the diagonal elements. It should be noticed that b_n^2 , being the inner product of a vector with itself is always positive.

By construction $|u_{n+1}\rangle$ is normalised to unity and orthogonal to $|u_n\rangle$ and $|u_{n-1}\rangle$. It is also orthogonal to $|u_{n-2}\rangle, |u_{n-3}\rangle, \ldots\ldots\ldots$, i.e., all the previous states in the chain. To see this, we take the inner product of both sides of (4.13) with $|u_{n-2}\rangle$ to obtain

$$b_{n+1} \langle u_{n-2} | u_{n+1} \rangle = \langle u_{n-2} | H | u_n \rangle .$$

since $\langle u_{n-2} | u_n \rangle$ and $\langle u_{n-2} | u_{n-1} \rangle$ vanish by construction. Thus

$$b_{n+1} \langle u_{n-2} | u_{n+1} \rangle = \langle u_n | H | u_{n-2} \rangle^*$$

$$= a_{n-2} \langle u_n | u_{n-2} \rangle^* + b_{n-1} \langle u_n | u_{n-1} \rangle^* + b_{n-2} \langle u_n | u_{n-2} \rangle^* .$$

Each term on the right hand side of this eqn. vanishes by construction, showing the orthogonality of $|u_{n+1}\rangle$ and $|u_{n-2}\rangle$.

This argument can be extended down the chain to show the orthogonality of $|u_{n+1}\rangle$ to all the previous states in the chain.

The transformation terminates when b_{n+1}^2 in (4.18) is zero. Since b_{n+1}^2 is the inner product of a vector with itself, this can happen only when the new vector $(H - a_n)|u_n\rangle - b_n |u_{n-1}\rangle$ is zero. In practice, there is a cumulative decay of orthogonality in the chain due to rounding error. Hence for a N dimensional matrix H, b_N may be small but nonzero, and the chain continues producing multiple eigenvalues for each eigenvalue of the original matrix. However, in order to

calculate the local DOS one needs to calculate only a small number of co-efficients and thus, in practice, we terminate the chain long before all degrees of freedom have been exhausted. The cumulative loss of orthogonality does not pose any problem until linear independence of chain states is lost. Although nonorthogonality accumulates, eigenvalues remain accurate to a single rounding error, provided the co-efficients a_n and b_n are calculated by the algorithm discussed above. This point has been discussed in detail by Haydock (refernce 95).

4.3(1b) NONSYMMETRIC RECURSION

In general the Hamiltonian matrix $[D_{\alpha\beta}]$ is nonhermitian or nonsymmetric. We recall that in the Anderson-Bullett scheme discussed in section (3.1), $D_{\alpha\beta}$ is given by eqn. (3.37), which is different from $D_{\beta\alpha}$ if the orbitals ϕ_α and ϕ_β are geometrically inequivalent. The algorithm discussed in the previous section assumes $\langle u_n | H = (H|u_n\rangle)^+$ for evaluating the inner product $b_{n+1}^2 \langle u_{n+1} | u_{n+1}\rangle$. If H is nonhermitian, the left and the right eigenvectors of H are different. In the chain model, this results in the left and the right chain states being different. Haydock and Kelly,[105] therefore used a two sided recursion algorithm based on Wilkinson's[106] description of the unsymmetric Lanczos method. They generate a biorthogonal sequence of vectors $\{|u_n\rangle\}$ and $\{|v_n\rangle\}$ by means of two three term recursion relations

$$b_{n+1}\,|u_{n+1}\rangle = (H - a_n)\,|u_n\rangle - b_n\,|u_{n-1}\rangle, \quad (4.20)$$

$$b_{n+1}\,|v_{n+1}\rangle = (H^{+} - a_n)\,|v_n\rangle - b_n\,|v_{n-1}\rangle, \quad (4.21)$$

where

$$\langle v_m | u_n \rangle = \delta_{mn},$$

and $$|u_0\rangle = |v_0\rangle,$$

the orbital whose local density is sought. The co-efficients a_n and b_{n+1} are now given by

$$a_n = \langle v_n | H | u_n \rangle = \langle u_n | H^{+} | v_n \rangle, \quad (4.22)$$

$$b_{n+1}^{2} = \frac{\left[(H^{+} - a_n)\,|v_n\rangle - b_n\,|v_{n-1}\rangle\right]^{+}\left[(H - a_n)\,|u_n\rangle - b_n\,|u_{n-1}\rangle\right]}{\langle v_n | u_n \rangle}. \quad (4.23)$$

Though the storage and time requirements are doubled, this still provides a fast algorithm to tridiagonalise the nonsymmetric Hamiltonian matrix. An important point to note is that b_{n+1}^{2} is no longer given by the inner product of a vector with itself and hence it can be negative. This may lead to complex eigenvalues and a negative DOS. If this occurs, the chain has to be terminated at that point.

4.31(c) LDS IN TERMS OF THE RECURSION CO-EFFICIENTS

In terms of the elements a_n and b_n of the tridiagonalised matrix, the local Green's function acquires a continued fraction representation:

$$G_0(E) = \langle u_0 | G(E) | u_0 \rangle$$

$$= \cfrac{1}{E - a_0 - \cfrac{b_1^2}{E - a_1 - \cfrac{b_2^2}{E - a_2 - b_3^2 \ \cdots\cdots}}} \qquad (4.24)$$

The derivation is simple and has been provided by Haydock, Heine and Kelly[98] (see also Heine, Ref. 95, p90 and Haydock, ibid., p252). Expression (4.24), even when truncated at a finite level, satisfies all the analyticity conditions for $G_0(E)$ discussed in section (4.2), provided a_n are real and b_n^2 are positive.

In practice, one computes only a finite number of co-efficients a_n and b_n and tries to approximate the remaining co-efficients. In case the co-efficients are not rapidly convergent or show oscillatory behaviour, one simply sets the remaining recursion co-efficients to zero. This truncation as well as the finiteness of the cluster causes the LDS to be strictly a set of delta functions. To obtain a smooth LDS curve one evaluates

$$\eta_0(E) = -\frac{1}{\pi} \operatorname{Im} G_0(E + i\varepsilon) \qquad (4.25)$$

for a small but positive ϵ, thus broadening the delta functions into Lorentzians. This method obscures details within an energy range of ϵ. Also the resulting LDS has blurred band edges and ripples from the poles. However, if one has sufficiently large number of delta functions, these effects are small.

An alternative method, implemented in the subroutine RECTAB of the Cambridge Recursion Library,[107] is based on the differentiation of the mean of the upper and lower limits to the integrated density of states. Details of this method have been discussed by Haydock (Ref. 95, p257) and Kelly (same Ref., p315).

For calculations involving an isolated band in a periodic solid (i.e., only one type of orbital per site), the co-efficients a_n and b_n settle down quickly to asymptotic values (a_∞, b_∞),[102,108] where a_∞ provides the center of the band and b_∞ determines the band width. In this case, one can analytically evaluate the remainder of the continued fraction (4.24) for $n > N$ with $a_n = a_\infty$ and $b_n = b_\infty$, and thus $G_0(E)$ can be obtained exactly.

When the co-efficients a_n, b_n do not show any signs of settling to some asymptotic values, as is the case in most applications, one has to decide about the number of co-efficients to be considered. Actually $G_0(E)$ is not sensitive to a_n, b_n for large n if the state $|b_0\rangle$ is localised, and often a fairly small number ($\sim$30) is sufficient to obtain a good approximation to $G_0(E)$. In any case one can decide as to where to terminate the chain, simply by studying

the variation in the LDS with increasing number of co-efficients. Certain rules of thumb to help one decide about this number have been discussed by Heine and Haydock.[95]

4.32 EQUATION OF MOTION METHOD

Equation of motion method was first used by Alben et al[109] to calculate the eletronic DOS in model disordered alloys. Beeman and Alben[110] used it to calculate the vibrational DOS in model amorphous semiconductors. Later Weaire and Williams applied this method to study localisation in the Anderson model of a disordered Hamiltonian.[111]

In this method one carries out a step by step numerical solution of the Schrodinger equation for the one-electron wavefunction. Suppose at time t=0, the electron is in a state $|\xi_0\rangle$, which has the form:

$$|\xi_0\rangle = \sum_\alpha a_\alpha(0)\,|\phi_\alpha\rangle \quad , \qquad (4.26)$$

where $\{|\phi_\alpha\rangle\}$ represents the localised basis. The state function $|\xi_t\rangle$ at time t satisfies the Schrödinger equation

$$\frac{\partial}{\partial t}|\xi_t\rangle = -i/\hbar\, H\,|\xi_t\rangle, \qquad (4.27)$$

where H is the one-electron Hamiltonian. Writing

$$|\xi_t\rangle = \sum_\alpha a_\alpha(t)\,|\phi_\alpha\rangle \quad , \qquad (4.28)$$

eqn.(4.27) is transformed into

$$\sum_{\alpha}\left[\frac{\partial}{\partial t}\left(a_{\alpha}(t)\right)\right]|\phi_{\alpha}\rangle = -i/\hbar \sum_{\alpha} a_{\alpha}(t)\, H|\phi_{\alpha}\rangle . \tag{4.29}$$

If the basis is orthogonal, then

$$H|\phi_{\alpha}\rangle = \sum_{\beta} H_{\beta\alpha}|\phi_{\beta}\rangle , \tag{4.30}$$

where $H_{\beta\alpha}$ represent the matrix elements of the Hamiltonian, i.e.,

$$H_{\beta\alpha} = \langle\phi_{\beta}|H|\phi_{\alpha}\rangle . \tag{4.31}$$

If the basis is nonorthogonal, then

$$H|\phi_{\alpha}\rangle = \sum_{\beta} D_{\beta\alpha}|\phi_{\beta}\rangle ; \tag{4.32}$$

where

$$D_{\beta\alpha} = \left(S^{-1}H\right)_{\beta\alpha} . \tag{4.33}$$

Using (4.32) in eqn.(4.29), we have

$$\sum_{\alpha}\left[\frac{\partial}{\partial t}\left(a_{\alpha}(t)\right)\right]|\phi_{\alpha}\rangle = -i/\hbar \sum_{\alpha\beta} D_{\beta\alpha}\, a_{\alpha}(t)|\phi_{\beta}\rangle . \tag{4.34}$$

Using the linear independence of the set $\{|\phi_{\alpha}\rangle\}$, we obtain

$$\frac{\partial}{\partial t} a_{\alpha}(t) = -i/\hbar \sum_{\gamma} D_{\alpha\gamma}\, a_{\gamma}(t) . \tag{4.35}$$

This equation can be solved numerically for a given set of $a_{\alpha}(0)$'s, i.e., amplitudes of the initial state of the electron on various basis vectors. Often one chooses the initial

state to be a particular basis state, i.e.,

$$a_\alpha(0) = \delta_{\alpha\mu} \,. \tag{4.36}$$

Knowing all $a_\alpha(t)$'s , we can obtain $|\xi_t\rangle$. To obtain the local DOS we write the formal solution of eqn. (4.27) as

$$|\xi_t\rangle = e^{-i/\hbar Ht}|\xi_0\rangle = \sum_n e^{-i/\hbar E_n t}|\psi_n\rangle\langle\psi_n|\xi_0\rangle,$$

where E_n and $|\psi_n\rangle$ are the eigenvalues and the eigenvectors of H. Thus

$$\langle\xi_0|\xi_t\rangle = \sum_n |\langle\psi_n|\xi_0\rangle|^2 e^{-i/\hbar E_n t} \,. \tag{4.37}$$

The local DOS is given by

$$\begin{aligned}
\eta_{\xi_0}(E) &= \sum_n |\langle\psi_n|\xi_0\rangle|^2 \delta(E-E_n) \\
&= \sum_n |\langle\psi_n|\xi_0\rangle|^2 \cdot \frac{1}{2\pi} \cdot \int_{-\infty}^{+\infty} e^{i(E-E_n)t}\, dt \\
&= \sum_n |\langle\psi_n|\xi_0\rangle|^2 \cdot \frac{1}{\pi} \, Re \int_0^{\infty} e^{i(E-E_n)t}\, dt
\end{aligned}$$

Using (4.37) we obtain

$$\eta_{\xi_0}(E) = \frac{1}{\pi} \, Re \int_0^{\infty} \langle\xi_0|\xi_t\rangle \, e^{iEt}\, dt \tag{4.38}$$

The expressions (4.26) and (4.28) yield $\eta_{\xi_0}(E)$ in terms of the amplitudes $a_\alpha(t)$,

$$\eta_{\xi_0}(E) = \frac{1}{\pi} \, Re \int_0^{\infty} \Big[\sum_{\beta\alpha} a_\beta^*(0) \, S_{\beta\alpha} \, a_\alpha(t) \Big] e^{iEt}\, dt \tag{4.39}$$

Particular simplifications occur when the basis is orthogonal and the initial amplitudes satisfy(4.36). Then eqn.(4.39) yields

$$\eta_{\xi_0}(E) = \eta_{\phi_\mu}(E) = \frac{1}{\pi} Re \int_0^\infty a_\mu(t)\, e^{iEt}\, dt \qquad (4.40)$$

while the equation to be solved is

$$\frac{d}{dt} a_\mu(t) = -\frac{i}{\hbar} \sum_\gamma H_{\mu\gamma}\, a_\gamma(t), \qquad (4.41)$$

with the initial conditions being given by (4.36). For a finite system, (4.40) is strictly a set of delta functions and to obtain a smooth LDS, we add a small but positive imaginary part ϵ to E as is done even in the time independent approach described in section (4.31). Thus LDS is calculated from

$$\eta_{\phi_\mu}(E) = \frac{1}{\pi} Re \int_0^\infty a_\mu(t)\, e^{iEt}\, e^{-\epsilon t}\, dt \qquad (4.40a)$$

The term $e^{-\epsilon t}$ acts as a convergence factor for the integral.

4.33 OTHER METHODS

Various other methods are available for calculating the LDS. The most widely used one is the method of moments,[112-114] where one calculates various power moments μ_n^α of the LDS:

$$\mu_n^\alpha = \langle \phi_\alpha | H^n | \phi_\alpha \rangle = \sum_i E_i^n |\langle \psi_i | \phi_\alpha \rangle|^2$$

$$= \sum_i |\langle \psi_i | \phi_\alpha \rangle|^2 \int_{-\infty}^{+\infty} \delta(E - E_i)\, E^n\, dE = \int_{-\infty}^{+\infty} E^n \eta_\alpha(E)\, dE . \qquad (4.42)$$

In principle, if one knows all the moments, then one can calculate the characteristic function

$$F(x) = \sum_{n=0}^{\infty} \frac{(ix)^n}{n!} \mu_n^\alpha ,$$

and obtain the LDS as the Fourier transform of $F(x)$:

$$\eta_\alpha(E) = \int_{-\infty}^{+\infty} e^{ixE} F(x)\, dx .$$

In practice, one calculates only a finite number of moments using eqn. (4.42) and tries to extract $\eta_\alpha(E)$ from them. Initial attempts in this regard lay in identifying $\eta_\alpha(E)$ with a function $f(E, \lambda_1, \lambda_2 \cdots \lambda_n)$, where $\lambda_1, \ldots \lambda_n$ were adjustable parameters to fit the first n moments of $\eta_\alpha(E)$.[112,113] Later on, a continued fraction method was developed, where the Hilbert transform of $\eta_\alpha(E)$ was expressed as[114]

$$R(z) = \int_{-\infty}^{+\infty} \frac{\eta_\alpha(E)\, dE}{z - E} = \sum_{n=0}^{\infty} \mu_n / z^{n+1}$$

$$= \cfrac{1}{z - c_1 - \cfrac{d_1}{z - c_2 - \cfrac{d_2}{z - c_3 - d_3 \cdots}}} \qquad (4.43)$$

The co-efficients C_i, d_i involve determinants constructed from the moments. In this form, this method is very similar to the recursion method discussed earlier. However, this method is not numerically as stable as the recursion method. Interrelations between these two methods have been discussed by Haydock, Heine and Kelly.[102]

Another useful approach in the study of electronic structure in disordered systems has been based on the cluster-Bethe lattice method.[115-118] The method involves treating part of an infinite connected network of atoms exactly as a cluster, and representing the effects of the rest of the environment by connecting a Bethe lattice (of the same co-ordination number as the cluster) to the surface of the cluster. The Bethe lattice (or the Cayley tree) is a lattice in which any closed loop of sequential bond is forbidden. The reasons for using the Bethe lattice as a boundary condition are threefold. First of all, the equations involving the Green's function at different sites can be solved exactly. Also attaching the Bethe lattice preserves the connectivity of the system. And finally, the DOS of the Bethe lattice is smooth and featureless. Hence, any structure found in the local density of states at the central atom is essentially determined by the local environment of this atom. A detailed discussion and review on this method has been provided by Joannopoulos and Cohen.[119]

Recently Lambin and Gaspard have used the idea of generalised moments[108]

$$\mu_{2K-1}^{\alpha} = \int_{-\infty}^{+\infty} P_K(E)\, P_{K-1}(E)\, \eta_{\alpha}(E)\, dE$$

to calculate the continued fraction co-efficients C_i, d_i in (4.43). Here $P_n(E)$ is a polynomial of degree n in E. This method is claimed to offer greater numerical stability than the power moment method.

An interesting method that has been used to study the excitations in disordered systems is based on the renormalisation group or the decimation approach. Da Silva and Koiller have used the method to calculate local density of phonon states in a disordered linear chain,[120] while Aoki has used this technique to calculate the electronic DOS and study Anderson localisation in a square lattice.[121]

V. CHAPTER (5)

COMPARISON OF RESULTS OBTAINED BY THE RECURSION METHOD AND THE EQUATION OF MOTION TECHNIQUE

To compare the local DOS obtained by the recursion and the equation of motion methods, calculations were performed on small clusters of 125 atoms representing bcc, amorphous and liquid iron. The reason for choosing such small clusters is the comparatively large computation time required by the equation of motion method. The liquid and amorphous clusters were obtained by the Monte Carlo technique as discussed in section (2.2). The pair distribution functions for these clusters are shown in Figs.(3) and (4). These clusters were of cubic shape.

The Hamiltonian matrices used in these calculations were obtained by following the empirical LCAO scheme described in section (3.3). The band structure for bcc iron obtained under this scheme is displayed in Fig.(8). The parameters obtained by fitting to this band structure were used to calculate the elements of the Hamiltonian matrices for various clusters, as functions of actual interatomic separations. The Hamiltonian matrices, thus generated, were symmetric. Thus for calculating the LDS by the recursion method, we used the symmetric version discussed in section (4.31a). Calculations for the LDS by the equation of motion method were performed by solving eqn.(4.41),

instead of (4.35), i.e., the basis was assumed orthonormal, despite the fact that the transfer matrix elements were obtained from the Slater type orbitals centered at the atomic sites and these orbitals have nonzero overlap. We note that the Slater type orbitals simply provide a means of directly parameterising the matrix elements and do not represent the basis orbitals. In all calculations, the results were obtained by applying the free condition to the respective clusters, i.e., the interaction of the atoms at the surface with the medium surrounding the cluster was set equal to zero.

In the equation of motion method, one has to carry out the numerical integration of the Schrödinger equation, i.e., solve an initial value problem of the type (see eqns.(4.35) and (4.41))

$$dy_i/dx = f_i(y_1, \ldots y_N)$$

$$y_i(0) = y_{i0} \quad , i = 1, 2, \ldots N \qquad (5.1)$$

where N is the total number of orbitals in the cluster. Since there are several numerical methods available for solving such problems, one has to find out whether there is any advantage in choosing a particular method over the others. In particular, one may be interested in saving on computation time by using sophisticated methods with larger step size. We carried out some preliminary calculations of LDS for a simple cubic cluster with

random on-site potentials and constant nearest neighbor interaction. We used the fifth order Runge-Kutta method[122,123] and the extrapolation method of Bulirsch and Stoer[124-126] for solving the system of equations (4.41) with the initial conditions (4.36). The results obtained by these two methods for a given step size were very similar. However, it was also found that similar results could be obtained in somewhat less time by using the simplest one-step method (known as the 'polygon method' of Euler[127]) with smaller step size. In this method the approximations η_i to the solutions $y_i = y(x_i)$ of a differential equation

$$dy/dx = f(x,y) \quad , \quad y(x_0) = y_0 \qquad (5.2)$$

are given by

$$\eta_0 = y_0 \qquad (5.3)$$

$$\eta_{i+1} = \eta_i + h\, f(x_i, \eta_i) \quad , \quad x_{i+1} = x_i + h$$

$$i = 0, 1, 2, \ldots \qquad (5.4)$$

Thus though the sophisticated methods allowed us to use a larger step size h, the simple prescriptions (5.3), (5.4) yielded similar results in less time provided a sufficiently small h was chosen. Hence, in our subsequent calculations of the LDS in the

clusters representing the various phases of iron, we decided to use the prescriptions (5.2),(5.3) with sufficiently small step size. Supposing that over such small steps in time the variation in the integrand of (4.40) would be linear, we employed the simple mid-point integration rule to obtain the Fourier transform $\eta_{\phi_\mu}(E)$. The Fourier transform and the solution to the Schrödinger equation were carried out simultaneously, i.e., at every step of the calculation we obtained an approximate solution to the Schrödinger equation (4.41) and then calculated the contribution to the Fourier integral (4.40).

In Figs.(9-14) we display the LDS obtained by the two methods for various clusters. For each cluster the LDS was calculated at a site near its center. For the recursion method, fifty recursion co-efficients were found sufficient to calculate the LDS, i.e., increasing the number of co-efficients beyond this point did not bring in new features in the LDS. The value for the imaginary part of the energy ε, which broadens the delta functions into Lorentzians was chosen to be 0.025 Ryd. The same value of ε was used in the equation of motion method to calculate the Fourier transform (4.40a). The step size of integration was chosen as 0.04 and sixteen hundred integration steps were used, bringing the upper limit of integration in (4.40a) to 64. The choice of this upper limit depends on several factors. It should actually depend on the inverse of the spacing between the eigenvalues. In practice, one chooses this limit depending on the broadening parameter ε. Another criterion to

follow is the variation of the Green's function with time. For an infinite system, the amplitude $a_\mu(t)$ or the local Green's function slowly decays to zero as the electron diffuses away from the initial localised orbital. However, for a finite cluster the local Green's function decays for some time and then starts rising due to reflections from the boundary.[ψ] The bigger the cluster, the longer the time before such a reversal in the variation of the local Green's function will take place. To avoid the contribution from the boundary one should follow the time evolution of the Green's function and truncate the integral in (4.40) at a time where it has become negligible. In our calculations, this criterion was combined with the additional condition that the results for the LDS should converge to those obtained by the recursion method. Thus we first obtained the LDS by the recursion method and then adjusted the step size h and the upper limit of integration T in the equation of motion method till we converged to these results. As can be seen in Figs. (9-14), this convergence is really good except at low energies where the effects of truncating the Fourier integral in the equation of motion method appear as oscillations in the LDS. Actually, truncating the integral at a lower time causes parts of the LDS at low E to become negative.

[ψ] Certain shapes of the boundary may be preferable to others to avoid a coherent superposition of the reflected waves at the central site. For example, for a simple cubic s band, a cubic shape is preferable to a spherical or octahedral one (see Heine, Ref. 95, page 75).

We will only briefly discuss the nature of the LDS for various clusters obtained in these calculations, as the emphasis in the present discussion is on the comparison of the results obtained by the two methods. Each of the Figs. (9-14) shows the LDS calculated at a single site chosen near the center of the corresponding cluster. For the d states in the bcc cluster, the LDS has a double peaked structure. However, the gap between the two peaks is not as pronounced as expected for the d states in a conventional bcc transition metal. This is a reflection on the corresponding band structure shown in Fig. (8), rather than the smallness of the cluster. The shape of this LDS curve, as we will see in the next chapter, remains essentially unchanged when the calculations are carried out on a bigger cluster. For the amorphous cluster, the small peak at lower energy changes to a shoulder, while it is smoothed further in the liquid. The maximum in the LDS for the amorphous cluster is lower than that for the bcc cluster. For the liquid cluster this maximum (Fig. 14) is higher than that in the amorphous cluster (fig. 12). However, this result is true only for the particular site where the LDS has been calculated. On the average the LDS for the liquid cluster has a lower maximum than the amorphous. The LDS for the s states in the amorphous and the bcc clusters is double peaked. This is also true in general for the liquid cluster. The deviation from this structure in Fig. (13) is typical of the particular site only. The peak near the top of the s band in the average DOS for the liquid is somewhat broader than that in the

amorphous cluster. Since we will come back to a detailed discussion on these points in the next chapter, we end the present discussion with the note that the convergence between the results obtained by the equation of motion and the recursion methods is remarkable and as far as resolving the structure in the LDS is concerned, both methods are equally good.

FIGURE CAPTIONS

FIG.(9-14).

Comparison of results for the LDS calculated by the recursion method and the equation of motion technique, in clusters of 125 atoms representing bcc, amorphous and liquid Fe. The vertical axis is labelled in states/Ryd./atom. The curves have been obtained by adding an imaginary part = 0.02 Ryd. to the energy.

DENSITY OF S STATES IN BCC Fe

FIG. (9)

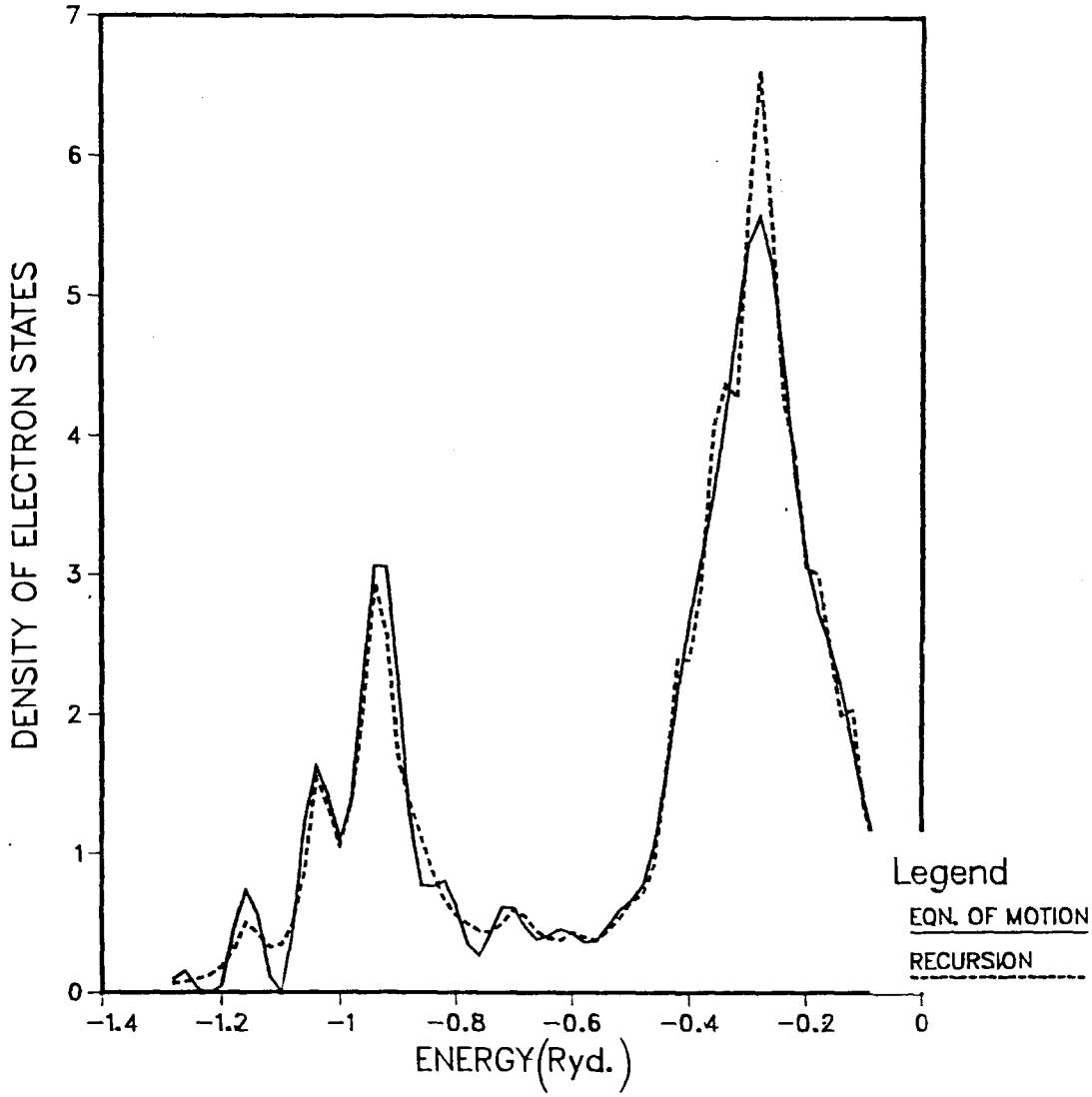

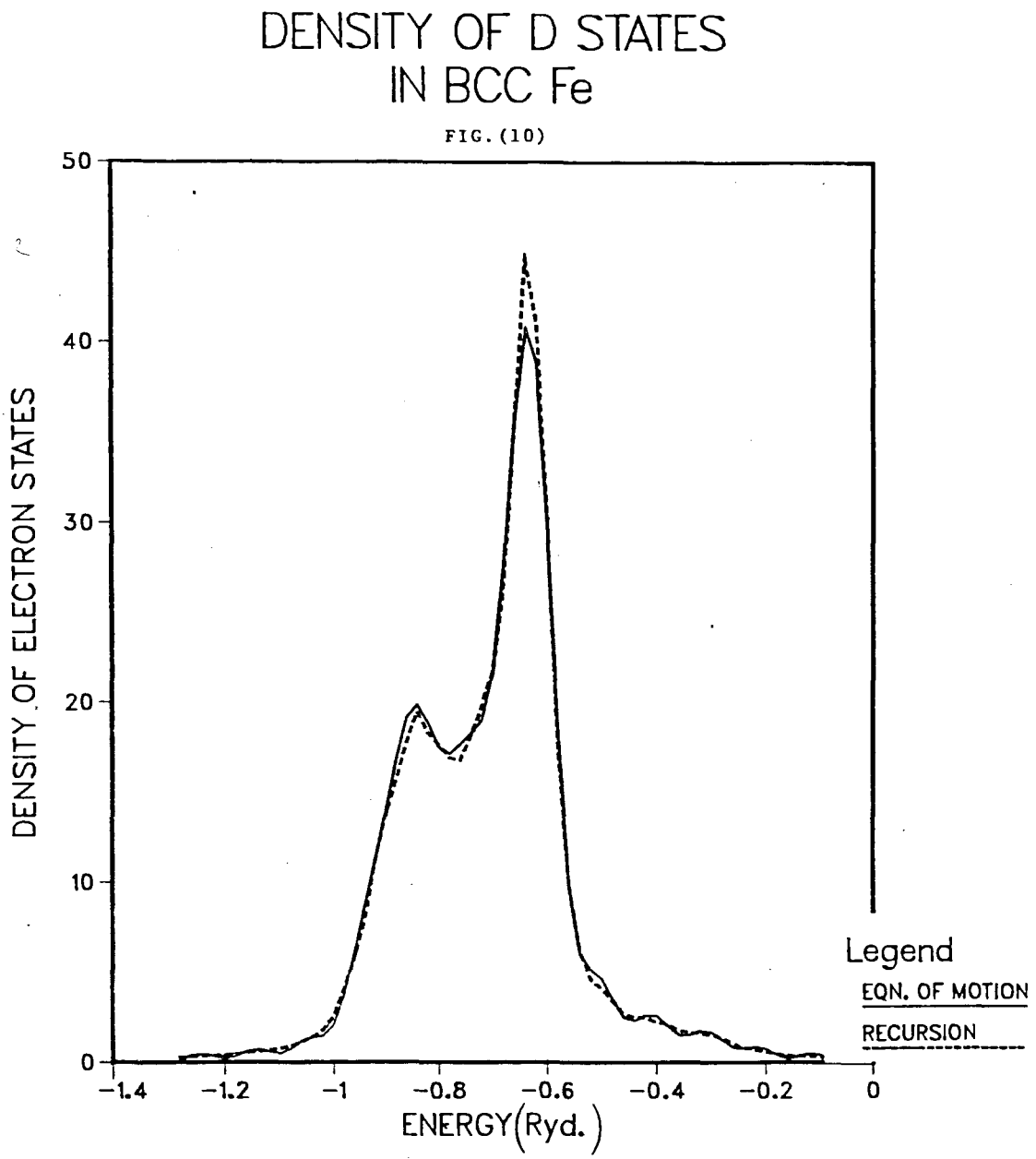
DENSITY OF D STATES
IN BCC Fe
FIG. (10)
DENSITY OF ELECTRON STATES
50
40
30
20
10
0
−1.4
−1.2
−1
−0.8
−0.6
−0.4
−0.2
0
ENERGY(Ryd.)
Legend
EQN. OF MOTION
RECURSION

DENSITY OF S STATES IN AMORPHOUS Fe

FIG. (11)

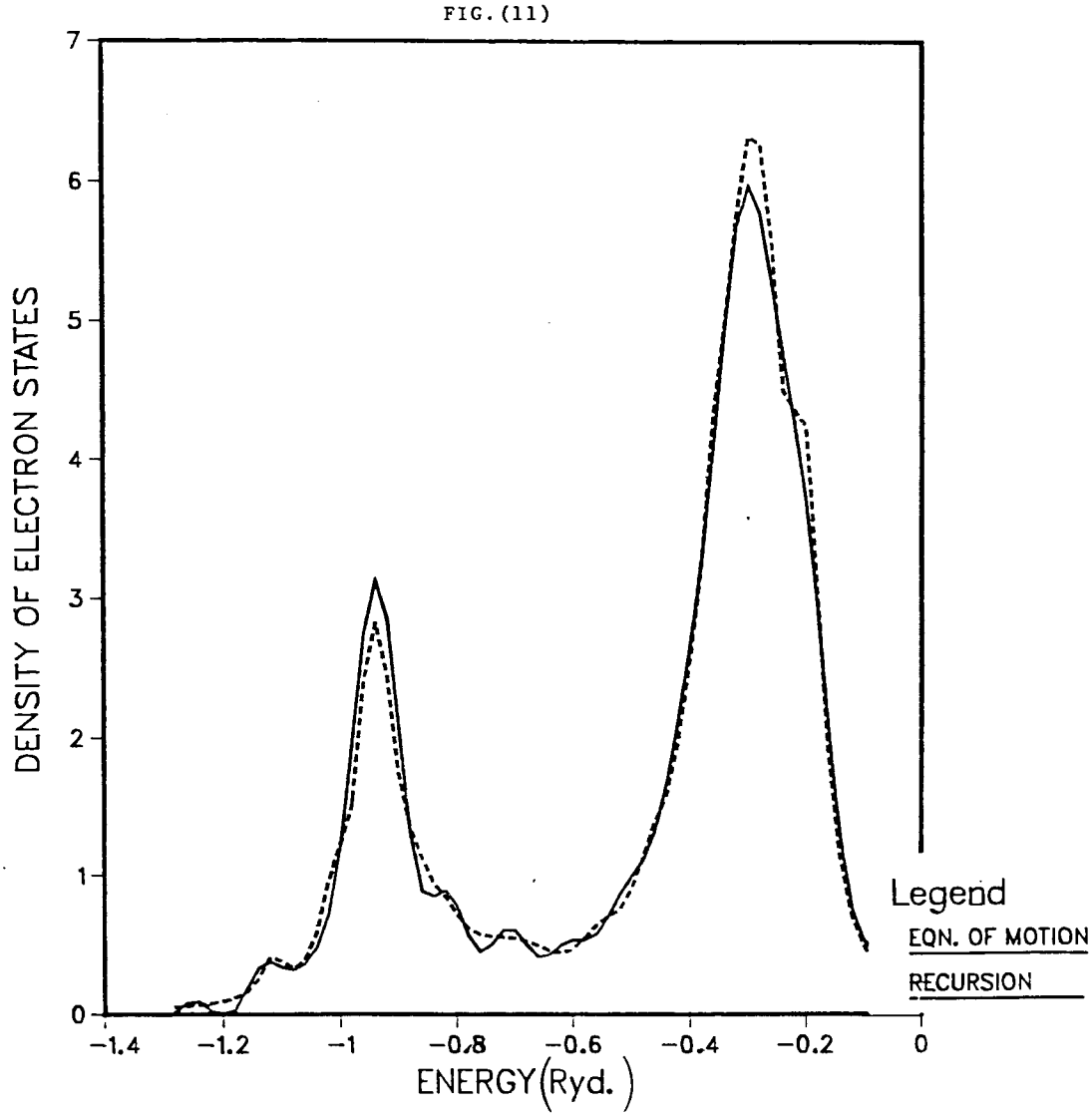

DENSITY OF D STATES IN AMORPHOUS Fe

FIG. (12)

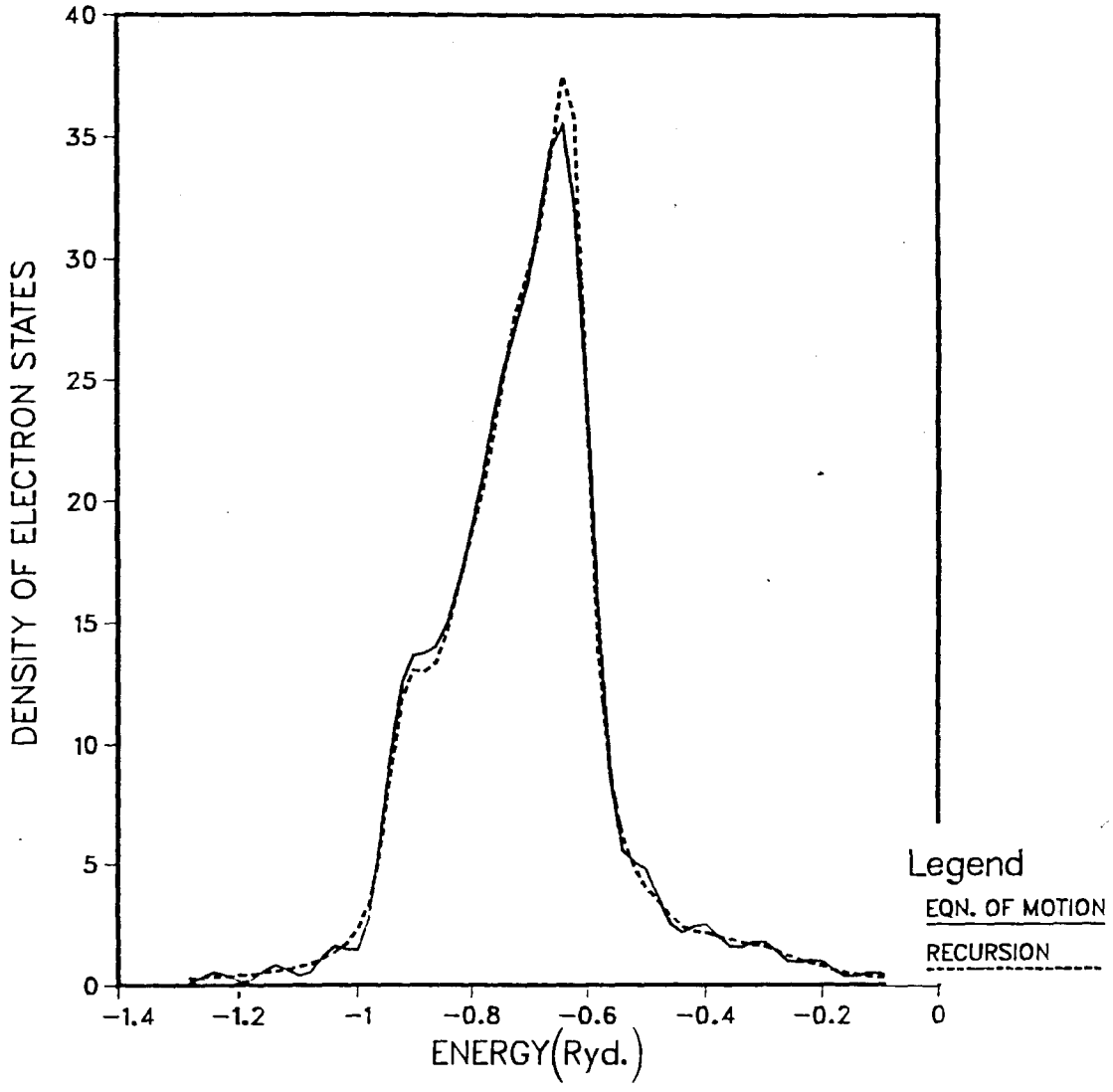

DENSITY OF S STATES IN LIQUID Fe

FIG. (13)

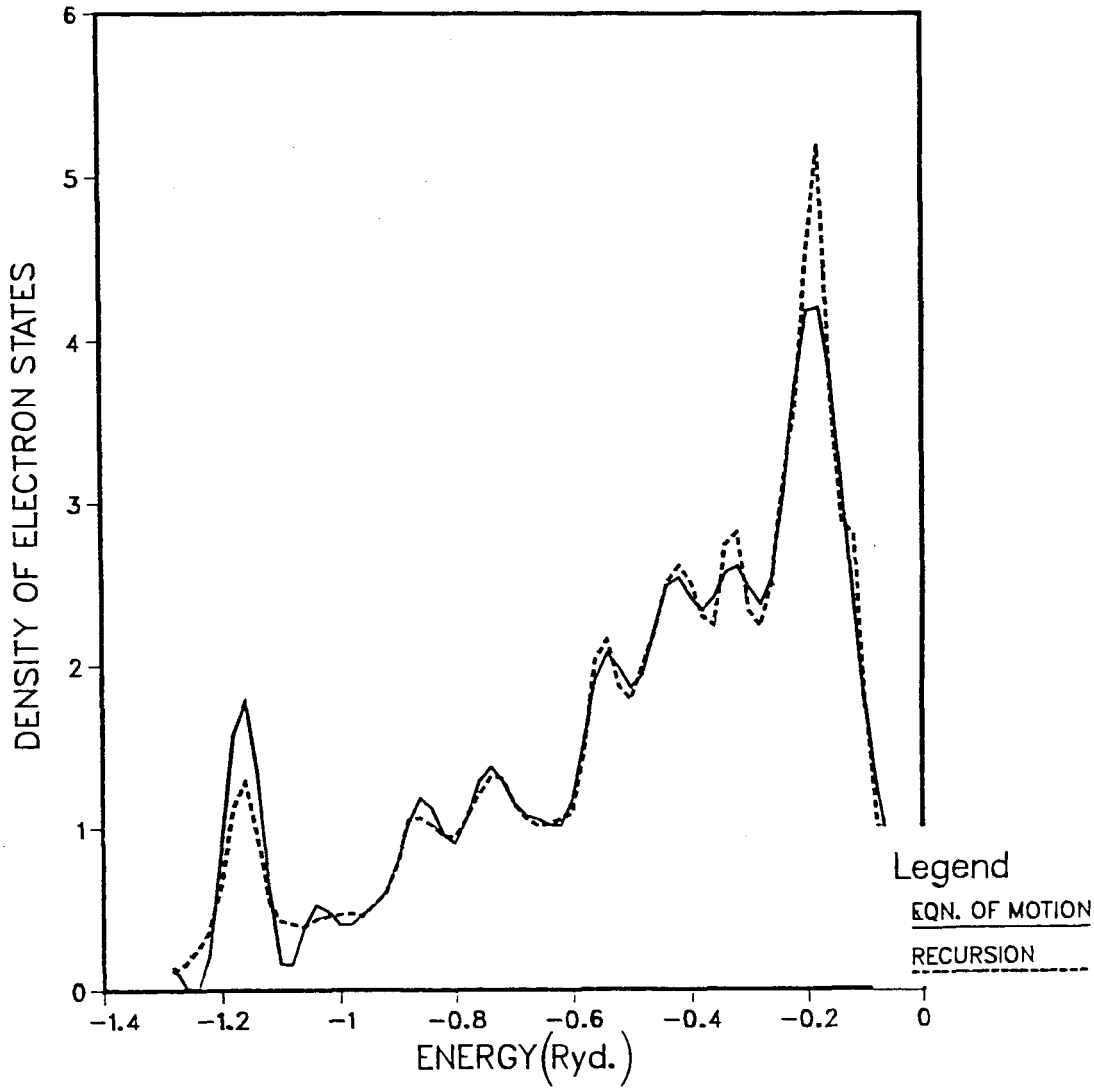

DENSITY OF D STATES IN LIQUID Fe

FIG. (14)

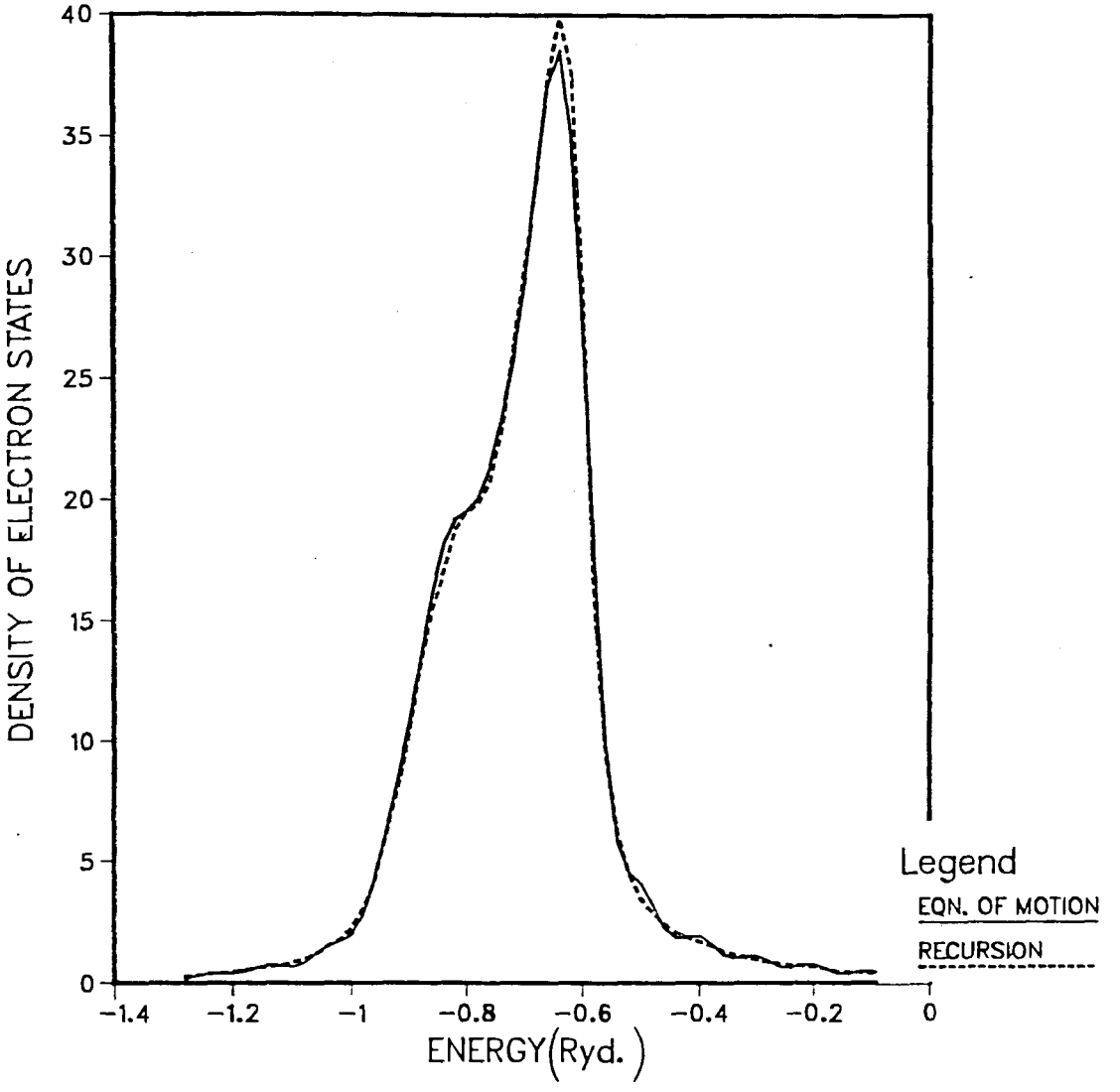

The important difference between the two methods lies in the computation time required by them. While the recursion method provides a fast algorithm to calculate the LDS, the equation of motion technique demands careful integration with sufficiently small step size, requiring large computation time. For clusters with 125 atoms and six orbitals per atom, the time required by the equation of motion method was approximately 42 times larger than the recursion method, where 50 recursion co-efficients were calculated. In the recursion method the time required to calculate the LDS (sampled at a given number of energy points) depends on the length of the chain (the number of co-efficients) and the system size (total number of orbitals in the cluster). If the state for which the LDS is sought is well localised, then only a modest number of co-efficients(30) are needed and this makes it an efficient method to calculate the LDS as well as any local properties depending on this quantity. In the equation of motion method the corresponding time depends on the system size and the number of integration steps. Unless the LDS is particularly featureless, the number of integration steps required to reproduce the required structure will be quite high, thus making this method unsuitable for the calculation of highly structured DOS as in transition metals.

One important point to note is that a substantial part of the information generated by the equation of motion method remains essentially unused, if one is interested only in obtaining the LDS. To calculate a particular orbital amplitude

$a_\mu(t)$ (see eqn. (4.41)) for different values of t, one has to follow the time evolution of all the amplitudes. The Fourier transforms of these amplitudes yield one entire row (or column) of the off-diagonal elements of the Green's function. These off-diagonal elements can be used to study other properties like the spectral functions etc.[2] In a disordered system, one can use these to calculate the inverse participation ratio

$$P_\alpha = \sum_{j=1}^{N} |\langle \psi_\alpha | \phi_j \rangle|^4, \qquad H|\psi_\alpha\rangle = E_\alpha |\psi_\alpha\rangle \quad (5.5)$$

and study localisation of energy eigenstates[111,128] as well as calculate electrical conductivity as has been done by Kramer and Wearie[129] and Kramer et al.[130] Thus although the equation of motion method is rather slow in calculating the local DOS, its real potential lies in generating the off-diagonal elements of the Green's function, which can be obtained in a modest amount of additional time. In the recursion method, calculation of each off-diagonal element G_{ij} involves calculating four diagonal elements for states that are linear combinations of $|\phi_i\rangle$ and $|\phi_j\rangle$ (see Haydock, Ref.95, section 17) and in that case the two methods are perhaps of comparable efficiency.

VI. CHAPTER (6)

6.1 LOCAL DOS BY RECURSION METHOD

6.1(a) NONSYMMETRIC HAMILTONIAN

In this section we will discuss the results for the LDS obtained by employing the Anderson-Bullett scheme described in section (3.1). The elements of the Hamiltonian matrix D are written as (see eqn.(3.37))

$$D_{\alpha\beta} = \langle \phi_\alpha | V_\alpha^\circ | \phi_\beta \rangle + \langle \phi_\alpha | \delta V_x | \phi_\beta \rangle \qquad (6.1)$$

where ϕ_α'S are the atomic orbitals (s and d) and V_α° is the free atom potential at the same center as ϕ_α. δV_x is a correction due to the non-additivity of exchange and correlation effects. We treat δV_x as a constant and adjust its value as well as the atomic s and d energy levels to reproduce a band structure appropriate to the bcc phase of iron (Fig.6). These parameters together with the atomic orbitals and potential are then used to compute the Hamiltonian matrices for the clusters representing bcc, fcc, amorphous and liquid iron. These clusters are bigger than those considered in the previous chapter. The liquid and the amorphous clusters, obtained by the Monte Carlo technique, are of 365 atoms each, while the clusters

representing the crystalline phases consist of about 400 atoms. The pair distribution functions for the liquid and the amorphous clusters are shown in Figs.(1) and (2) respectively. For each cluster, the size of the Hamiltonian matrix is kept within reasonable limits by retaining the overlap integrals only upto the second nearest neighbour distance in the crystal.

Since, the Hamiltonian matrices defined by (6.1) are nonsymmetric, we employ the nonsymmetric recursion method discussed in section(4.31(b)). The results are obtained by employing the free boundary conditions to the clusters. In Figs.(15-20) we display these results, comparing two systems at a time. The curve for bcc iron, obtained as a check against known results, compares well with that obtained by Callaway and Wang(CW).[82] The two main peaks in the d region, characteristic of any bcc transition metal, are at the right places. The small peak towards the bottom of the d band that appears in the calculation of CW is missing from ours. This is indicative of smaller s-d hybridisation in our model. In this respect, our curve for bcc iron is similar to that obtained by Gallagher and Haydock,[131] who use localised d orbitals obtained by minimising the hybridisation with the conduction band. The fine structure in the DOS curve for solid iron that can be obtained by the conventional Brillouin zone summation method, cannot be seen in our results for a finite cluster (387 atoms), where, in order to obtain a smooth spectrum, we have added an imaginary part equal to 0.02 Ryd. to the energy(see section 4.31(c)). The DOS, in

this case, is a set of delta functions that have been broadened into Lorentzians obscuring fine details. This is why the DOS curves in Figs. (15-20) do not show any sharp band edges. However, these curves indicate that the change in the bandwidth from one system to another is inappreciable.

The DOS for the amorphous iron retains the double-peaked structure of bcc iron in the d region, while the s peak is broadened. For the liquid, this double-peaked structure vanishes, the peak towards the bottom of the band merging into a shoulder. For both the liquid and the amorphous clusters, the LDS for the s states is observed to undergo significant changes from one site to another. The d states are affected to a much lesser degree. Because of the small weight associated with the s states, their variation from one site to another only slightly affects the overall DOS and hence averaging over a few sites near the center of the cluster is sufficient to obtain the complete DOS curves. In Figs. (15-20), we have displayed the results obtained by averaging over four sites near the center of the amorphous and liquid clusters. It is interesting to note that the DOS for the amorphous and the liquid cluster is closer to that of fcc than bcc iron, a result similar to that obtained by Asano and Yonezawa[32] for liquid Ni. Comparison of the DOS curves for the crystalline and the amorphous phases seems to suggest that the short range order in the amorphous system is somewhat intermediate between the bcc and fcc structure (Fig. 21). However, this conclusion is only tentative and should be

verified by a direct observation and analysis of the structure in amorphous iron.

In Figs. (15-20), small oscillations near the maximum of the DOS curves for the liquid and the amorphous clusters are actually spurious. These arise because of the small number of recursion co-efficients used in the calculation. The nonhermiticity of the Hamiltonian sometimes causes the recursion co-efficients, b_n , to become imaginary, thus stopping the chain.[105] Though this never happened for the clusters representing the crystal, it occurred frequently for the liquid and somewhat less often for the amorphous clusters. In obtaining the results displayed in Figs. (15-20), we have used 50 recursion co-efficients, except for the cases where the chain had to be terminated due to b_n^2 becoming negative. The minimum number of co-efficients was 10 for the liquid and 16 for the amorphous clusters. The LDS calculated from such small number of co-efficients shows spurious peaks, since it consists of only a small number of Lorentzian broadened delta functions.

Some features of these results are summarised in table (1). Here E_f and $N(E_f)$ denote the Fermi level and the DOS at the Fermi level respectively, and n_d stands for the number of d electrons per atom. The subscripts 1 and 2 associated with $N(E_f)$ imply results obtained by employing two different smoothing procedures, the former referring to the Lorentzian broadening of delta functions and the latter to the method based on the differentiation of the mean of the upper and lower bounds to the

integrated density of states, and implemented in subroutine RECTAB of the Cambridge Recursion Library (see C. M. M. Nex, Ref.107). We note that there is no significant change in the number of d electrons due to a change of phase.

TABLE (1)

Some characteristics of the DOS in solid, liquid and amorphous iron, obtained by using nonsymmetric hamiltonian matrices

CLUSTER	E_f (Ryd.)	$N(E_f)_1$ * states/-atom/Ryd.	$N(E_f)_2$ # states/-atom/Ryd.	n_d electrons/atom
BCC	-0.59	40.5	48	7.4
FCC	-0.58	30.0	33.5	7.4
AMORPHOUS	-0.59	34.0	36	7.4
LIQUID	-0.58	30.0	31	7.4

* Results obtained by adding an imaginary part equal to 0.02 Ryd. to the energy.

Results obtained by using the subroutine RECTAB of the Cambridge Recursion Library (reference 107).

FIGURE CAPTIONS

FIG.(15-20).

DOS in various clusters obtained by applying the recursion method to nonsymmetric Hamiltonian matrices(eqn. 3.37). The vertical axis is labelled in states/Ryd./atom. The curves have been obtained by adding an imaginary part ε = 0.02 Ryd. to the energy.

FIG.(21).

DOS in bcc, amorphous and fcc clusters obtained by applying the recursion method to nonsymmetric Hamiltonian matrices(eqn. 3.37). The vertical axis is labelled in states/Ryd./atom. The curves have been obtained by adding an imaginary part ε = 0.02 Ryd. to the energy.

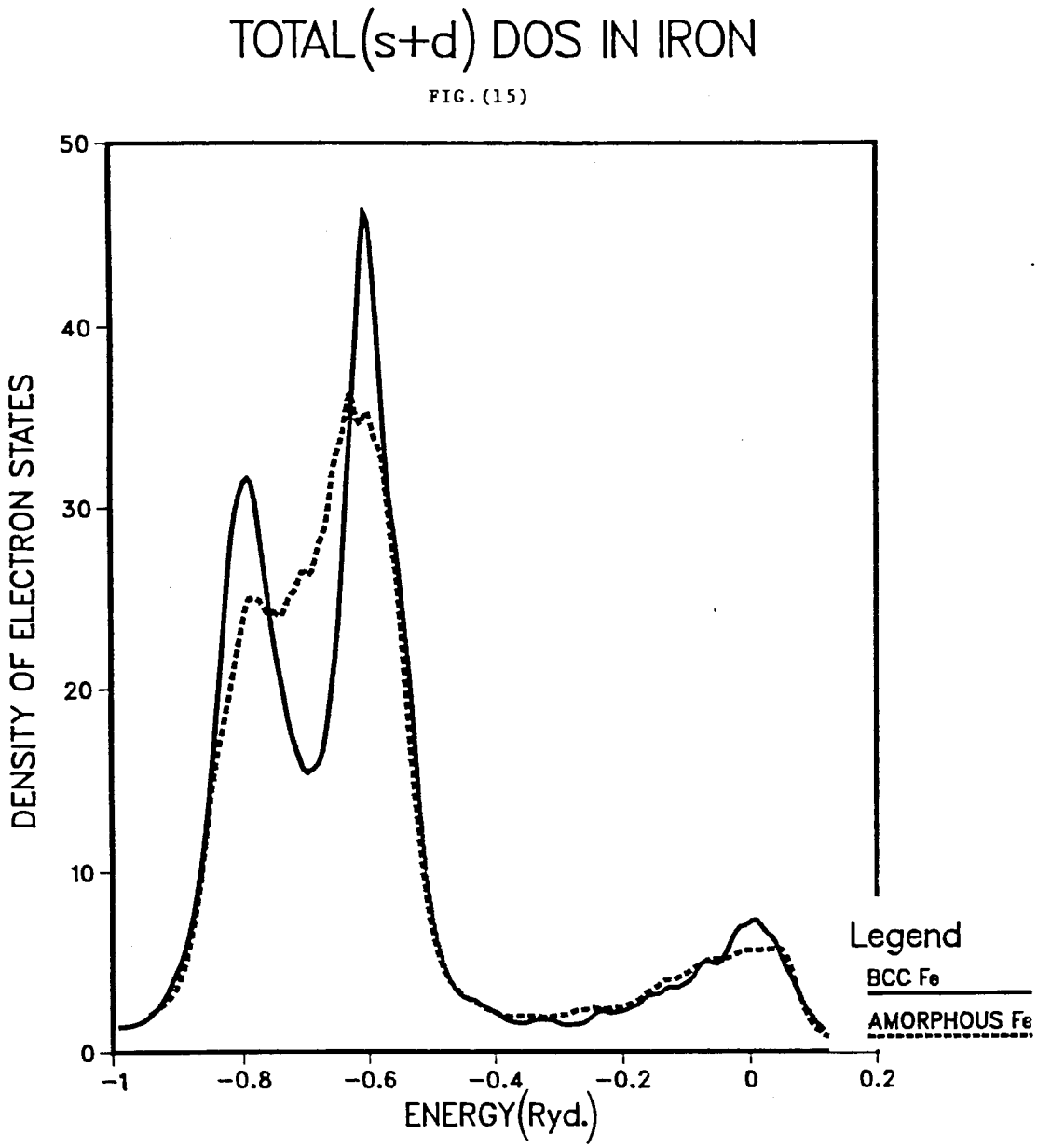
TOTAL(s+d) DOS IN IRON
DENSITY OF ELECTRON STATES
50
40
30
20
10
0
−1
−0.8
−0.6
−0.4
−0.2
0
0.2
ENERGY(Ryd.)
Legend
BCC Fe
AMORPHOUS Fe

FIG. (15)

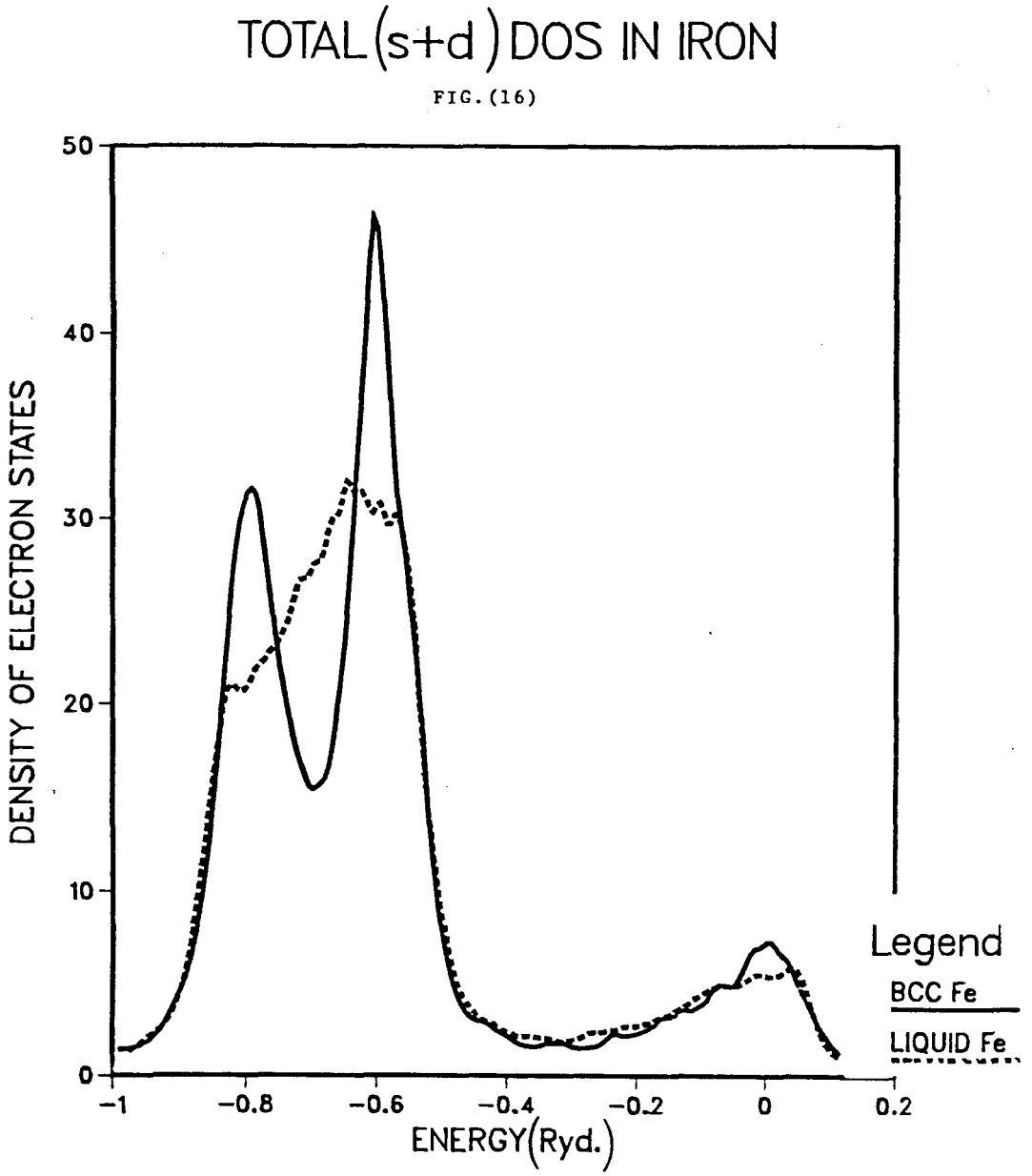
TOTAL (s+d) DOS IN IRON
DENSITY OF ELECTRON STATES
50
40
30
20
10
0
−1
−0.8
−0.6
−0.4
−0.2
0
0.2
ENERGY (Ryd.)
Legend
BCC Fe
LIQUID Fe

FIG. (16)

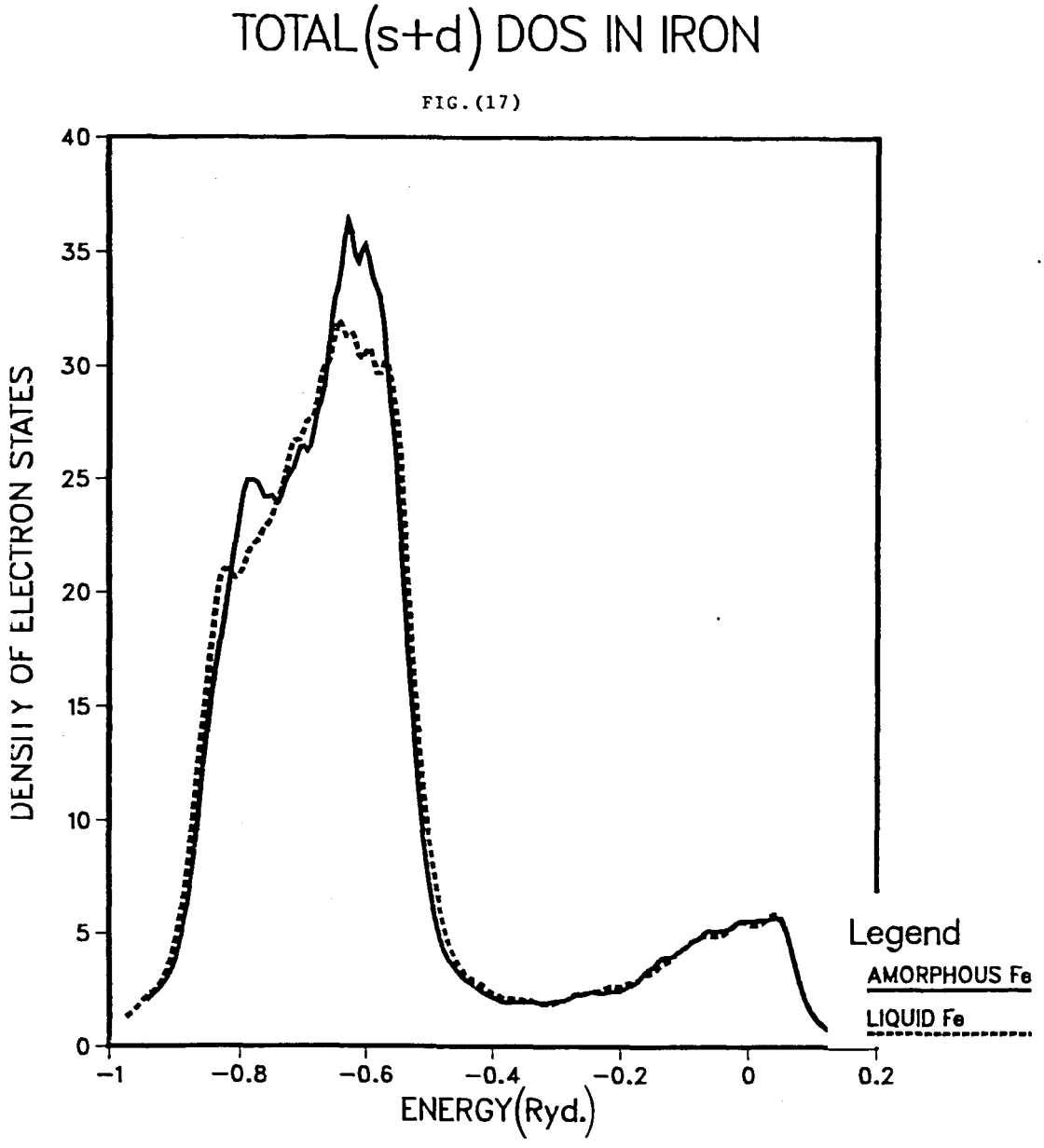
TOTAL (s+d) DOS IN IRON
DENSITY OF ELECTRON STATES
40
35
30
25
20
15
10
5
0
−1
−0.8
−0.6
−0.4
−0.2
0
0.2
ENERGY (Ryd.)
Legend
AMORPHOUS Fe
LIQUID Fe

FIG. (17)

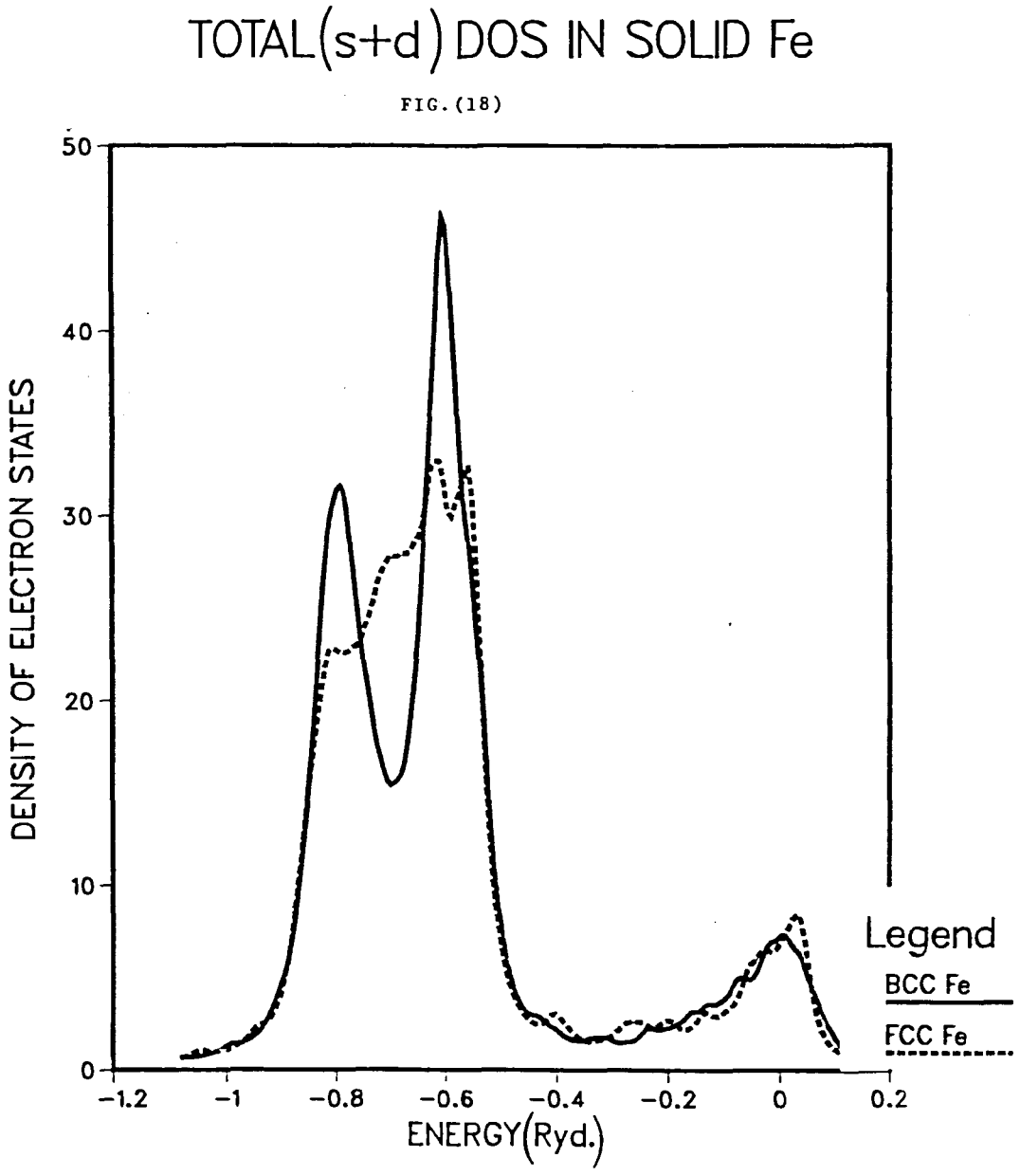
TOTAL(s+d) DOS IN SOLID Fe
DENSITY OF ELECTRON STATES
50
40
30
20
10
0
−1.2
−1
−0.8
−0.6
−0.4
−0.2
0
0.2
ENERGY(Ryd.)
Legend
BCC Fe
FCC Fe

FIG. (18)

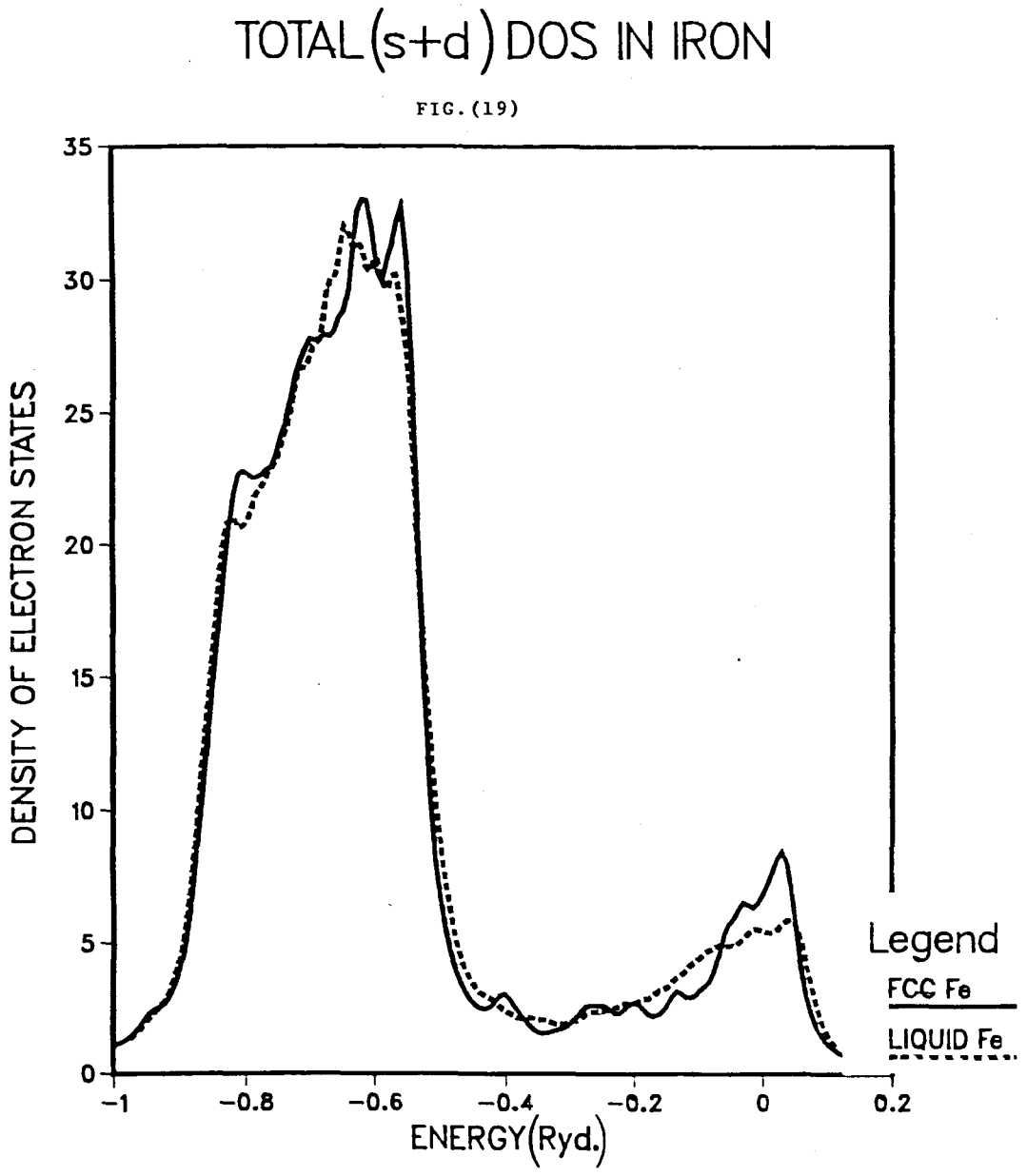
TOTAL (s+d) DOS IN IRON
DENSITY OF ELECTRON STATES
35
30
25
20
15
10
5
0
−1
−0.8
−0.6
−0.4
−0.2
0
0.2
ENERGY (Ryd.)
Legend
FCC Fe
LIQUID Fe

FIG. (19)

TOTAL (s+d) DOS IN IRON

FIG. (20)

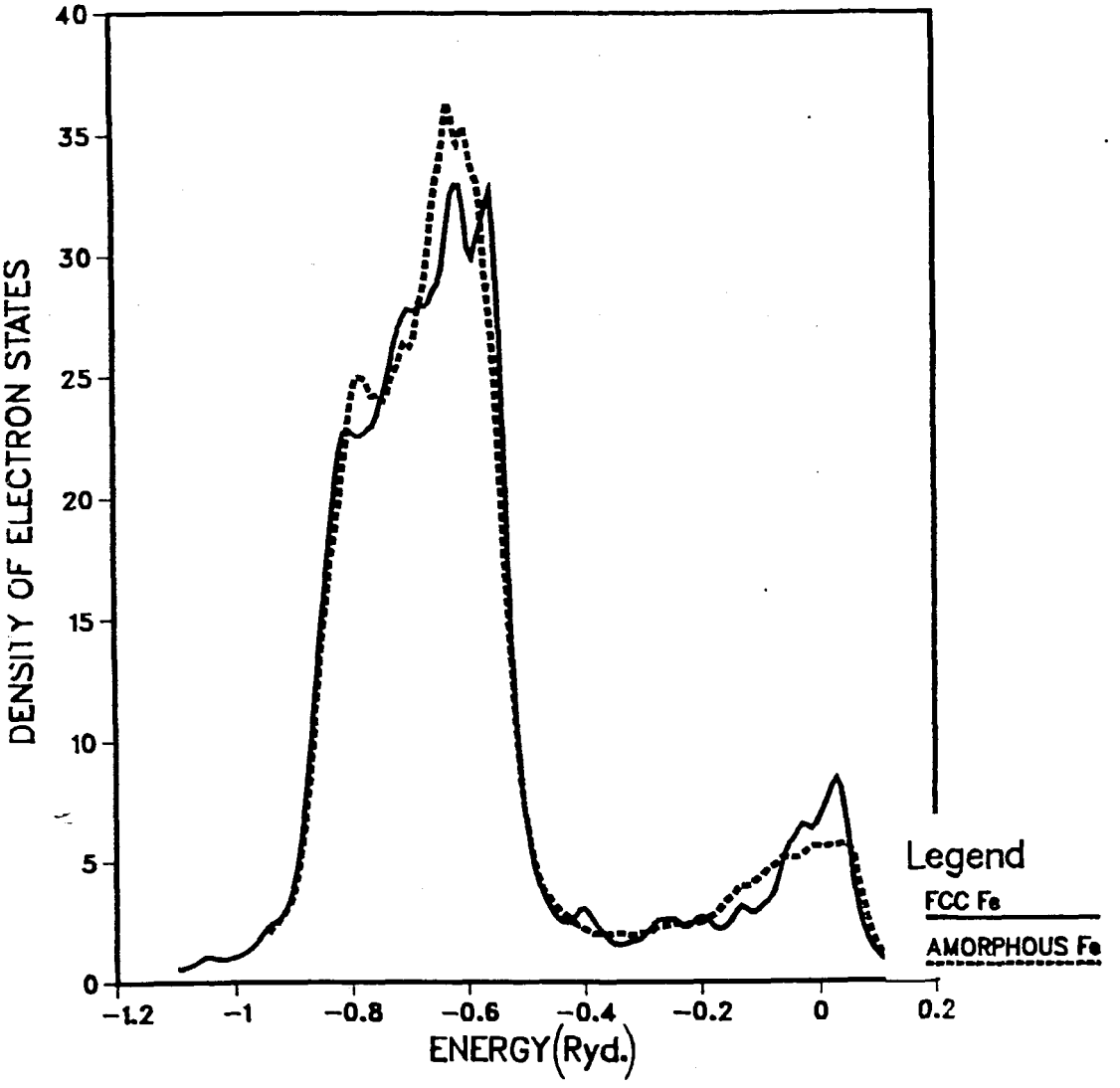

TOTAL (s+d) DOS IN IRON

FIG. (21)

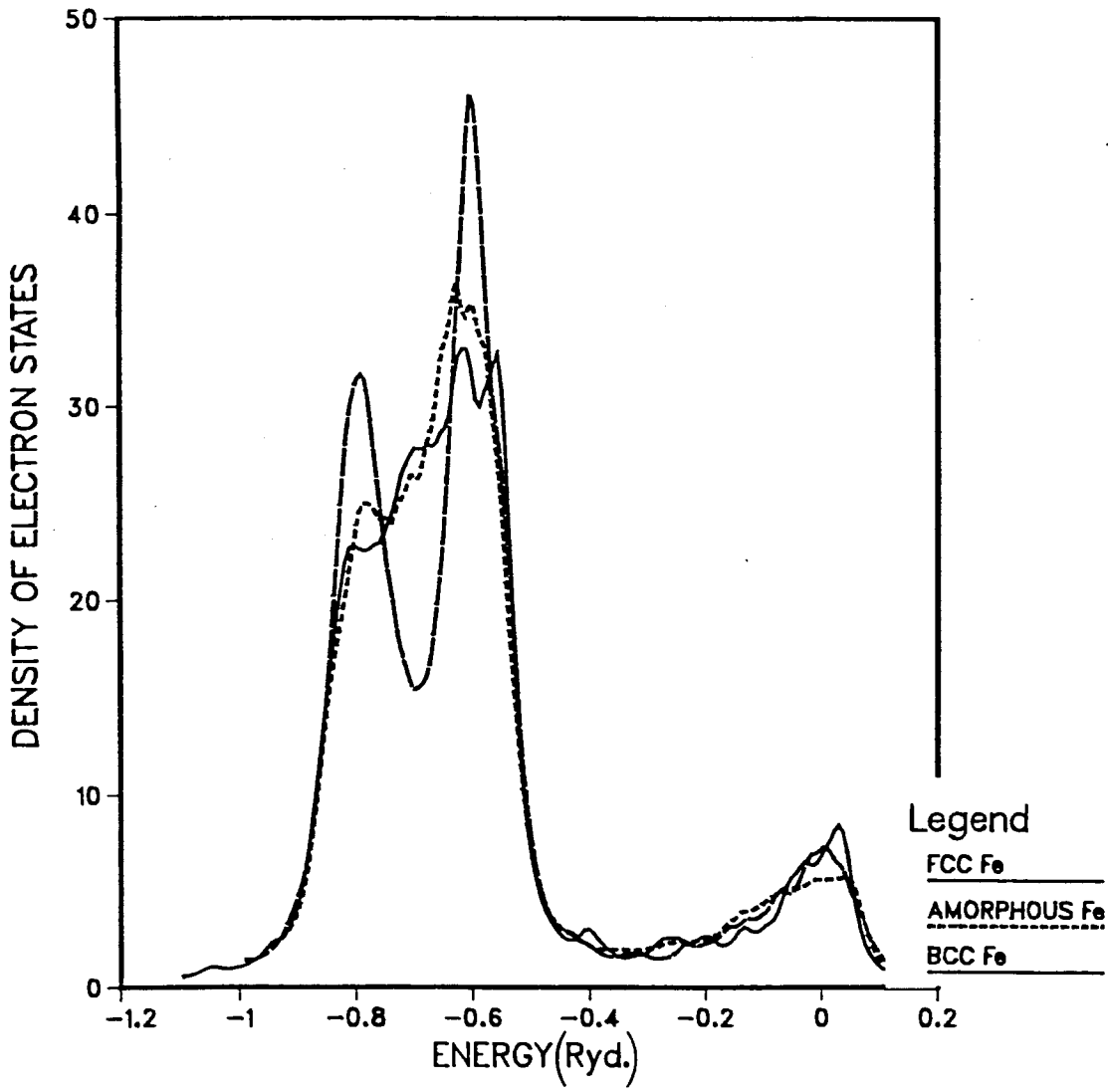

6.1(b) SYMMETRIC HAMILTONIAN

Since the hybridisation gap produced in the nonsymmetric Hamiltonian model is smaller than that in the calculation of CW,[82] we resorted to a different LCAO scheme with more adjustable parameters in an attempt to better represent the hybridisation. In section(3.3) we discussed this alternative parameterisation scheme, in which we directly parameterise the matrix elements of the Hamiltonian by fitting to the band structure of CW. This scheme generates a symmetric Hamiltonian, i.e.,

$$H_{ij} = H_{ji} \qquad (6.2)$$

We use the parameters obtained by fitting to the band structure of CW to compute the Hamiltonian matrices for the same clusters considered in the previous section(6.1(a)).Symmetric version of the recursion method outlined in section 4.31(a) was used to calculate the LDS in various clusters. In all calculations 50 recursion co-efficients were used and we employed free boundary conditions to the clusters. For the liquid and the amorphous clusters the DOS was obtained by averaging the LDS over 4 sites chosen near the center. These results are displayed in Figs.(22-27), where we compare two systems at a time. These curves are similar to those obtained for smaller clusters (125 atoms) considered in chap.5. The two main peaks for the LDS in the bcc cluster are not distinctly resolved as for the nonsymmetric Hamiltonian. Though the s-d hybridisation gap is

larger in this case (compare Figs.(6) and (8)), we still do not obtain the small peak near the bottom of the d-band, which appears in the calculation of CW.

Though these curves are different (in terms of the relative peak heights) from the corresponding curves for the nonsymmetric Hamiltonians, the change observed from one system to another is essentially the same. For example, there is no appreciable change in the bandwidth. The LDS for the amorphous or the liquid cluster is closer to that of the fcc than bcc iron. The curve for the amorphous cluster lies in between those of the bcc and fcc iron (Fig.28), indicating that the short range order in the amorphous cluster is intermediate between the two crystalline structures. The smaller of the two peaks in the bcc phase gradually merges into a shoulder as we go from the bcc to the amorphous and then to the liquid phase.

In table(2) we indicate the Fermi level, the DOS at the Fermi level and the number of d electrons for various clusters. The DOS at the Fermi level is slightly higher (except for the bcc system) than that for the nonsymmetric Hamiltonians, while the number of d electrons essentially remains unaltered.

TABLE (2)

Some characteristics of the DOS in solid, liquid and amorphous iron, obtained by using symmetric hamiltonian matrices

CLUSTER	E_f (Ryd.)	$N(E_f)^*$ states/atom/-Ryd.	n_d electrons/atom
BCC	-0.61	39	7.5
FCC	-0.62	33	7.4
AMORPHOUS	-0.61	38	7.5
LIQUID	-0.62	34	7.5

* $N(E_f)$ is calculated by adding an imaginary part equal to 0.02 Ryd. to the energy.

FIGURE CAPTIONS

FIG.(22-27).

DOS in various clusters obtained by applying the recursion method to the symmetric Hamiltonian matrices(eqn. 3.41-3). The vertical axis is labelled in states/Ryd./atom. The curves have been obtained by adding an imaginary part ε = 0.02 Ryd. to the energy.

FIG.(28).

DOS in bcc, amorphous and fcc clusters obtained by applying the recursion method to the symmetric Hamiltonian matrices(eqn. 3.41-3). The vertical axis is labelled in states/Ryd./atom. The curves have been obtained by adding an imaginary part ε = 0.02 Ryd. to the energy.

TOTAL(s+d) DOS IN IRON

FIG.(22)

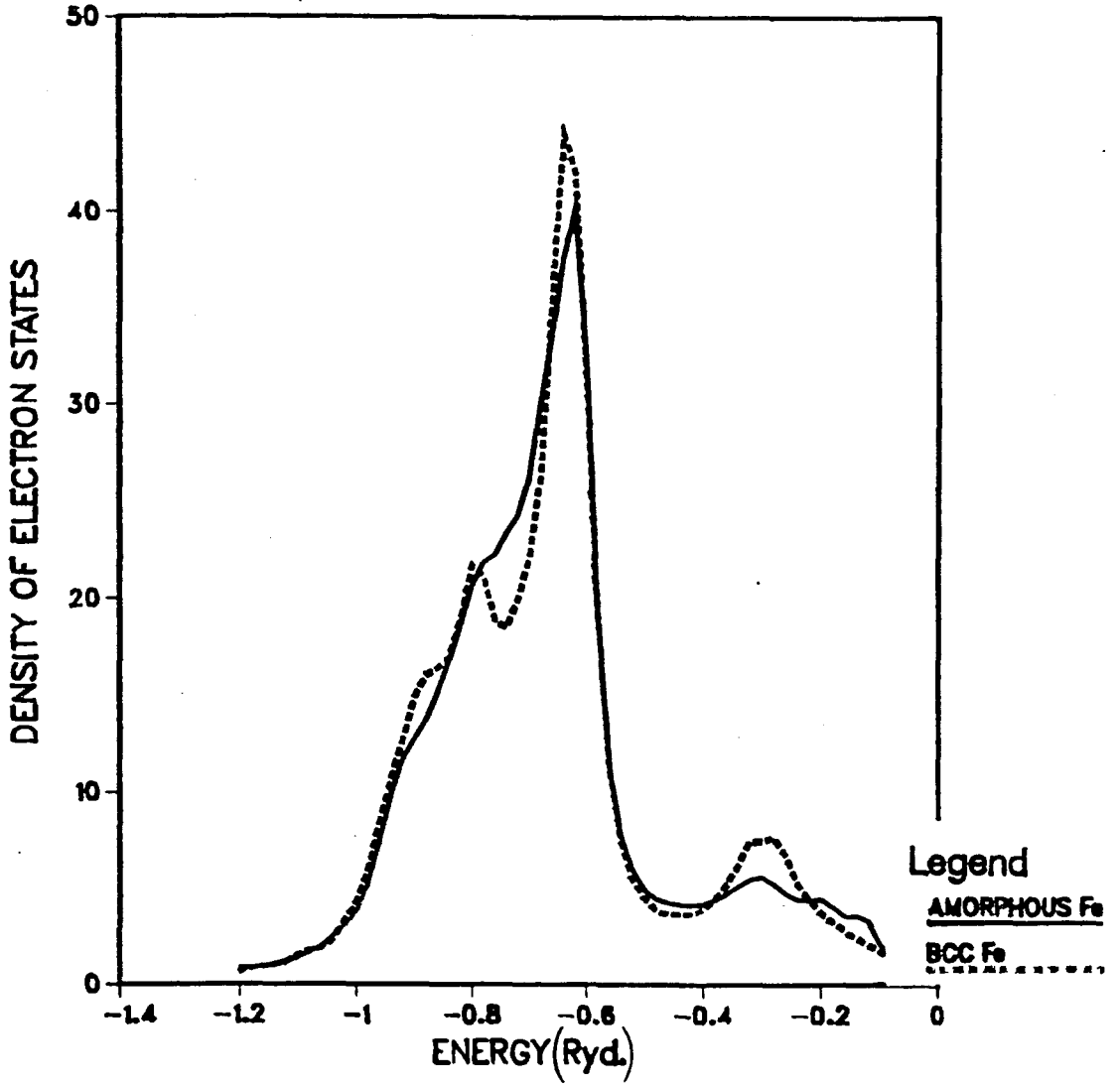

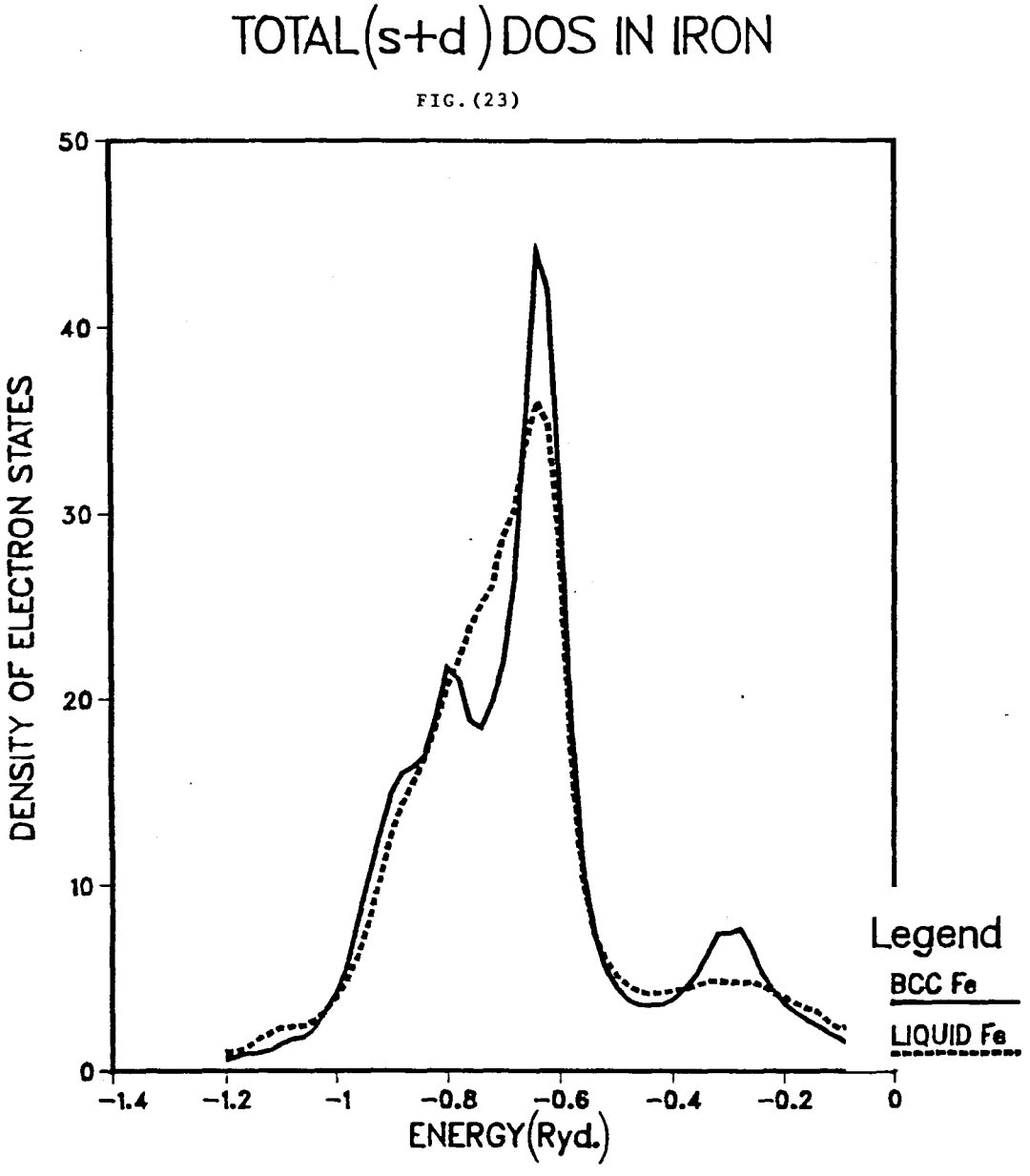
TOTAL(s+d) DOS IN IRON
50
40
30
20
10
0
DENSITY OF ELECTRON STATES
−1.4
−1.2
−1
−0.8
−0.6
−0.4
−0.2
0
ENERGY(Ryd.)
Legend
BCC Fe
LIQUID Fe

FIG. (23)

TOTAL (s+d) DOS IN IRON

FIG. (24)

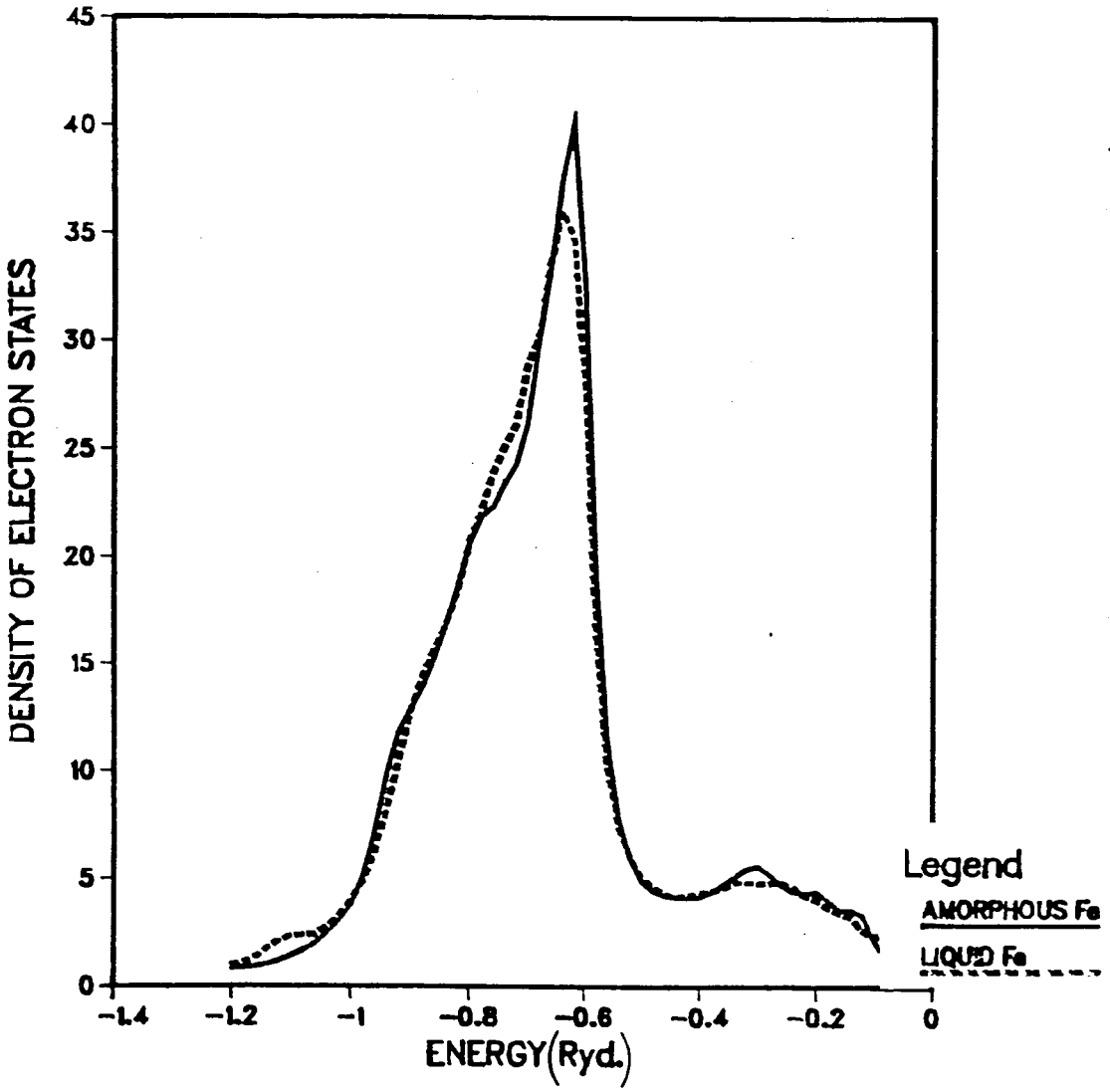

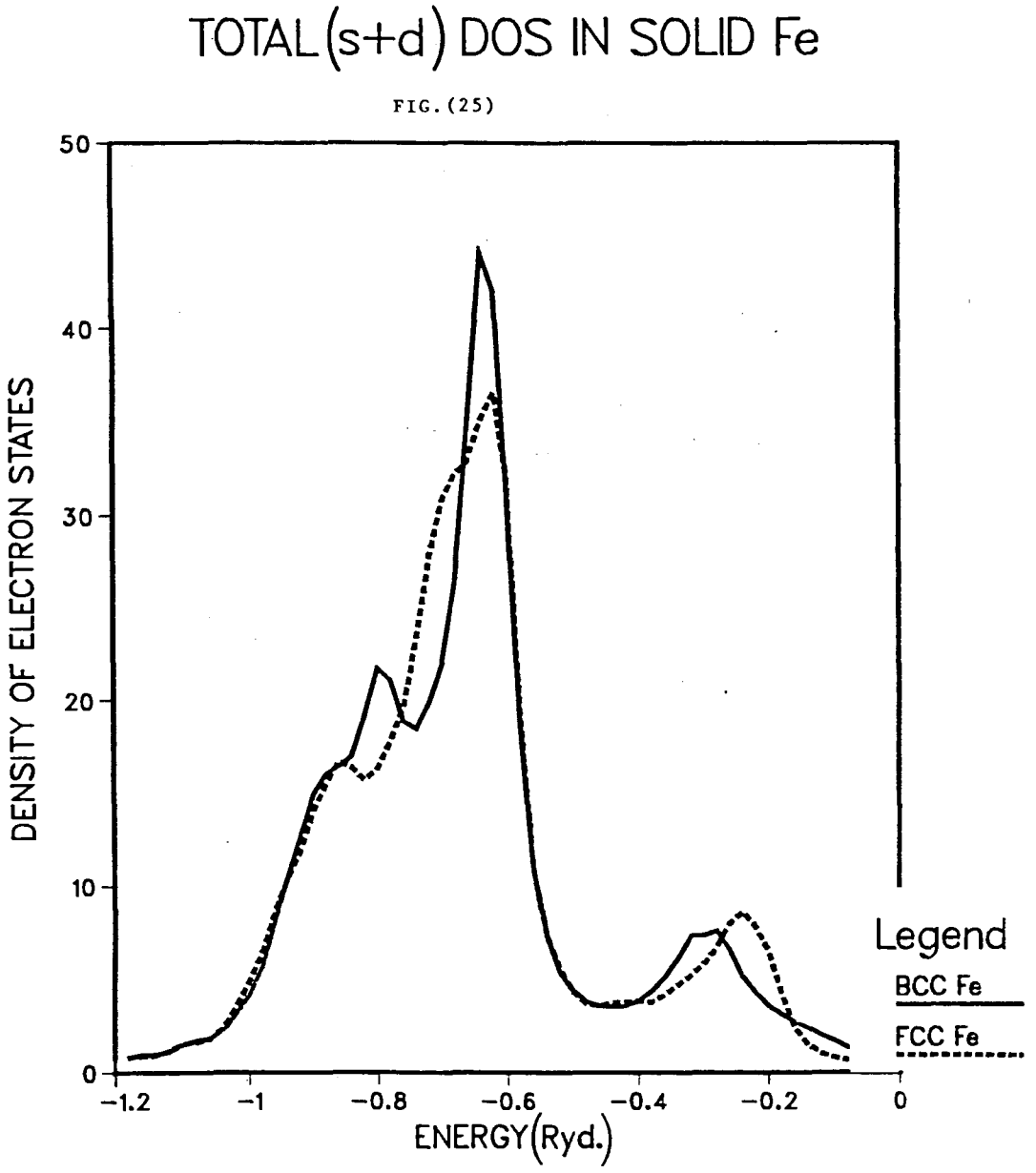
TOTAL (s+d) DOS IN SOLID Fe
DENSITY OF ELECTRON STATES
50
40
30
20
10
0
−1.2
−1
−0.8
−0.6
−0.4
−0.2
0
ENERGY (Ryd.)
Legend
BCC Fe
FCC Fe

FIG. (25)

TOTAL(s+d) DOS IN IRON

FIG.(26)

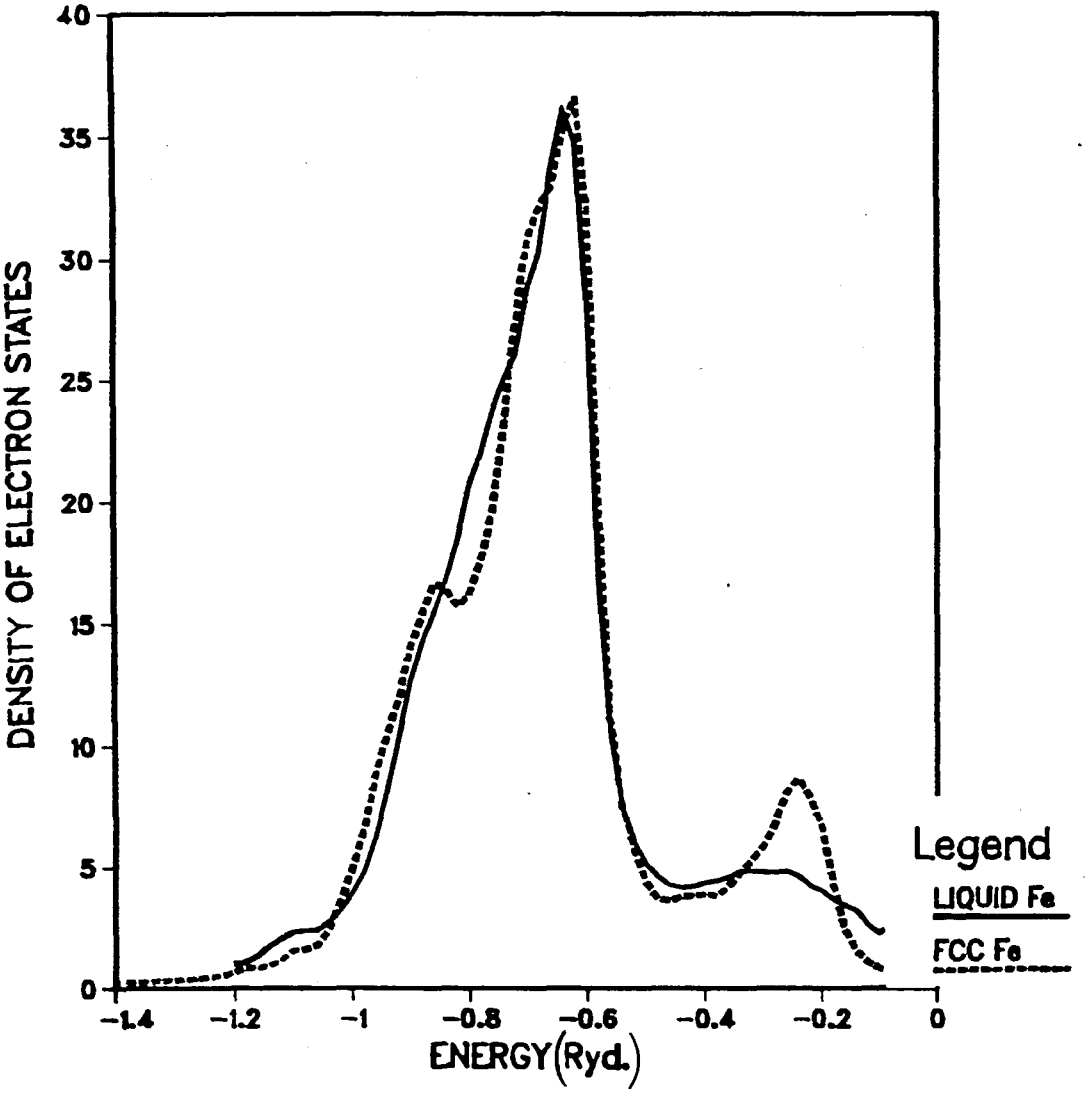

TOTAL (s+d) DOS IN IRON

FIG. (27)

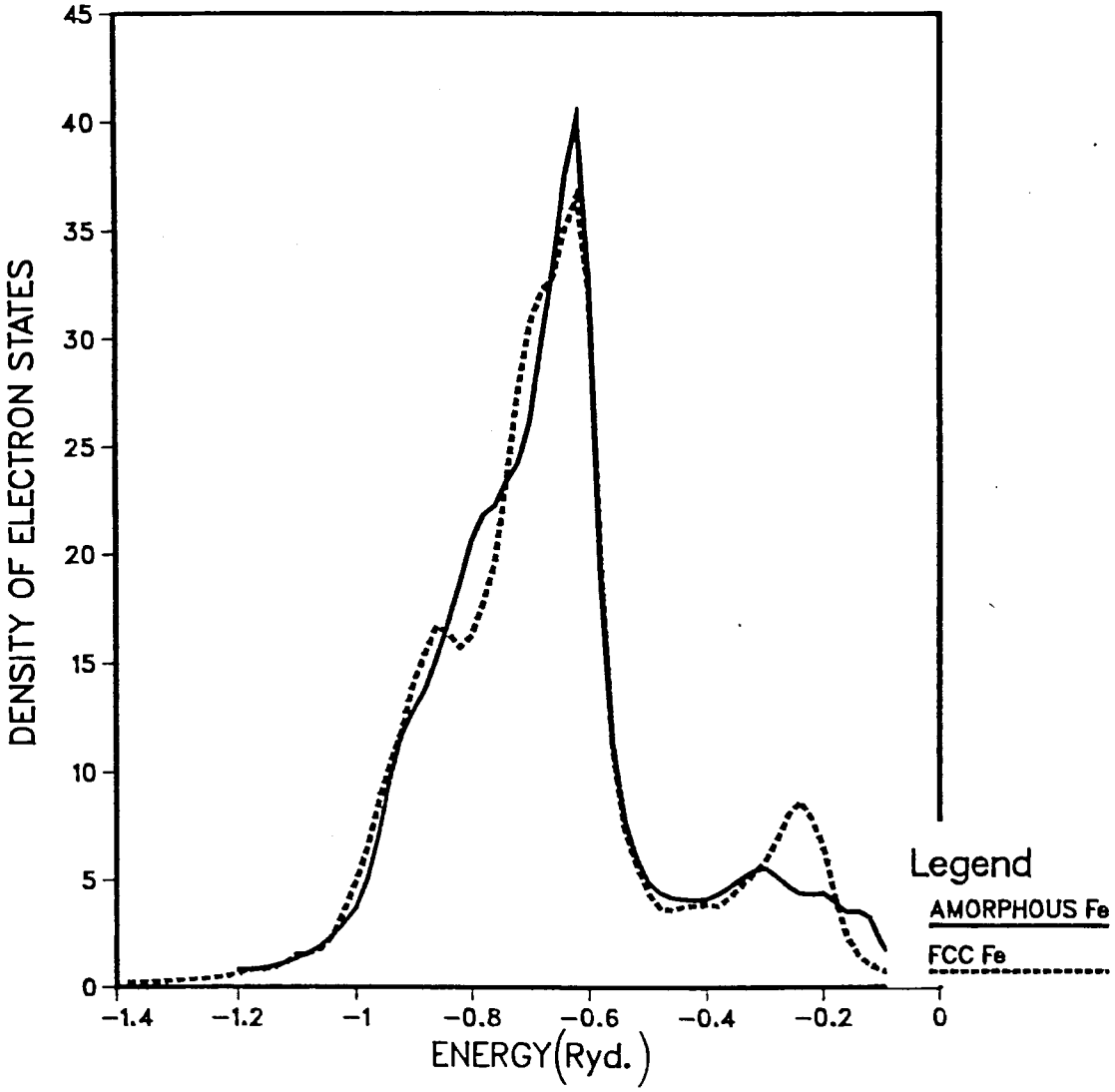

TOTAL (s+d) DOS IN IRON

FIG. (28)

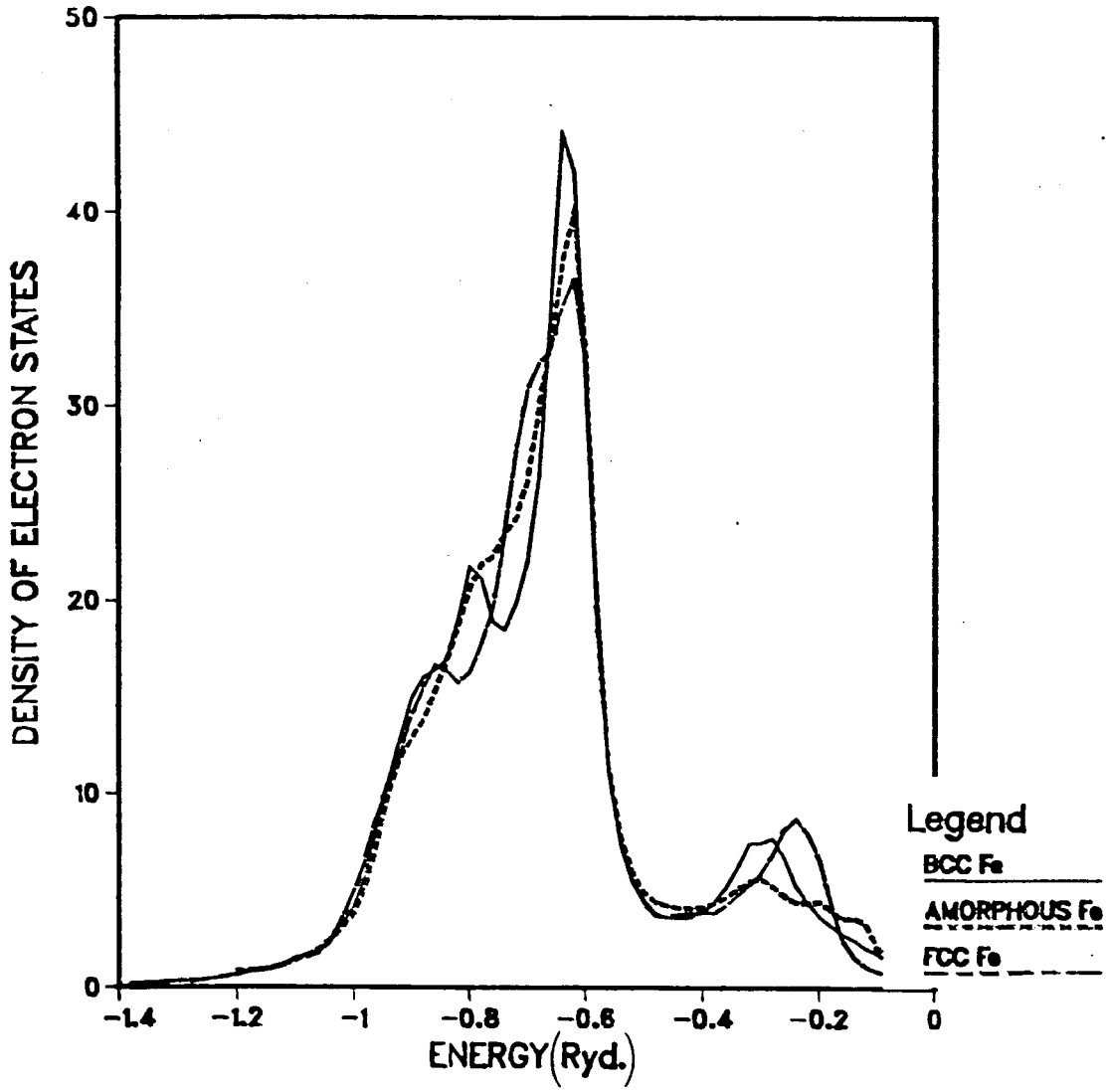

In Figs. (29,30) we have compared the DOS obtained by using two different Hamiltonian matrices for the bcc and the amorphous clusters. While the curves for the bcc cluster refer to the LDS at a single site, the curves for the amorphous cluster show the LDS averaged over the same four sites for the two Hamiltonians. The peak towards the top of the band, due to the s states, occurs at a higher energy for the nonsymmetric Hamiltonian. The d band width is a little larger for the symmetric Hamiltonian.

FIGURE CAPTIONS

FIG.(29,30).

Comparison of the DOS obtained by the two different LCAO schemes (sections 3.1 and 3.3) for bcc and amorphous clusters.

DENSITY OF STATES IN BCC Fe

FIG. (29)

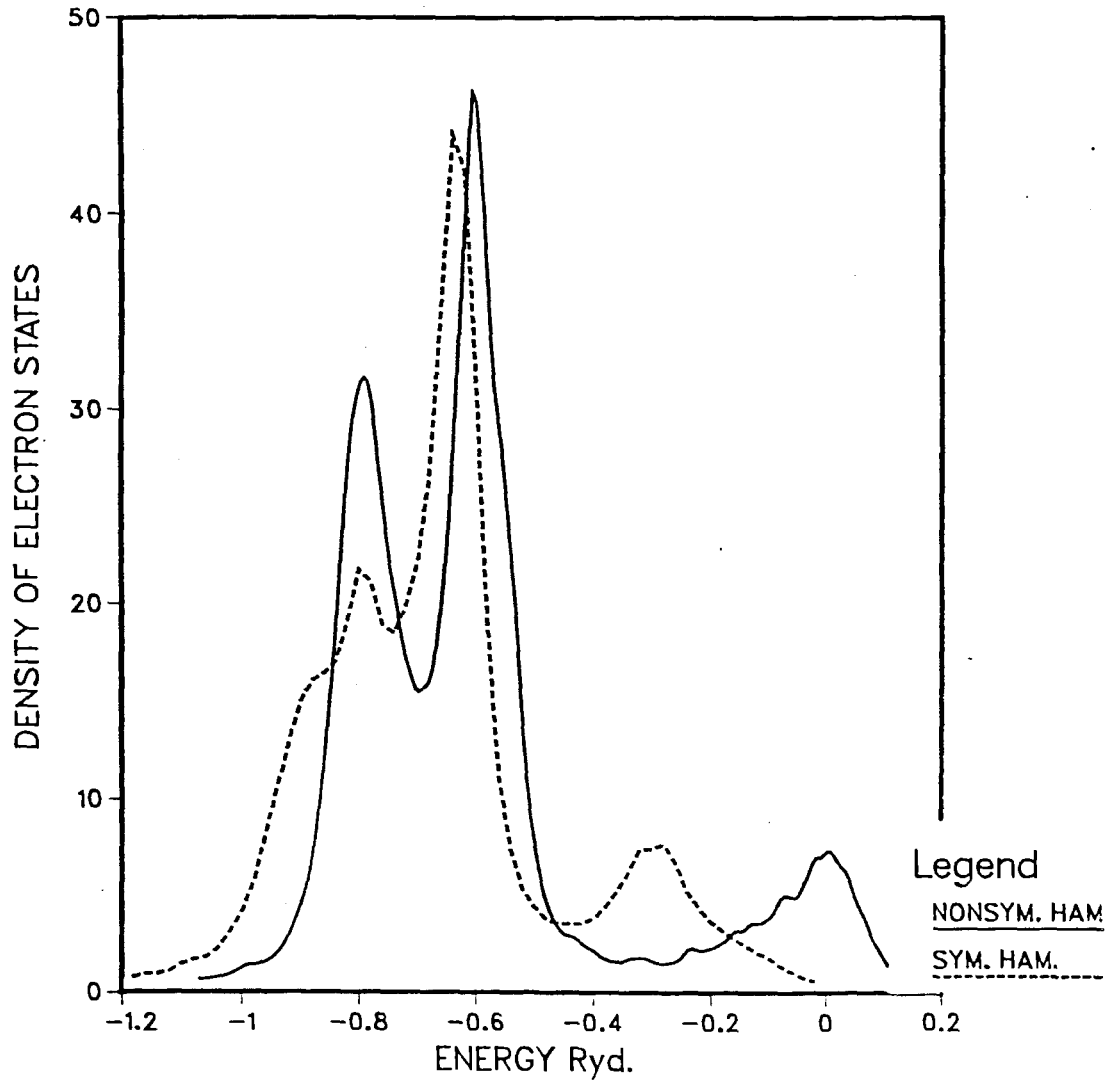

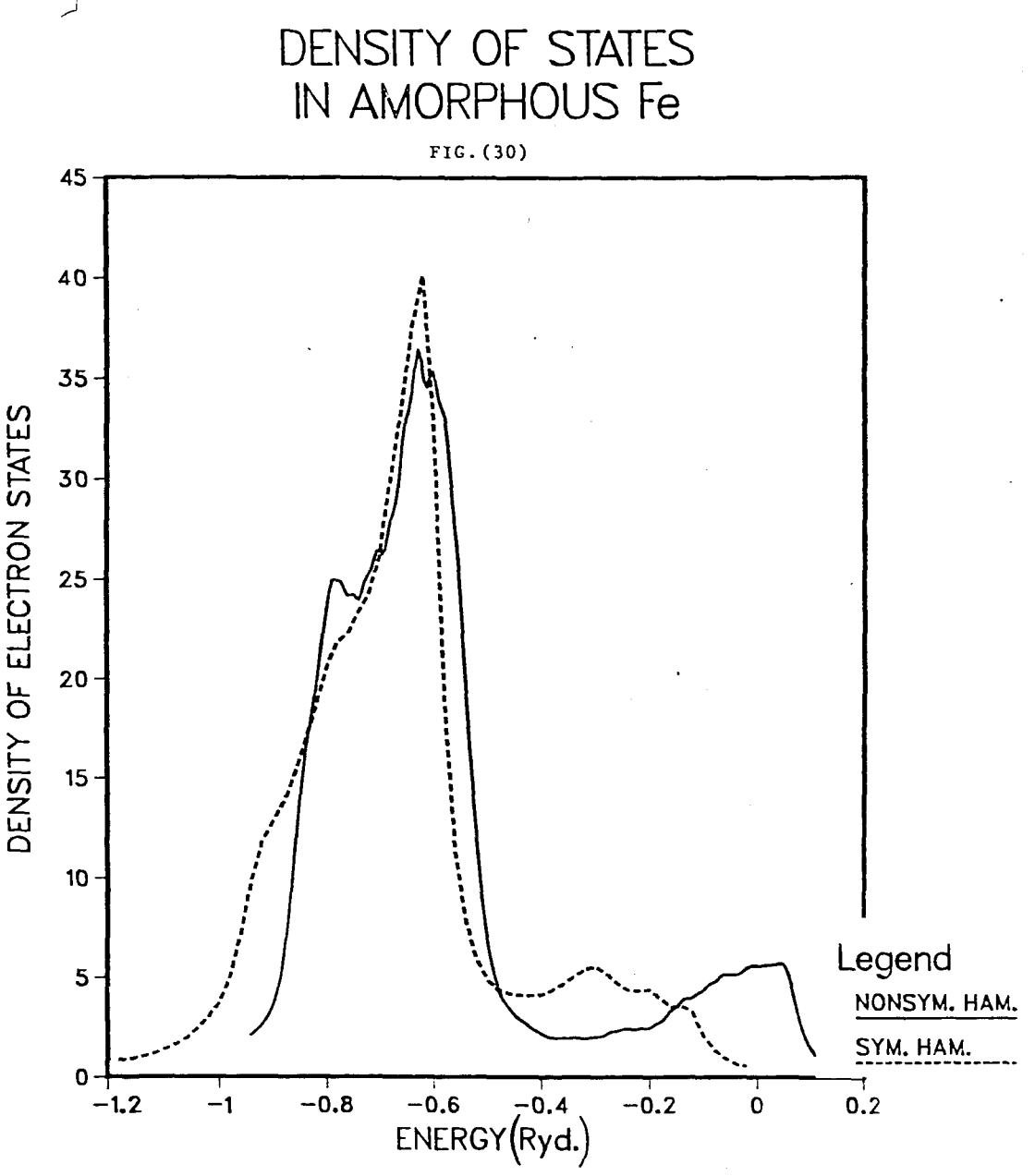
DENSITY OF STATES
IN AMORPHOUS Fe
DENSITY OF ELECTRON STATES
45
40
35
30
25
20
15
10
5
0
−1.2
−1
−0.8
−0.6
−0.4
−0.2
0
0.2
ENERGY(Ryd.)
Legend
NONSYM. HAM.
SYM. HAM.

FIG. (30)

6.2 HYBRIDISATION EFFECTS

To find the effect of hybridisation in our model, we have calculated the density of d states with the full Hamiltonian (s and d orbitals on each site) and the Hamiltonian generated by the d orbitals only. In Figs.(31,32) we show the d density of states obtained with these two Hamiltonians for the bcc and the amorphous clusters. The curves for the bcc cluster refer to the LDS at a single site, while the curves for the amorphous cluster have been obtained by averaging over the same four sites. We have used only the nonsymmetric Hamiltonian model for these calculations. For this model, the effect of hybridisation on the d-band width is not significant. There is a small increase in the band width due to the hybridisation, but no appreciable change near the Fermi level is observed. We recall that for this model the size of the hybridisation gap is small compared with that in the band structure of CW and hence the above result is not surprising. For the symmetric Hamiltonian model, the hybridisation gap is larger. Hence for that model, we expect a more pronounced effect of the hybridisation on the DOS.

The effect of hybridisation on the LDS for the s states is more pronounced. In Fig.33 we show the s DOS (averaged over 4 sites) in amorphous cluster with and without hybridisation. The peaks in the DOS for the s states are observed to be pushed outwards as a result of hybridisation with the d states. Similar effect is expected for the s states in the liquid cluster.

FIGURE CAPTIONS

FIG.(31,32).

Density of d states in bcc and amorphous clusters with and without hybridisation (nonsymmetric Hamiltonian model).

FIG.33.

Density of s states in amorphous cluster with and without hybridisation (nonsymmetric Hamiltonian model).

DENSITY OF D STATES IN BCC Fe

FIG. (31)

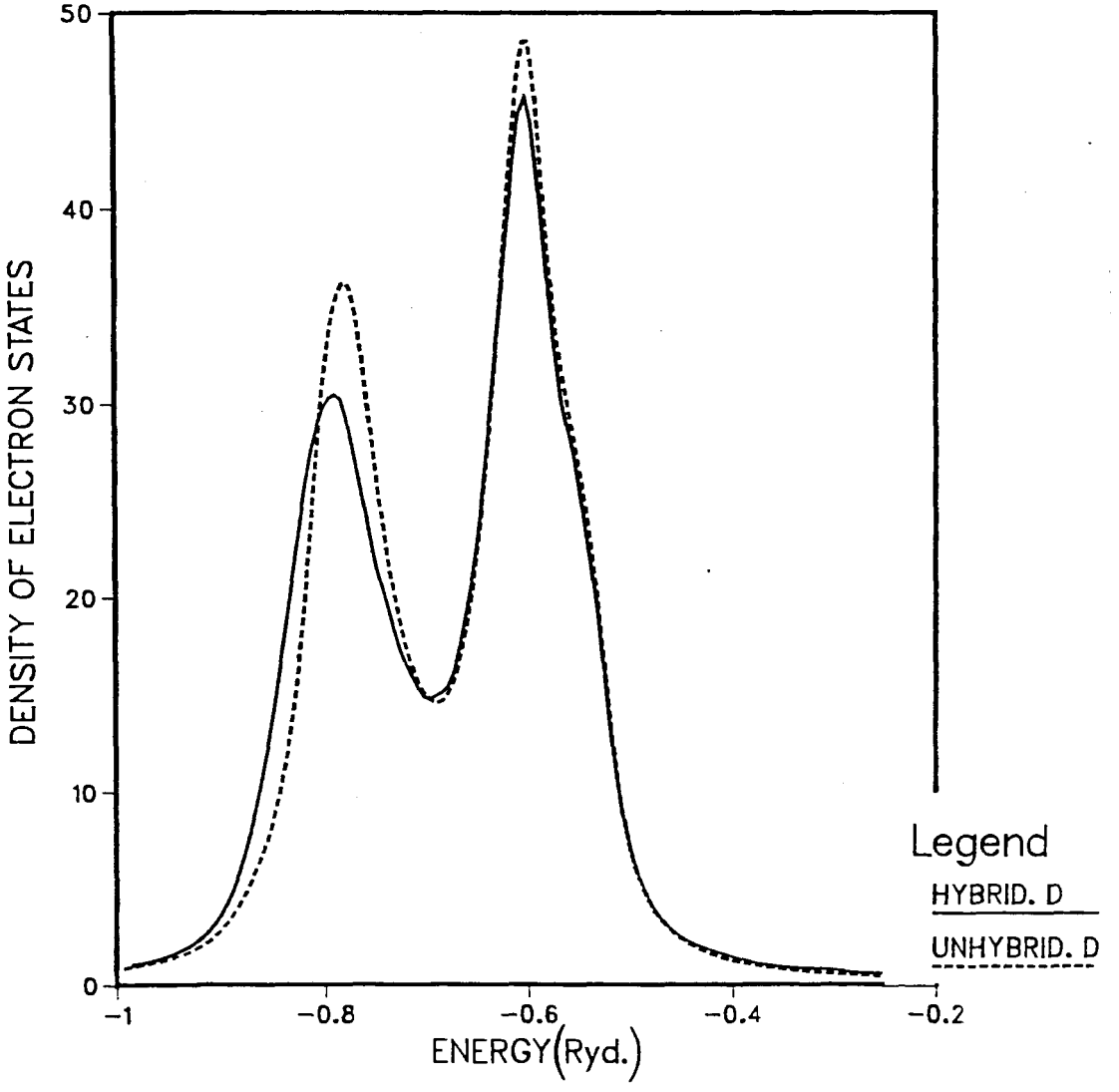

DOS IN AMORPHOUS Fe

FIG. (32)

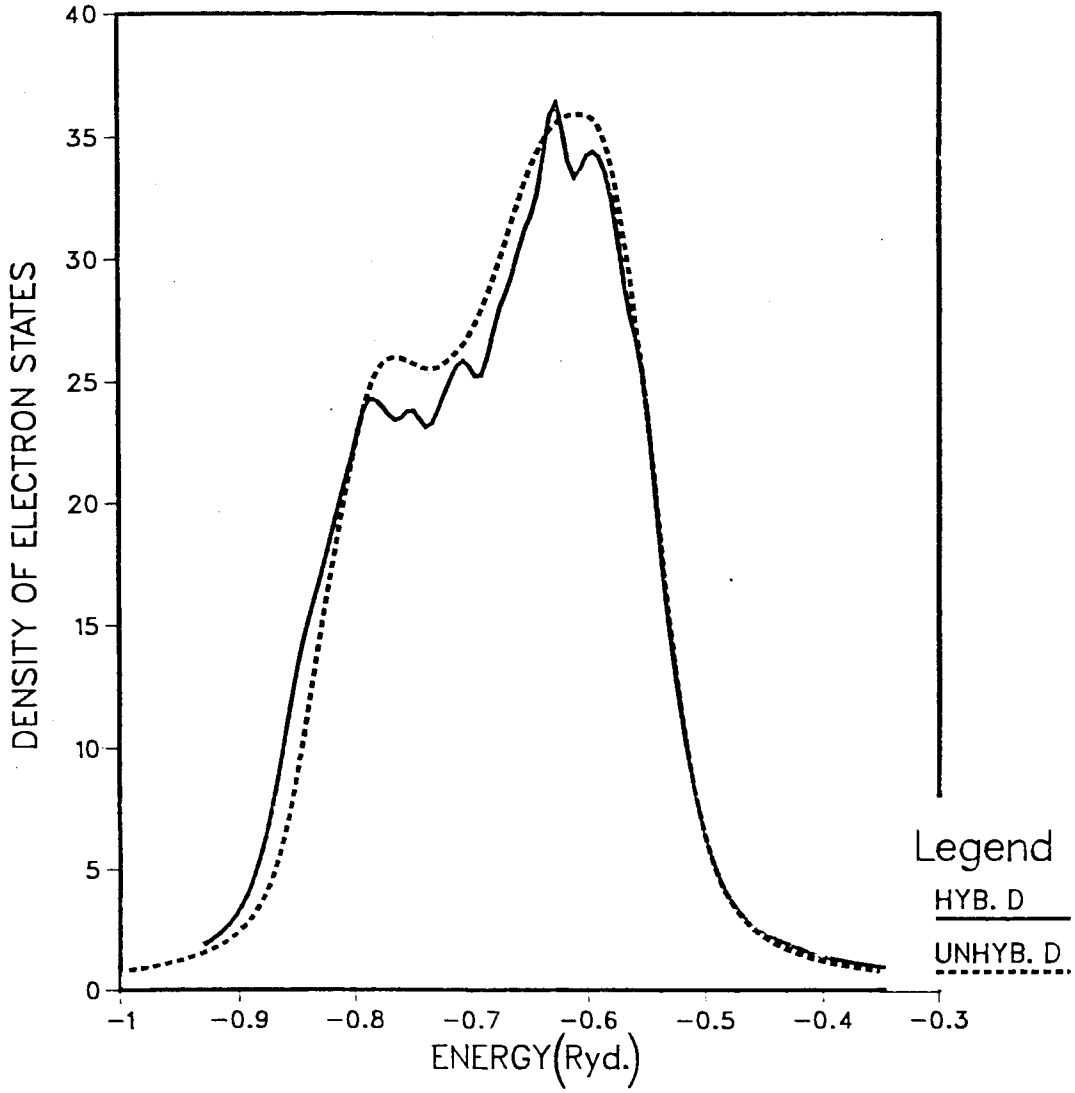

DENSITY OF STATES IN AMORPHOUS Fe

FIG. (33)

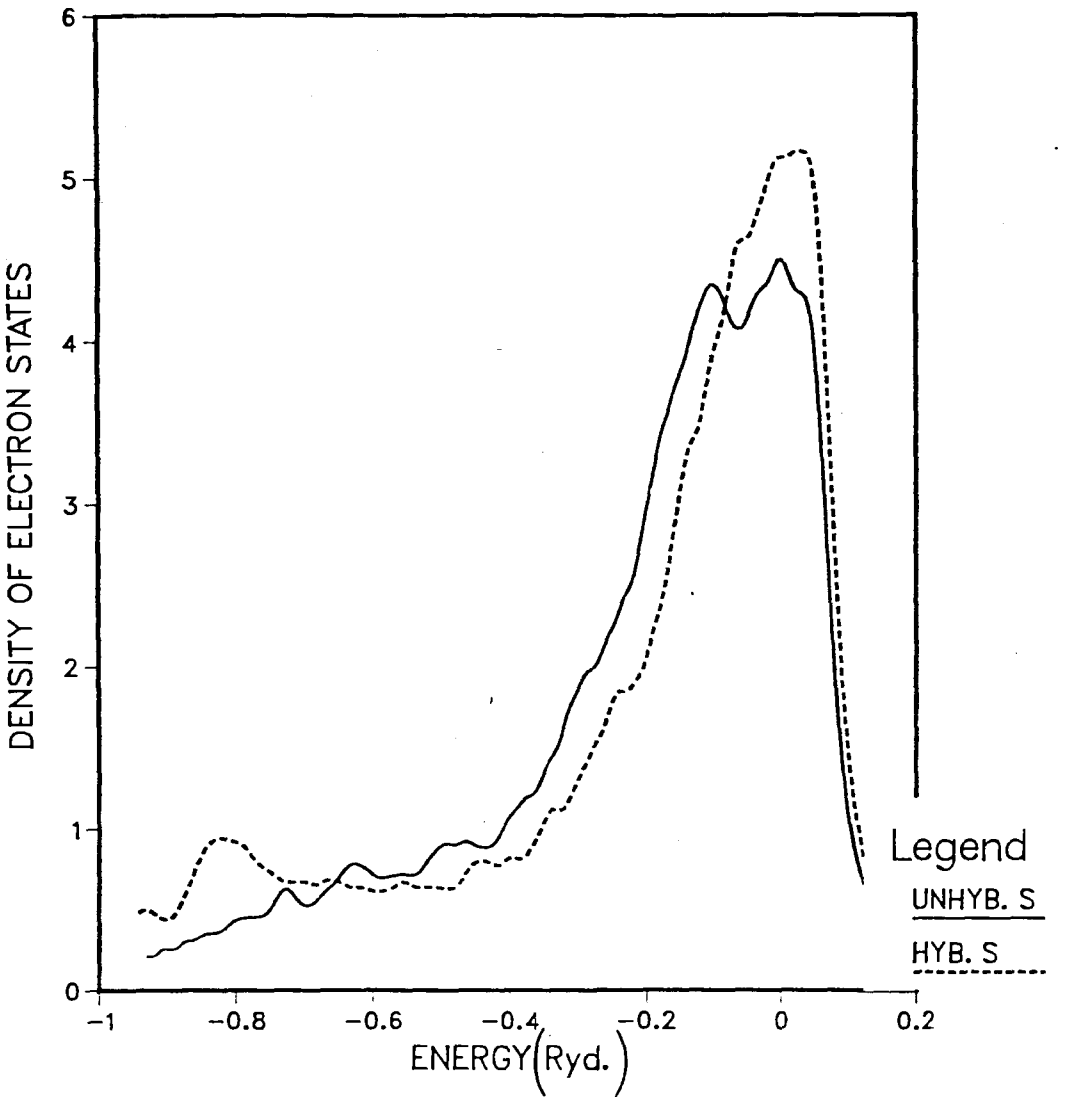

6.3 SIZE EFFECTS

Figs.(34,37) display the density of states obtained for the symmetric Hamiltonian model applied to the clusters with 365 and 125 atoms. The effect due to the cluster size on the density of d states is negligible. Since, in both the liquid clusters the density of s states undergoes significant changes from one site to another (in terms of the peak positions and the heights), one has to obtain an average over a large number of sites to resolve any difference due to the cluster size only. Our results show an average over five sites for the bigger cluster and fifteen for the smaller. The multiple subpeaks in the main peak towards the top of the s band in the liquid clusters are due to averaging over insufficient number of sites. In this case we cannot say anything conclusive about the size effect. For the amorphous case, the two main peaks in the s band seem to broaden with an increase in the cluster size. Whatever the effect of the system size on the s DOS may be, due to their small weight on the total DOS we expect very little change in the latter as the system size is increased from 125 to 365. In any case, there is no appreciable change near the Fermi level for the symmetric Hamiltonian model.

FIGURE CAPTIONS

FIG.(34-37)

Effect of cluster size on the DOS obtained by using the symmetric Hamiltonian model.

DENSITY OF S STATES IN AMORPHOUS Fe

FIG. (34)

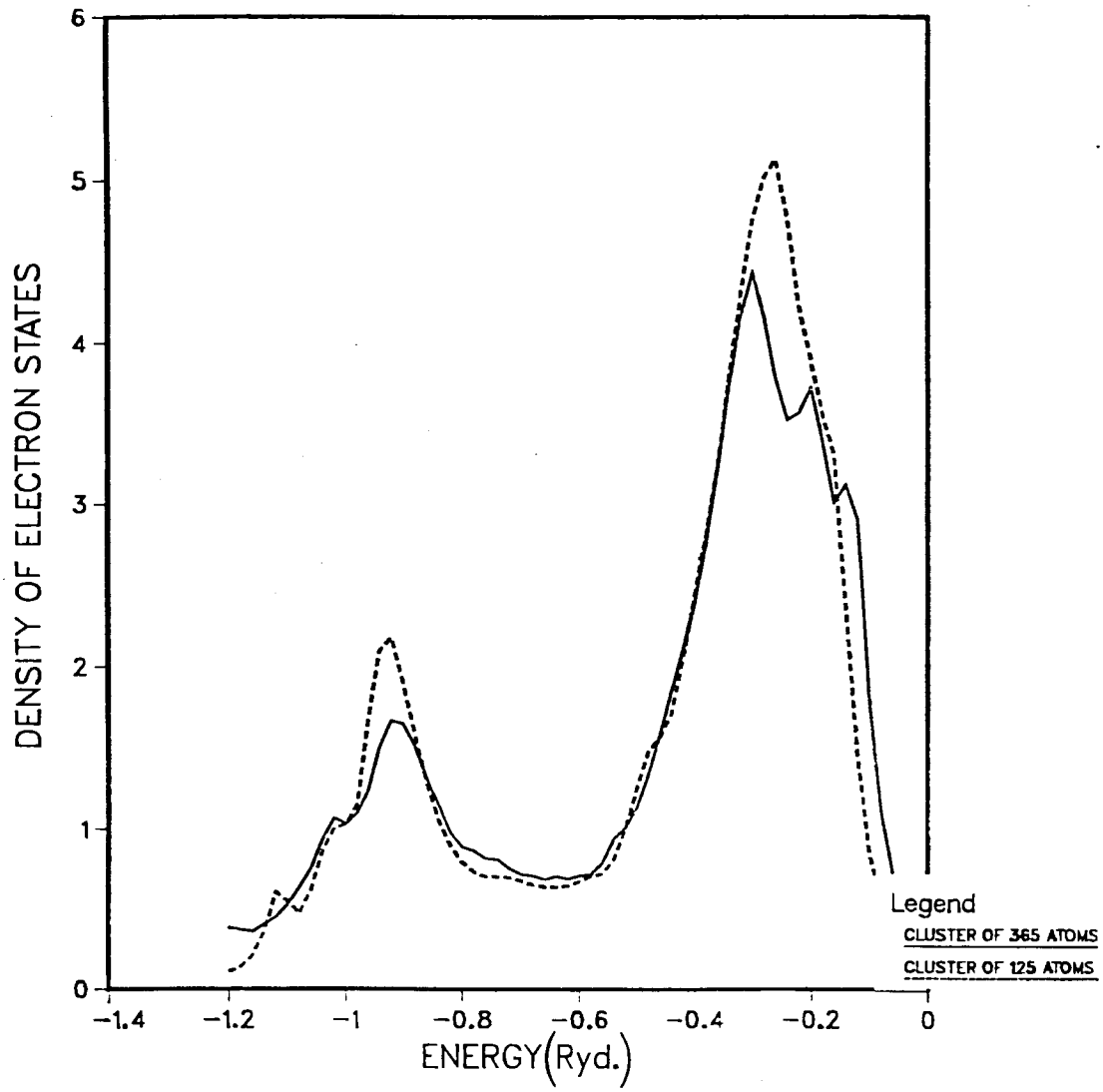

DENSITY OF D STATES IN AMORPHOUS Fe

FIG. (35)

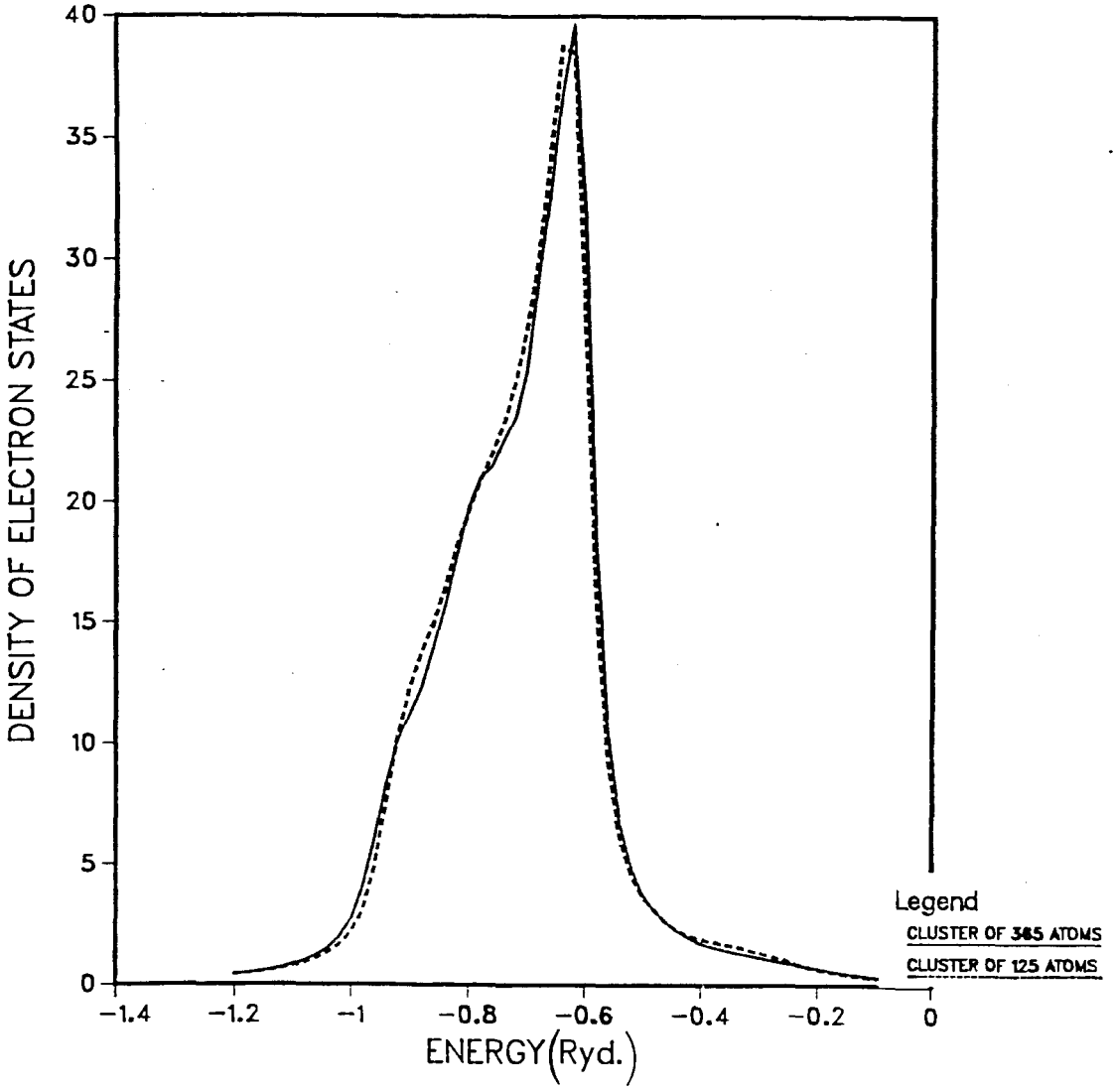

DENSITY OF S STATES IN LIQUID Fe

FIG. (36)

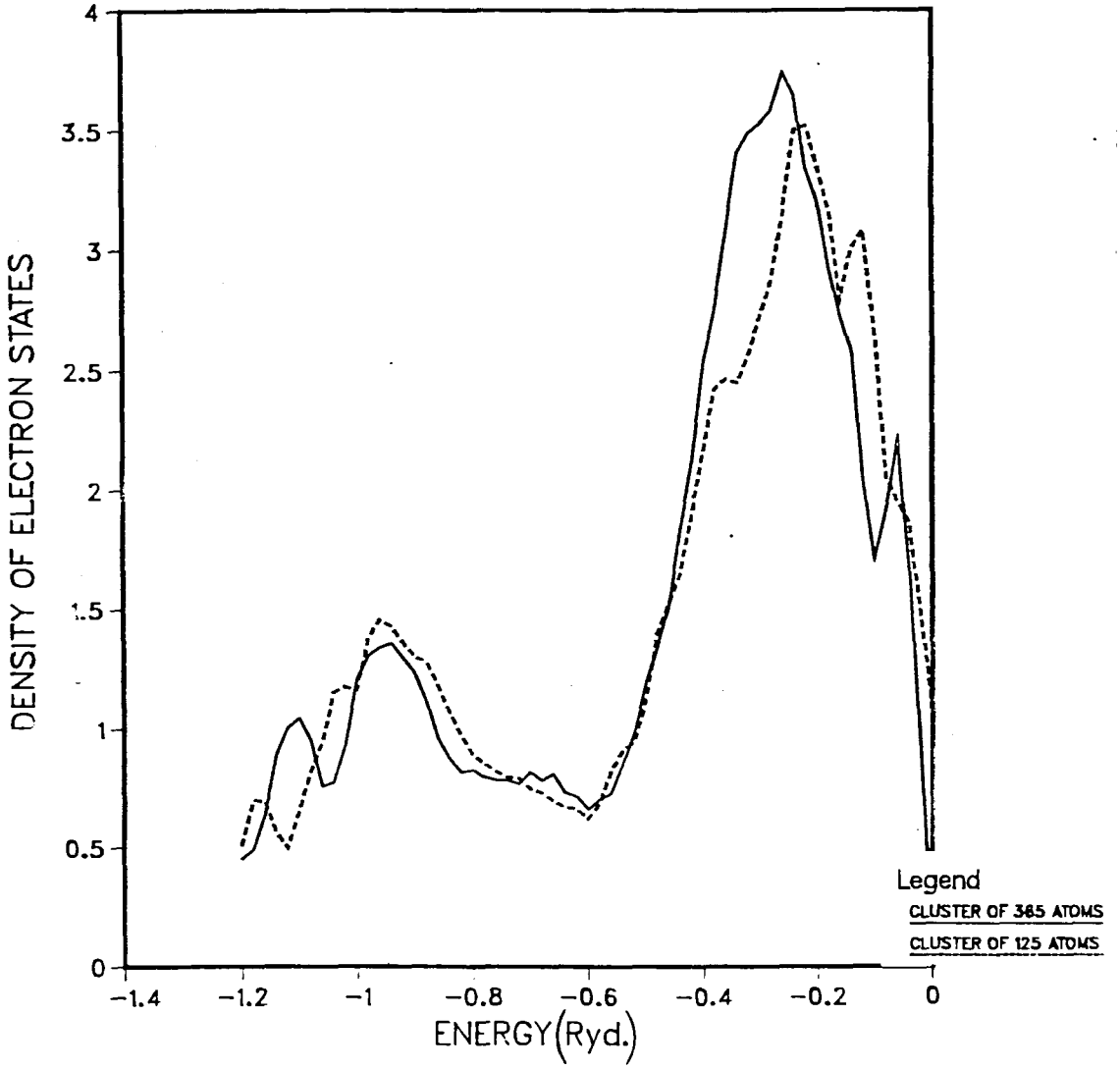

DENSITY OF D STATES IN LIQUID Fe

FIG. (37)

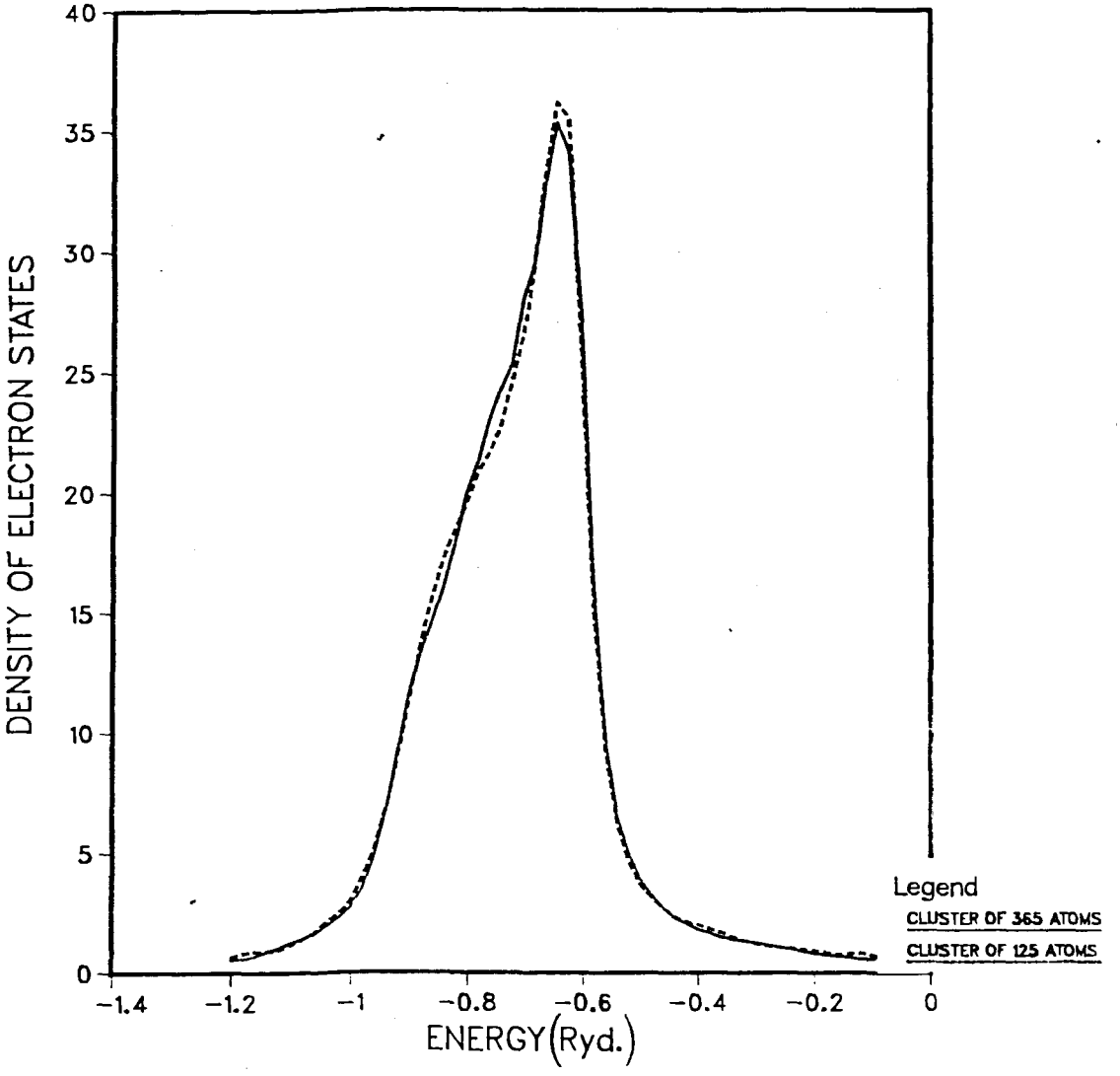

VII. CHAPTER (7)

STUDY OF THE PROPAGATING CHARACTER OF THE STATES

In transition metals like iron, the electrical transport properties are often described according to a picture developed by Mott,[132] which divides the conduction electrons into two categories, namely the s and the d electrons. Thus one can calculate the electrical conductivity by utilising the Boltzmann equation and making an assumption about which of these two types of electrons provides the effective current carriers. Such calculations for liquid iron have been performed on the assumption that it is the s electrons that provide the effective current.[133] On the other hand, calculations based on a hybrid nearly free electron tight-binding (NFE-TB) model and the Kubo-Greenwood formula indicate important d electron contribution to the electrical conductivity in such systems.[134] In order to shed some light on this issue, we have studied the propagating character of the s and the d states in various clusters. We employ a method used by Ballentine[59] to carry out similar studies in liquid La.

For the various clusters, we form Bloch-like running waves of wave vector K,

$$|u_{\vec{k}}^{(\ell)}\rangle = \sum_i e^{i\vec{K}.\vec{R}_i} |\phi_i^{(\ell)}\rangle \quad , \ell = 0, 2 \qquad (7.1)$$

where $\vec{R}_i$ denote the positions of the atomic sites and the $|\phi_i^{\ell}\rangle$'s are either the s or the d states. We then calculate the electronic DOS projected onto this state $|U_{\vec{K}}^{(\ell)}\rangle$. This projected DOS, which we will call the spectral function can be studied as a function of K. If the spectral function shows a sharp peak at a particular energy, then this energy E can be associated with the corresponding K value. A shift in the peak position with changing K would then suggest a dispersion (E vs. K) relation and hence a propagating character of the states. The absence of such a variation can be taken as an indication of weakly propagating or nonpropagating states. This method of studying the propagating character of the states can be considered as the K-space analogue of the method that studies the imaginary part of the Green's function as a function of the position in real space.[135] Similar studies have been carried out by Fujiwara and Tanabe[136] on model amorphous systems with hydrogen-like 1s wave functions.

Figs.(38,39) show the s and the d state spectral functions for several values of K for the liquid cluster, obtained by using the nonsymmetric Hamiltonian model. Figs.(40,41) show similar curves for the amorphous system. The s state spectral functions exhibit well-defined peaks, although they are quite broad in the midband region where s-d hybridisation is strong. The positions of the peaks yield a dispersion relation, suggesting propagating nature of these states. In other words these states retain the memory of the band structure in the

solid to a large extent. The d state spectral functions, on the other hand, show almost complete lack of such memory. These curves, shown in Figs. (39,41), exhibit very little K-dependence. For both the amorphous and the liquid clusters, these d state spectral functions show a sharp peak for small K, which gradually becomes broad as the K value is increased. There is a small change in the peak position with changing K for the amorphous cluster. For the liquid cluster this change is almost imperceptible. Thus the dispersion relation for the d states in the liquid is almost flat, while there is, perhaps, a very small change of E with K in the amorphous cluster. In view of these results, one can at best conclude that these states are only weakly propagating. For comparison, in Fig. (42), we show similar curves for the d state spectral functions in bcc iron, where a definite dispersion can be seen. We conclude that the s electron states in iron retain their propagating character in the disordered phases, while the d states appear to lose this property to a considerable extent.

FIGURE CAPTIONS

FIG.(38,39).

s and d state spectral functions for liquid iron (nonsymmetric Hamiltonian model).

FIG.(40,41).

s and d state spectral functions for amorphous iron (nonsymmetric Hamiltonian model).

FIG.42.

d state spectral functions for bcc iron (nonsymmetric Hamiltonian model).

SPECTRAL FNS. FOR S-STATES IN LIQUID Fe

FIG.(38)

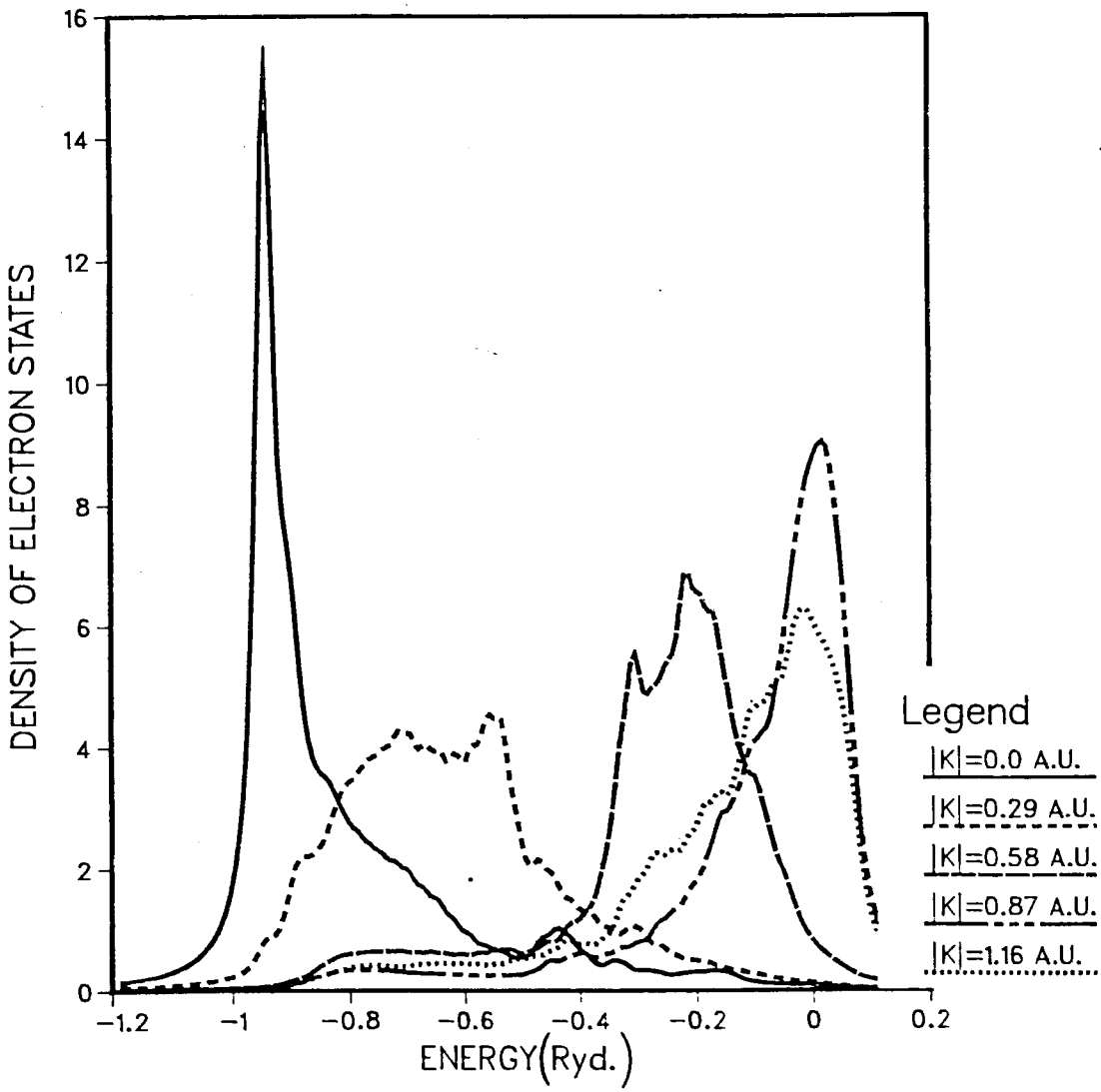

SPECTRAL FNS. FOR D–STATES IN LIQUID Fe

FIG. (39)

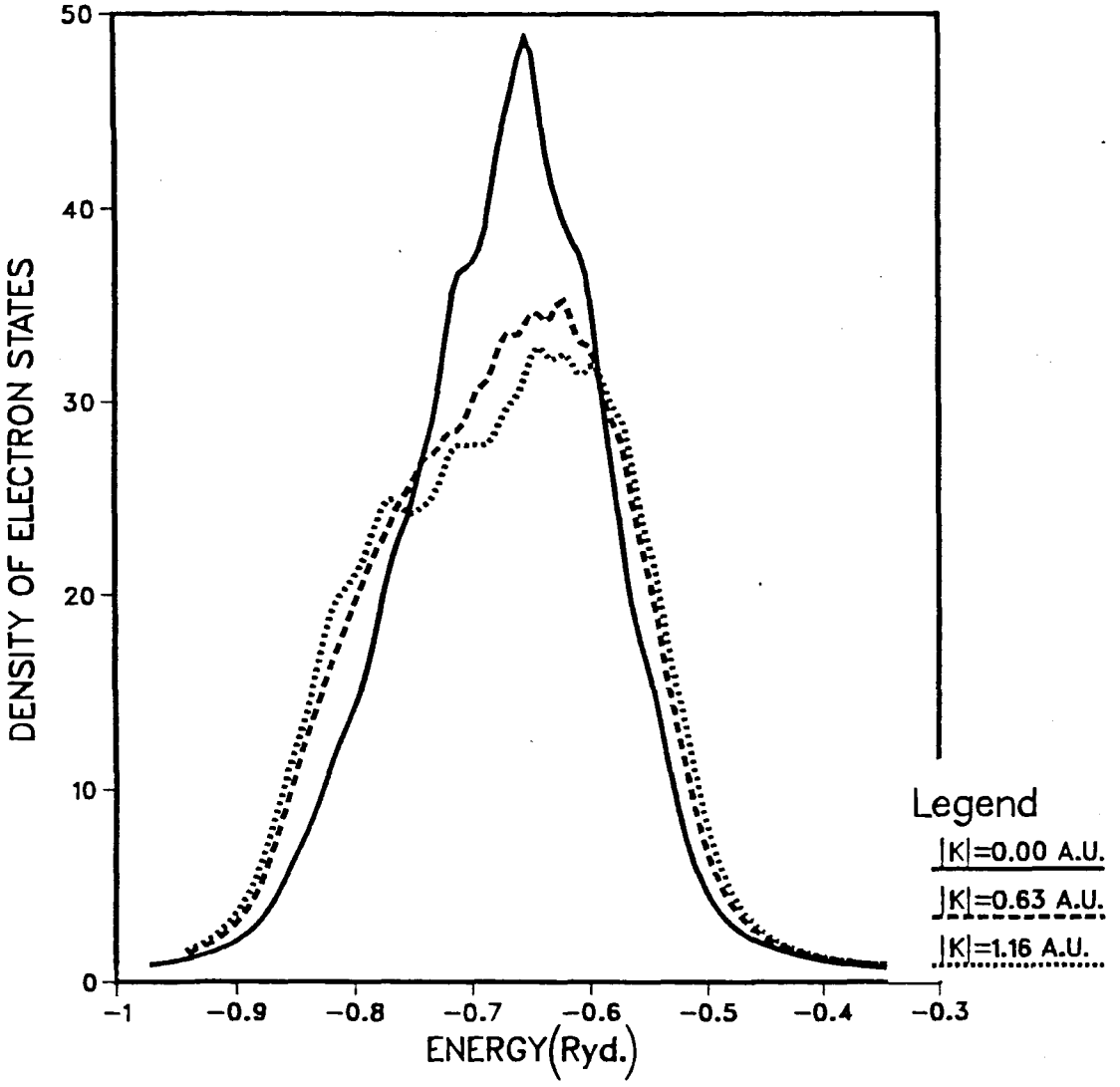

SPECTRAL FNS. FOR S–STATES IN AMORPHOUS Fe

FIG. (40)

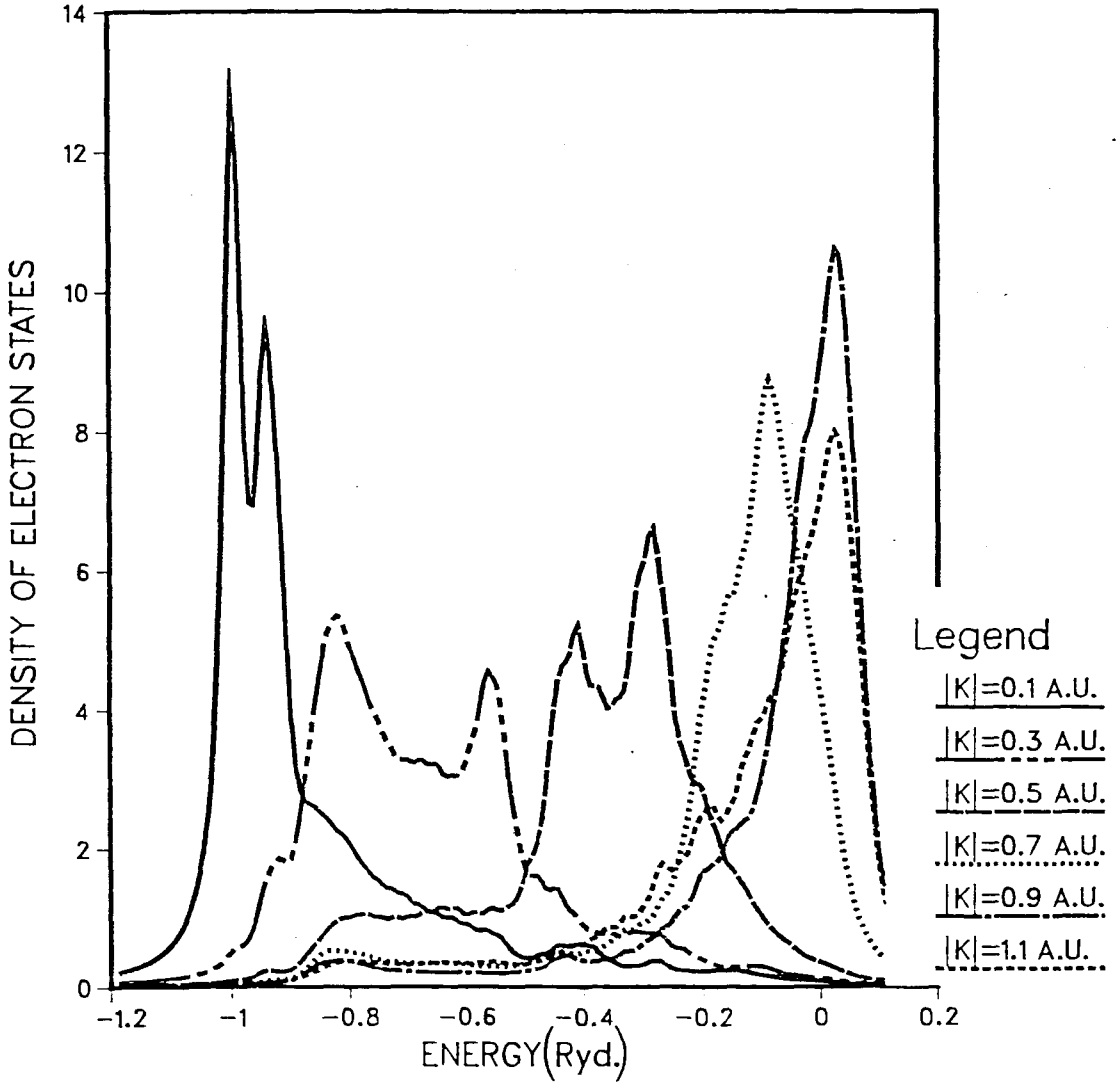

SPECTRAL FNS. FOR D–STATES IN AMORPHOUS Fe

FIG. (41)

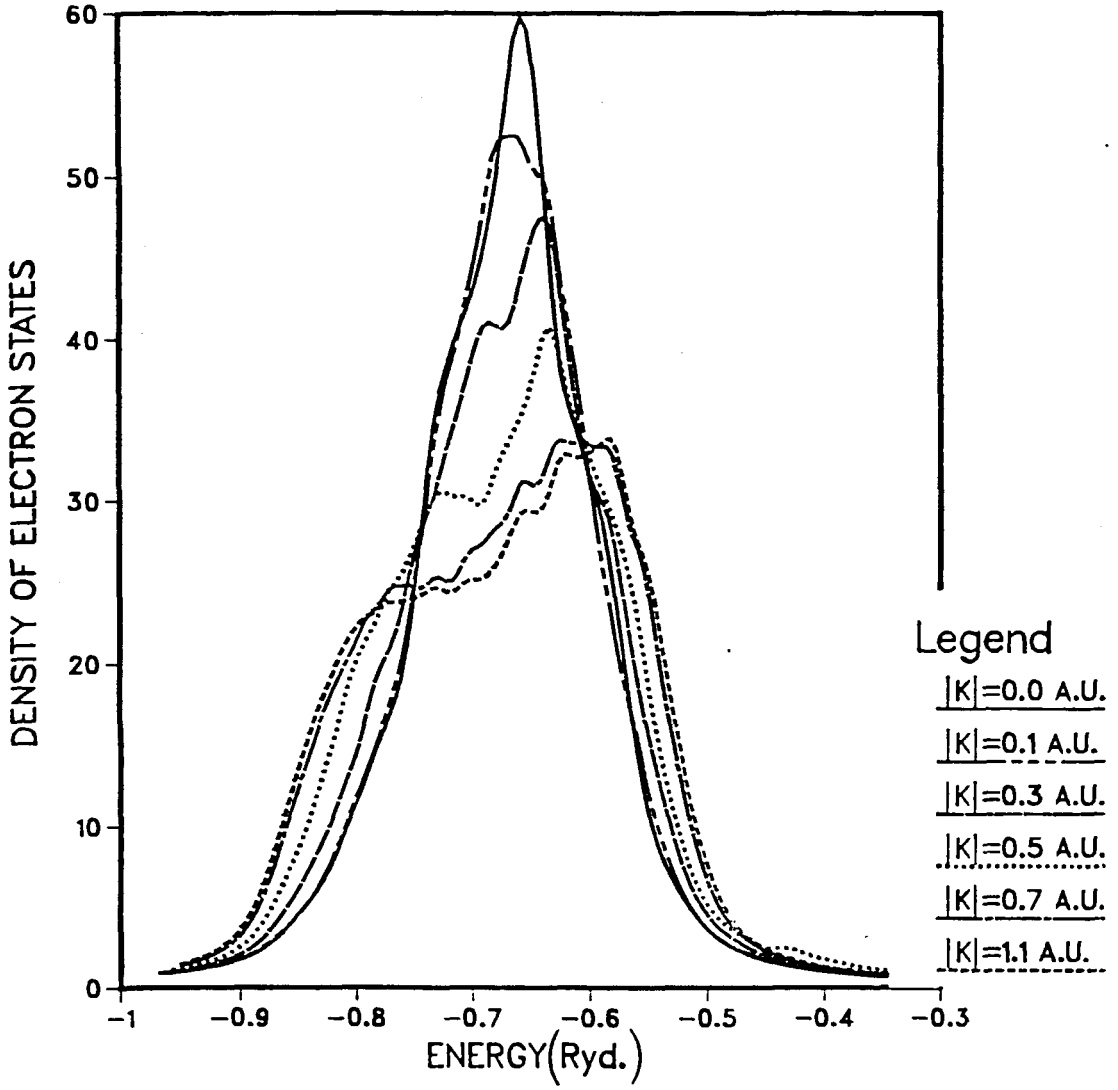

SPECTRAL FNS. FOR D–STATES IN BCC Fe

FIG. (42)

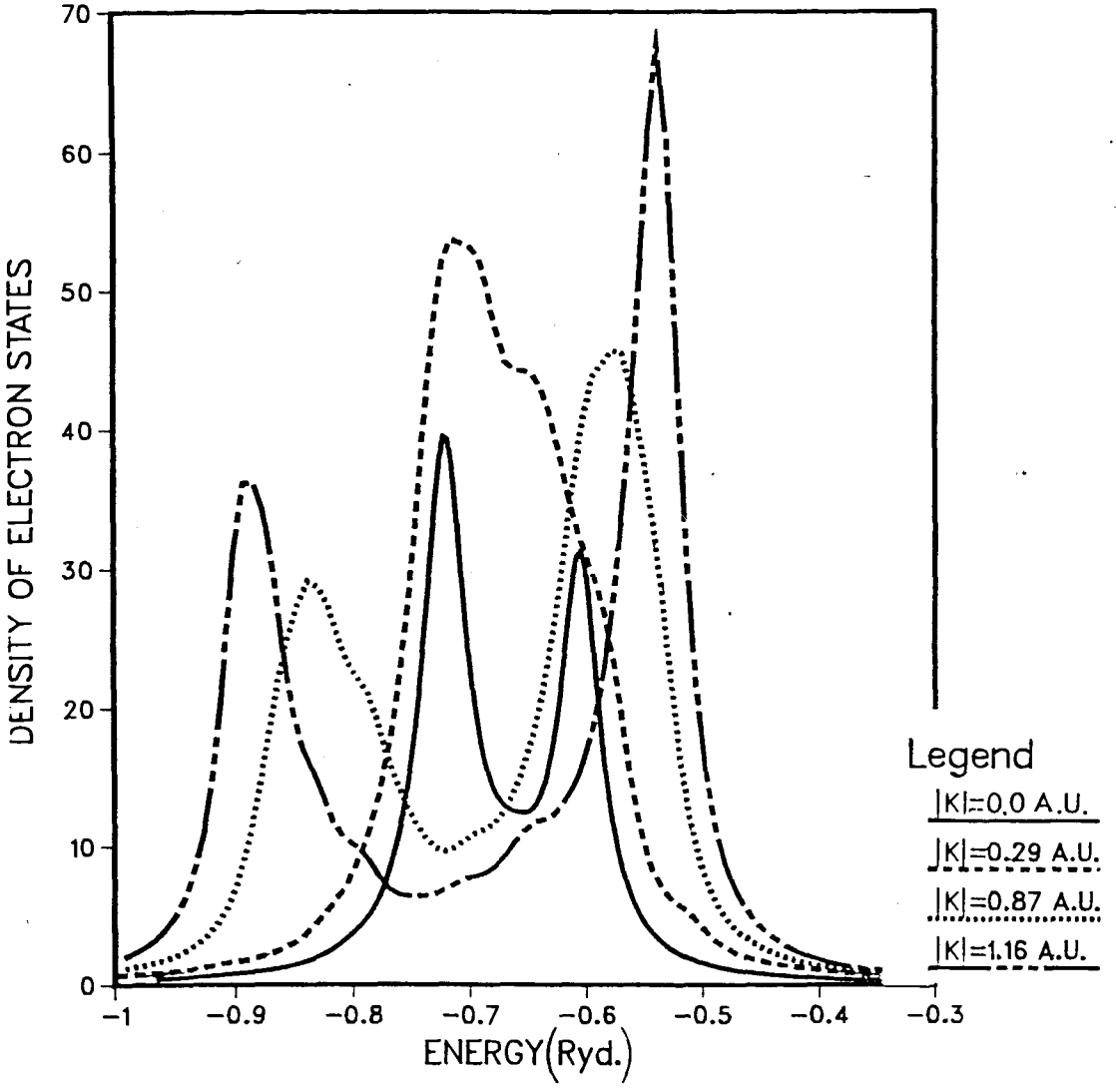

Figs. (43,46) exhibit the results of similar studies done on the symmetric Hamiltonian model. For both the amorphous and the liquid clusters (Figs. 43,45), the s state spectral functions exhibit dispersions, suggesting strongly propagating character of these states. The d state spectra are sharply peaked for small K. These peaks broaden to some extent as the K value is increased. However, there is no appreciable change in the peak position. For higher values of K, these curves look like the local density of states in these systems. It seems that the d states are only weakly propagating compared to the s states in these systems.

FIGURE CAPTIONS

FIG.(43,44).

s and d state spectral functions for liquid iron (symmetric Hamiltonian model).

FIG.(45,46).

s and d state spectral functions for amorphous iron (symmetric Hamiltonian model).

SPECTRAL FNS. FOR S-STATES IN LIQUID Fe

FIG. (43)

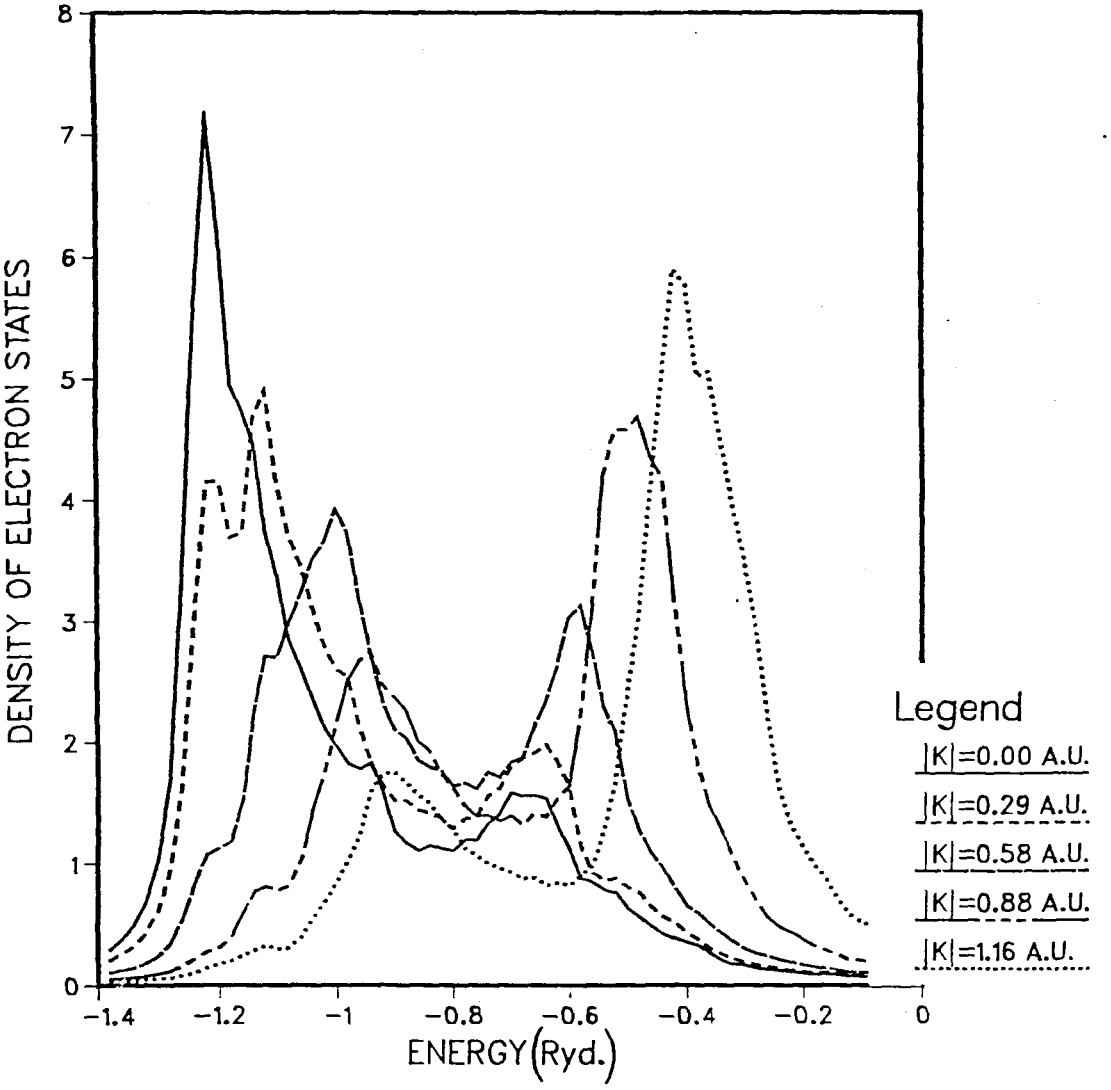

SPECTRAL FNS. FOR D–STATES IN LIQUID Fe

FIG. (44)

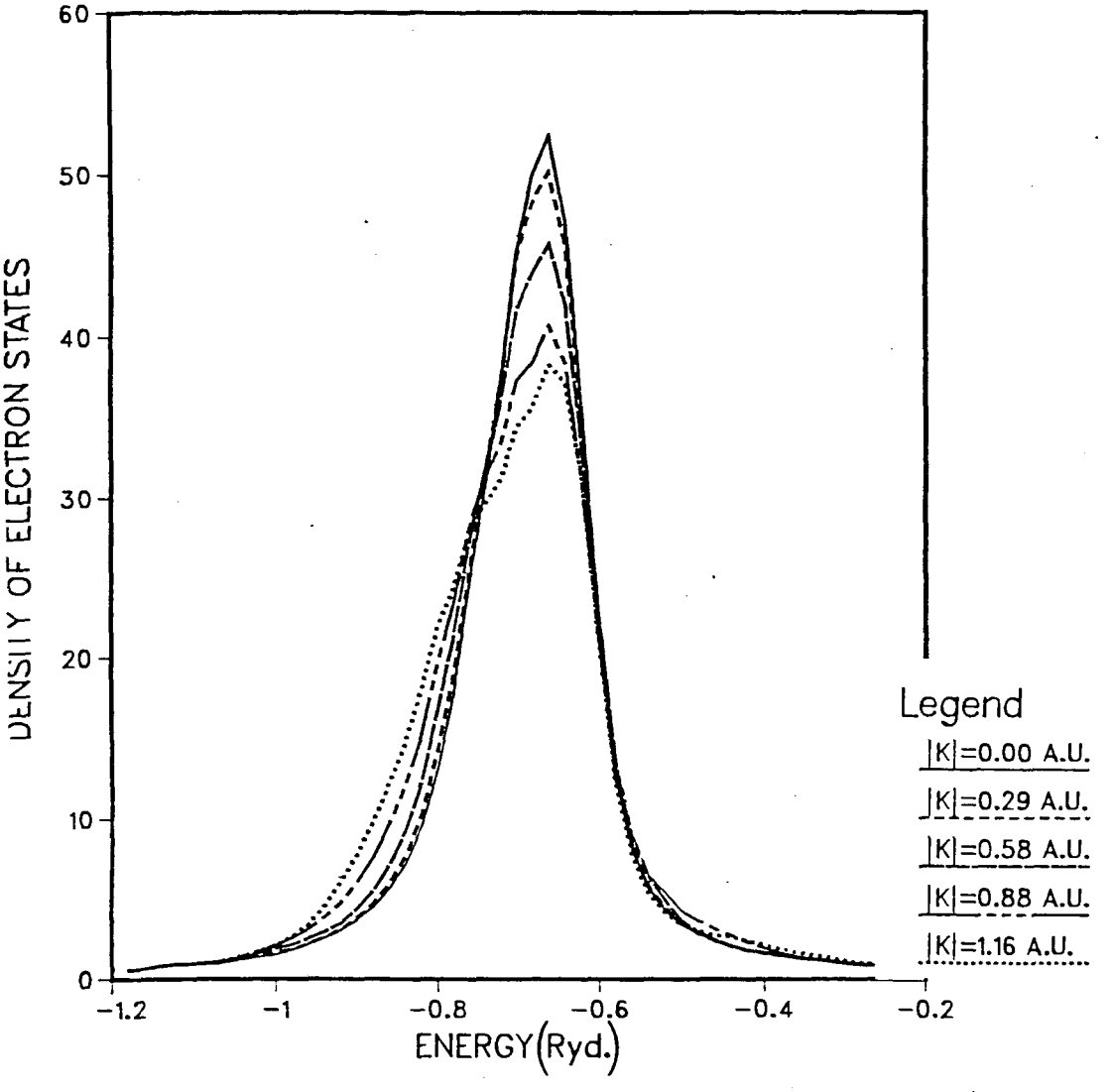

SPECTRAL FNS. FOR S–STATES IN AMORPHOUS Fe

FIG. (45)

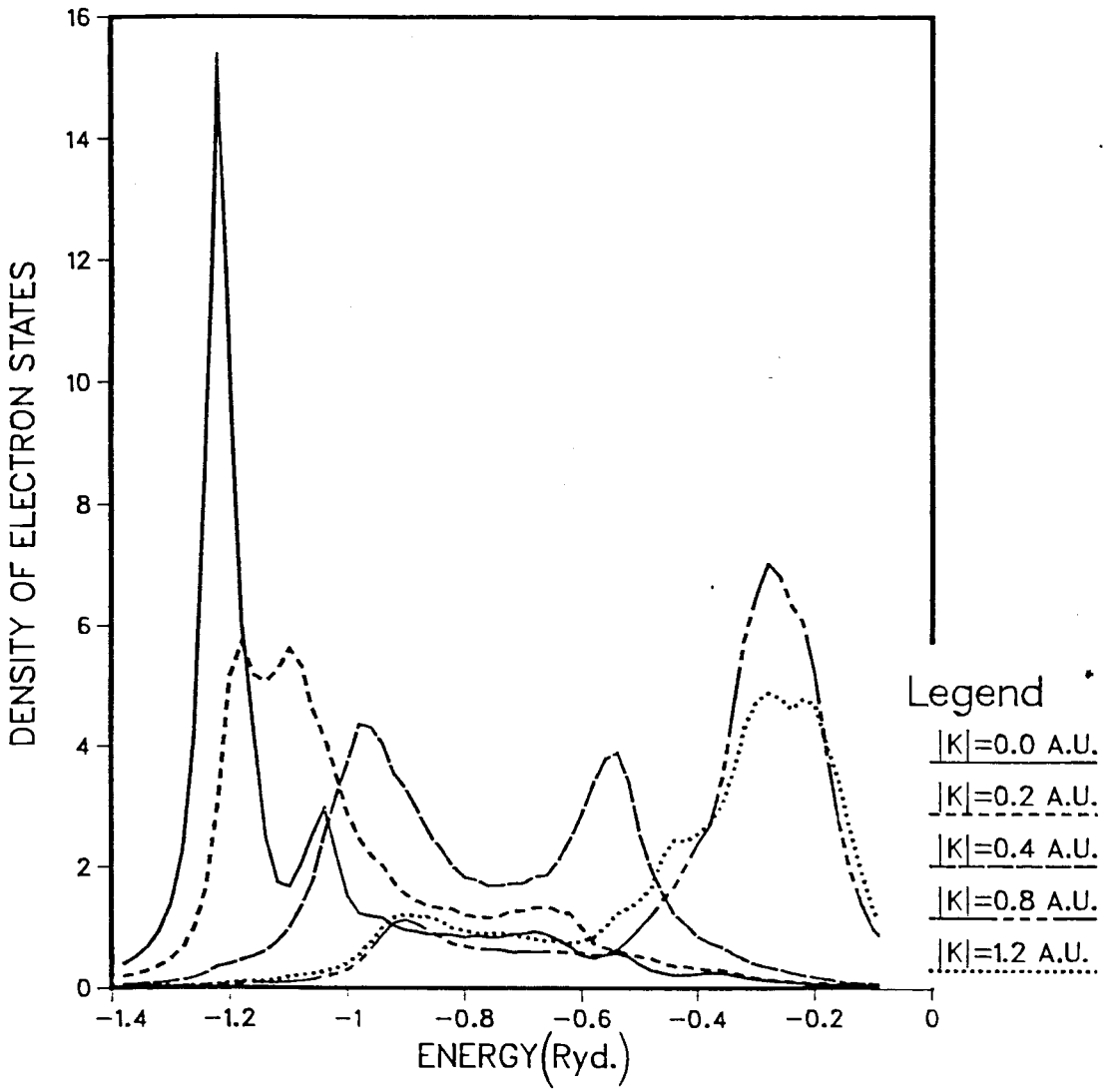

SPECTRAL FNS. FOR D–STATES IN AMORPHOUS Fe

FIG. (46)

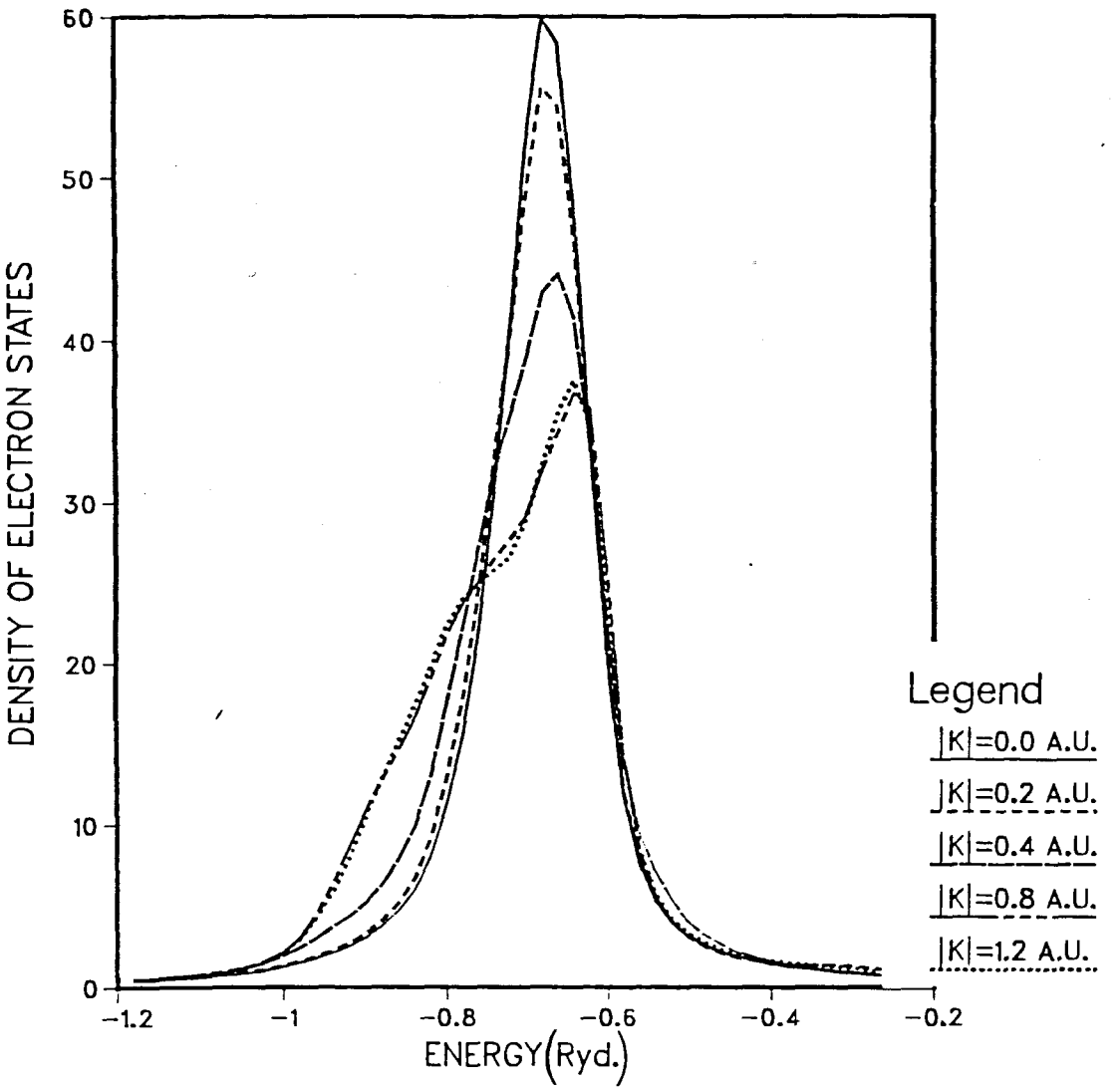

In Figs.(38-46), we have considered the K values in a particular direction (001) only. For a proper comparison one should probably average over various directions for the same value of K. However, in a randomly disordered system like the liquid there should be no significant dependence of the results on the orientation of K with respect to the sides of the cube. We have performed some calculations to verify this for the liquid cluster in both the symmetric and the nonsymmetric Hamiltonian models. Figs.(47-50) show the results for the nonsymmetric Hamiltonian model, while Figs.(51-53) show similar results for the symmetric Hamiltonian model. In both models, the s state spectra for a particular K value in various directions show some change in the peak heights and some fine structure, although the peak position remains the same. This is most probably due to the fact that these states have somewhat large orbit and feel the presence of the boundary to some extent. The d states are more localised than the s and less prone to the effects of the finite cluster size. Thus the d state spectra essentially remain unaltered for various directions of K. Since the shape of the spectral functions is independent of the direction of K, our conclusions regarding the nature of the s and the d states are, therefore, not subject to any changes.

FIGURE CAPTIONS

Spectral functions for s and d states in liquid iron cluster(365 atoms) with $\vec{K}$ in various directions, but having a constant magnitude (indicated in a.u.)

FIG.(47-50) show results for the nonsymmetric Hamiltonian model.

FIG.47. s state,

K_x, K_y, K_z = (0.0,0.0,0.6276) ————————
= (0.6276,0.0,0.0) ----------
= (0.1500,0.4309,0.4309) .....

FIG.48. s state,

K_x, K_y, K_z = (0.0,0.6276,0.0) ————————
= (0.3623,0.3623,0.3623) ----------

FIG.49. d state,

K_x, K_y, K_z = (0.0,0.0,0.6276) ————————
= (0.1500,0.4309,0.4309) ----------

FIG.50. d state,

K_x, K_y, K_z = (0.0,0.6276,0.0) ————————
= (0.6276,0.0,0.0) — — — —
= (0.3623,0.3623,0.3623) ----------

FIG. (47)

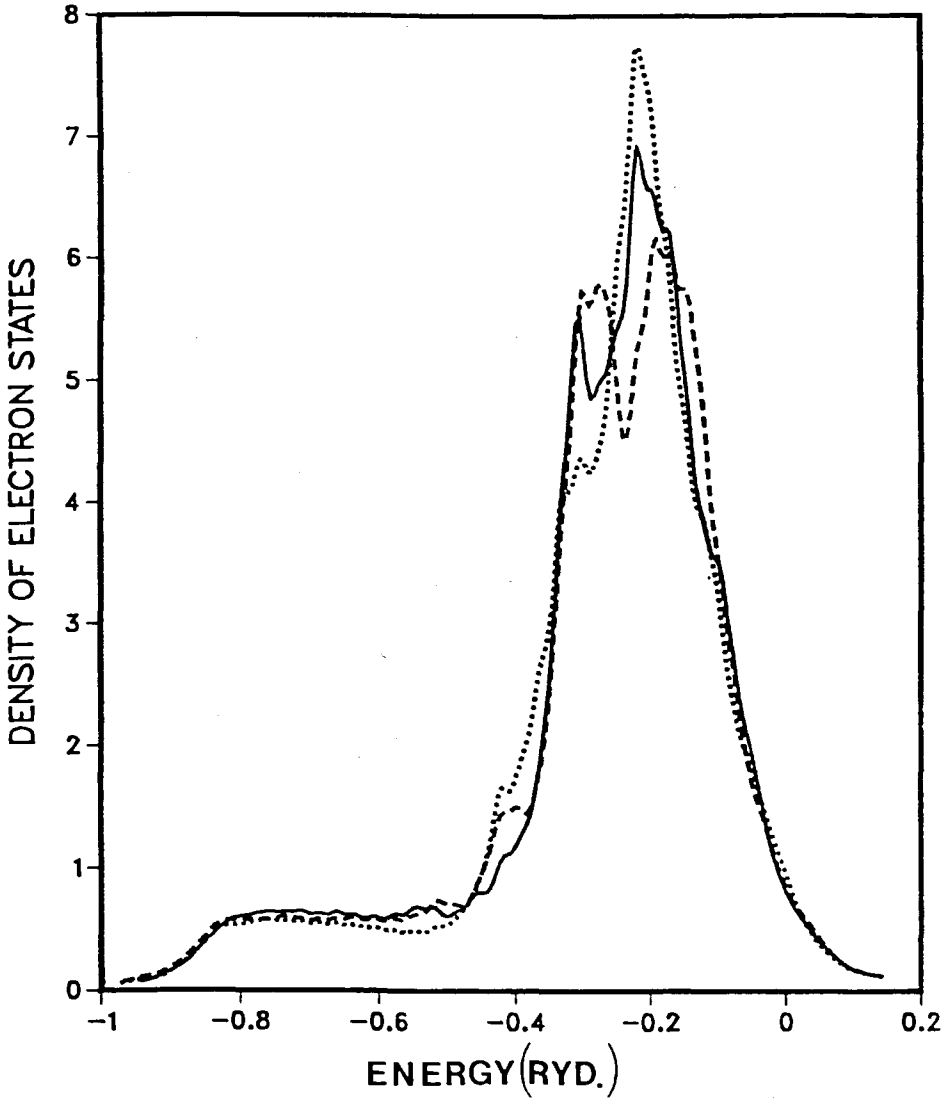
DENSITY OF ELECTRON STATES
8
7
6
5
4
3
2
1
0
−1
−0.8
−0.6
−0.4
−0.2
0
0.2
ENERGY(RYD.)

FIG. (48)

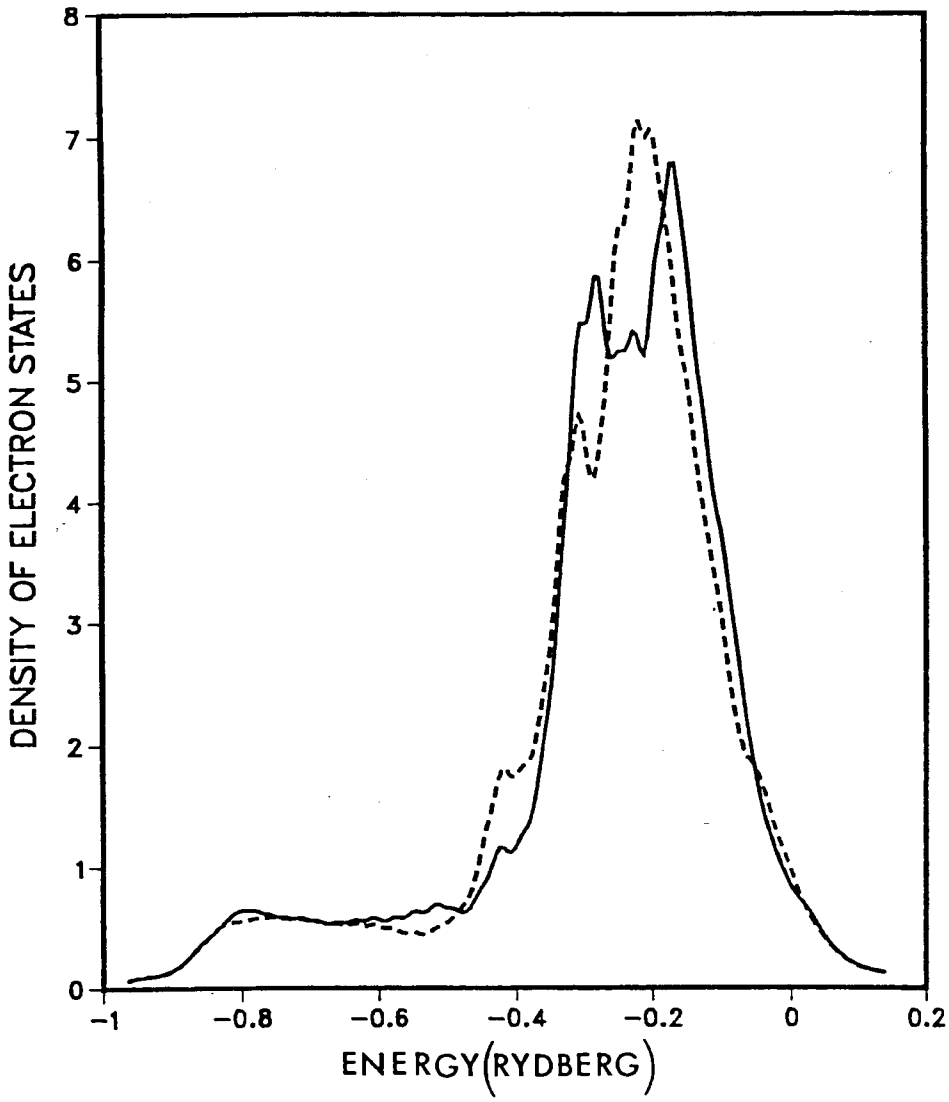
DENSITY OF ELECTRON STATES
8
7
6
5
4
3
2
1
0
−1
−0.8
−0.6
−0.4
−0.2
0
0.2
ENERGY(RYDBERG)

FIG. (49)

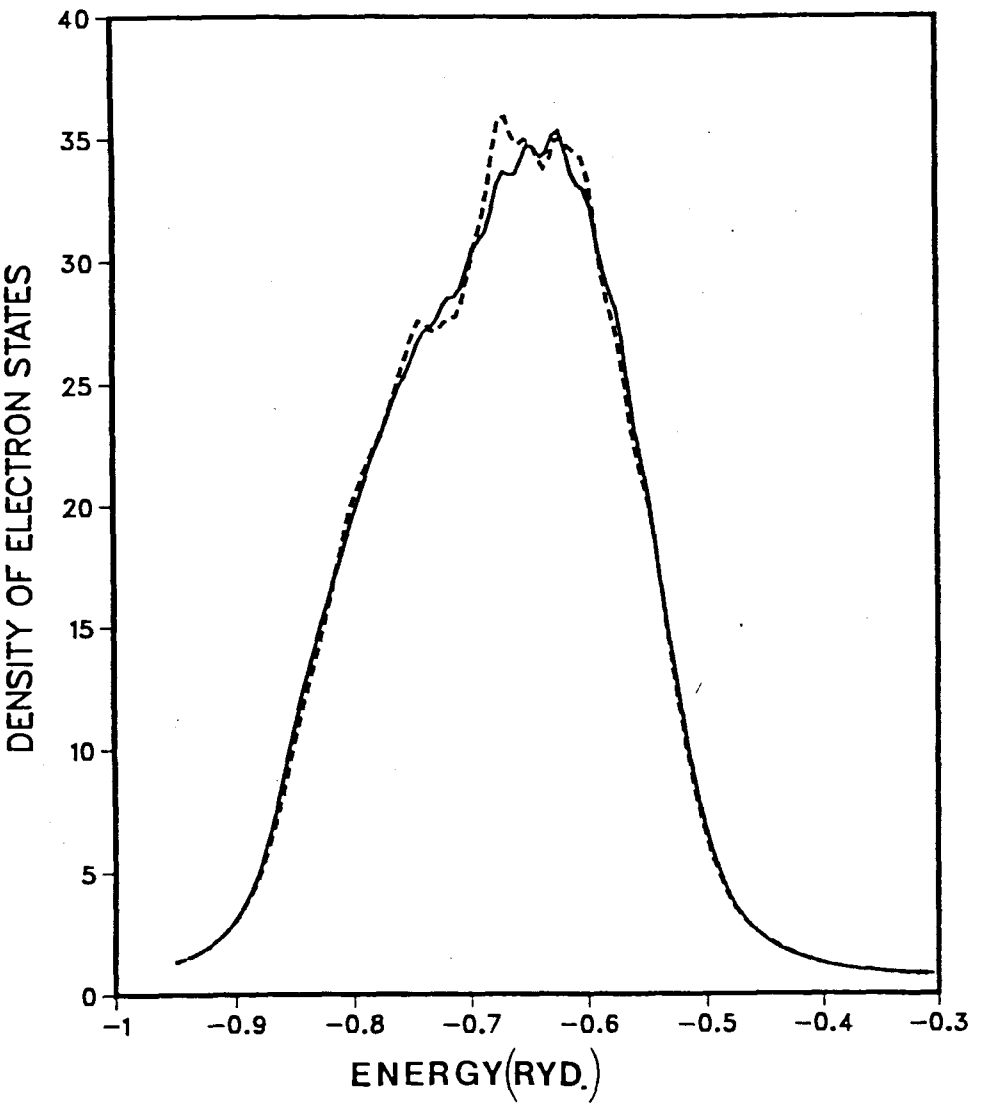
DENSITY OF ELECTRON STATES
40
35
30
25
20
15
10
5
0
−1
−0.9
−0.8
−0.7
−0.6
−0.5
−0.4
−0.3
ENERGY(RYD.)

FIG. (50)

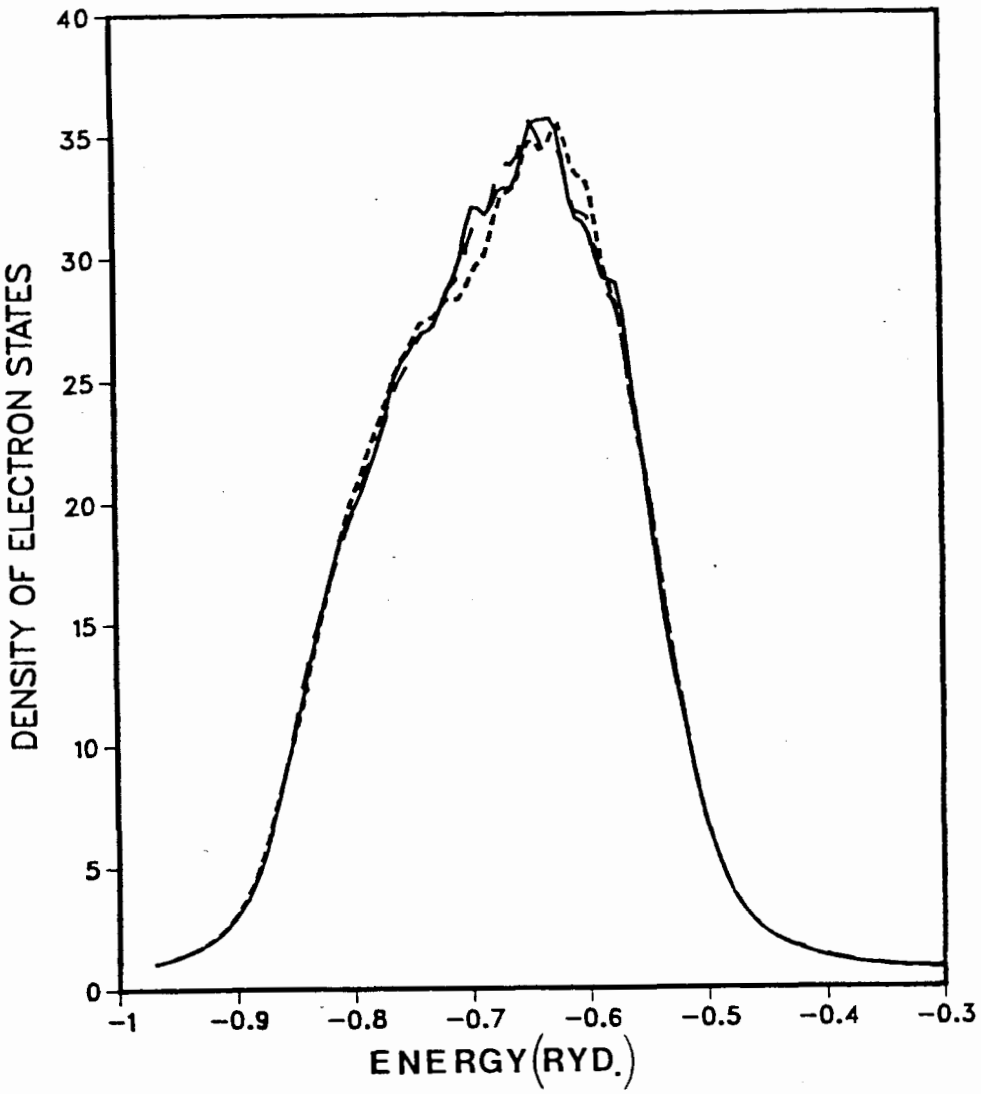
DENSITY OF ELECTRON STATES
40
35
30
25
20
15
10
5
0
−1
−0.9
−0.8
−0.7
−0.6
−0.5
−0.4
−0.3
ENERGY (RYD.)

FIGURE CAPTIONS

Spectral functions for s and d states in liquid iron cluster(365 atoms) with $\vec{K}$ in various directions, but having a constant magnitude (indicated in a.u.)

FIG.(51-53) show results for the symmetric Hamiltonian model.

FIG.51. d state,

K_x, K_y, K_z = (0.0,0.0,0.6276) ————————
= (0.0,0.6276,0.0) ---------
= (0.3623,0.3623,0.3623)
.....

FIG.52. s state,

K_x, K_y, K_z = (0.0,0.0,0.6276) ————————
= (0.0,0.6276,0.0) ---------
= (0.3623,0.3623,0.3623)
.....

FIG.53. s state,

K_x, K_y, K_z = (0.6276,0.0,0.0) ————————
= (0.1500,0.4309,0.4309)

FIG. (51)

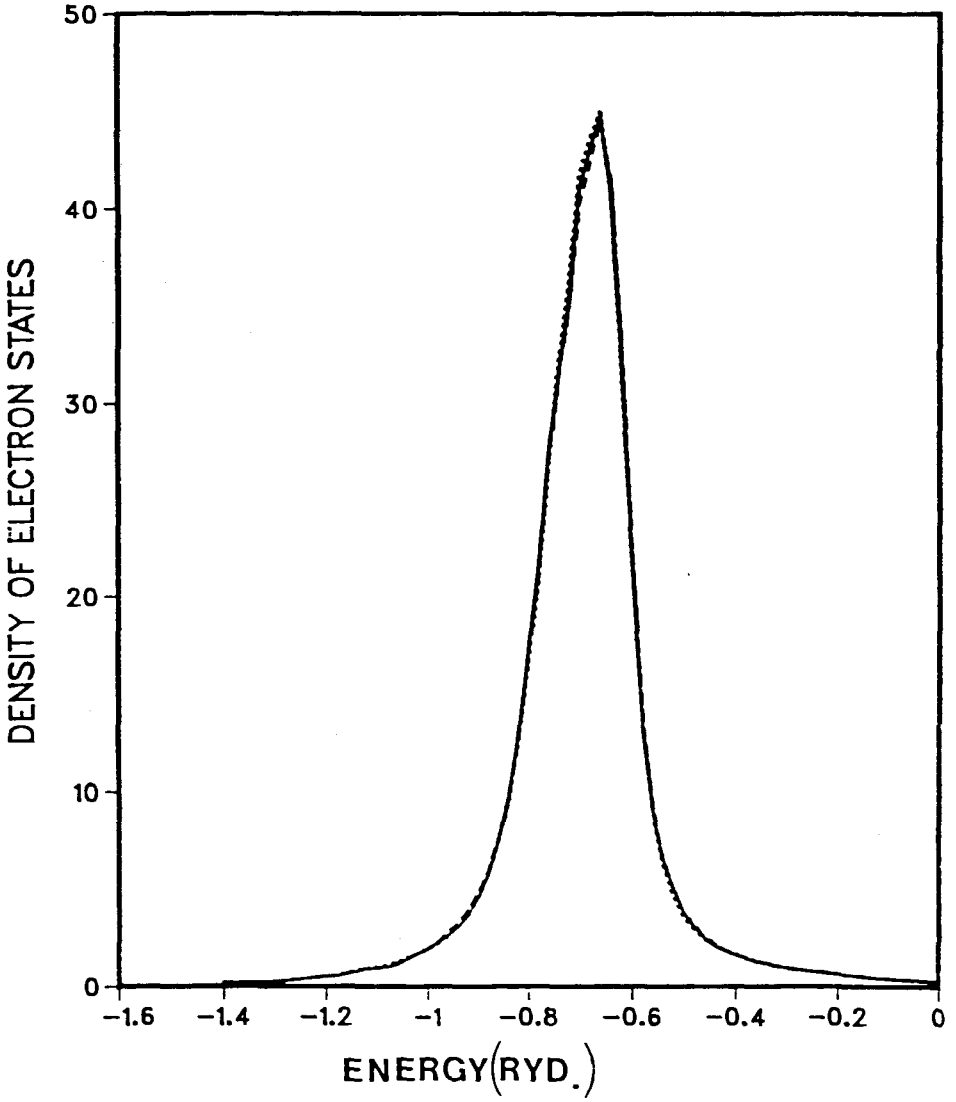
50
40
30
20
10
0
DENSITY OF ELECTRON STATES
−1.6
−1.4
−1.2
−1
−0.8
−0.6
−0.4
−0.2
0
ENERGY(RYD.)

FIG. (52)

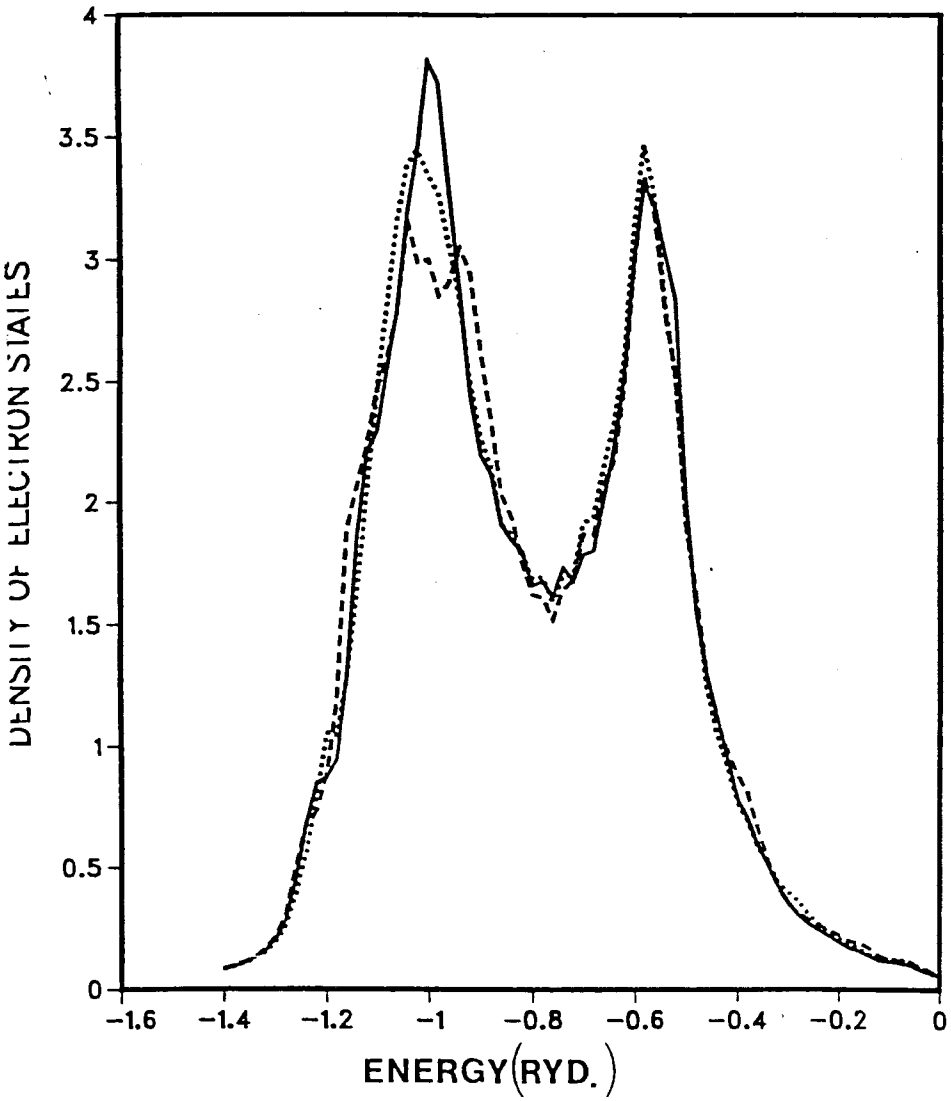
DENSITY OF ELECTRON STATES
4
3.5
3
2.5
2
1.5
1
0.5
0
−1.6
−1.4
−1.2
−1
−0.8
−0.6
−0.4
−0.2
0
ENERGY(RYD.)

FIG.(53)

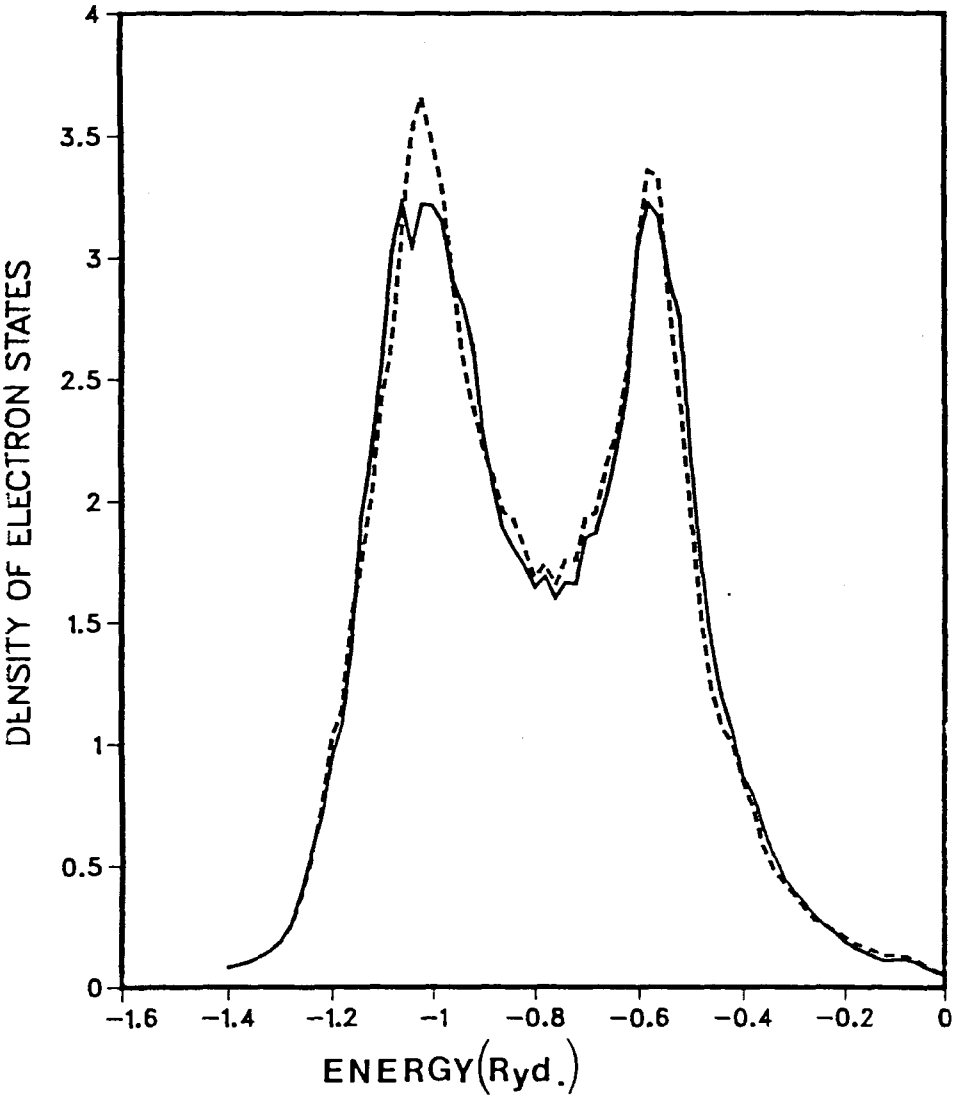
DENSITY OF ELECTRON STATES
4
3.5
3
2.5
2
1.5
1
0.5
0
−1.6
−1.4
−1.2
−1
−0.8
−0.6
−0.4
−0.2
0
ENERGY(Ryd.)

VIII. CHAPTER (8)

COMMENTS AND CONCLUSIONS

In this section we compare our results with similar calculations carried out for liquid and amorphous iron. We also indicate how our results compare with the available experimental data on these systems. And finally we present a summary of the results of the present calculation.

8.1 COMPARISON WITH OTHER CALCULATIONS

Tight-binding cluster calculations like ours have been carried out on models of liquid and amorphous iron by Fujiwara[35] and Fujiwara and Tanabe.[36] However, the Hamiltonian matrices used in these calculations consist of d states only and hence these calculations do not consider the hybridisation effects. Also the transfer matrix elements in these calculations are somewhat artificial in that they are assumed to have a certain distance dependence. These are expressed in terms of the Slater and Koster[137] hopping parameters ($dd\sigma, dd\pi, dd\delta$) and the latter are assumed to have a form

$$dd\mu = V_\mu \left(1 + x + x^2/3\right) exp(-x), \quad x = \frac{|\vec{R}_{ij}|}{A_\mu} \qquad (8.1)$$

where μ stands for either of σ, π or δ and $\vec{R}_{ij}$ is the vector joining the sites i and j, and V_μ and A_μ are constants depending on the particular hopping parameter. This is in contrast with our calculation, where instead of assuming an arbitrary form for the transfer matrix elements, we calculate these explicitly for the actual interatomic separations.

The DOS in the calculation of Fujiwara and Tanabe, obtained by employing the moment method, shows qualitative resemblance with our results. For example, the DOS for the liquid is single-peaked, while that for the amorphous cluster is double-peaked, though the difference in the peak heights is much smaller than in ours. The d band width for the amorphous cluster is approximately the same as in our calculations (0.5Ryd.). However, they obtain a larger d band width for the liquid, while no appreciable change in the band width is observed in our calculations. The density of the d states at the Fermi level is smaller in their calculation (30 states/atom/Ryd. for amorphous and 26 states/atom/Ryd. for the liquid iron, compared to 34 states/atom/Ryd. for amorphous and 30 states/atom/Ryd. for the liquid in our calculation). However the Fermi level in their calculation is only approximate, since it is obtained by assuming that there are 7 d electrons per atom in the liquid and the amorphous systems. This number varies between 7.4 and 7.5 according to our calculations(see tables (1) and (2)).

Fujiwara's results, obtained by employing the recursion method, are similar to those obtained by Fujiwara and Tanabe.

The LDS in both clusters is found to undergo significant changes from one site to another. Such drastic changes are not seen in our calculations.

A recent calculation for amorphous iron by Fujiwara,[37] based on the linear combination of muffin-tin orbital method in the atomic sphere approximation (see Bullett, Ref. 95, section 15), offers better agreement with our results. In this calculation the model consists of both the s and the d electron states. The density of states at the Fermi level (~31 states/atom/Ryd.) is close to the value obtained by us (34 states/atom/Ryd.). This calculation by Fujiwara shows significant change in the DOS due to s-d hybridisation in the entire energy range. The curve for the unhybridised d density of states is much narrrower than the hybridised one. Also the double peaked nature of the d density of states is much more pronounced without hybridisation. Our calculations show similar hybridisation effects, only to a lesser degree.

Asano and Yonezawa[32] have calculated the electronic DOS in liquid transition metals by using the KKR method for the Green's function. The liquid is treated as a system with nonoverlapping muffin tin potentials, and the ensemble averaged Green's function is calculated by employing various self-consistent single site approximations. Among these approximations, only the effective medium approximation of Roth[30] is found to yield reasonable result for the DOS over the entire energy range. Asano and Yonezawa carry out the explicit calculations only for

liquid Ni and then predict the DOS curves for other 3d transition metals by appealing to the rigid band approximation. This DOS curve is similar to ours in shape. The d band width is 0.5 Ryd. as in our calculation. However, N(Ef) i.e. the DOS at the Fermi level is 36 states/atom/Ryd. as compared with a value of 30 states/atom/Ryd. in our calculation.

Keller et al[24] have used the cluster method of Mcgill, Klima and Ziman[25] to calculate the DOS in solid and liquid iron. Their calculation generates somewhat different results. The DOS curve for the bcc iron shows one narrow and high peak with three low peaks, as compared with the double peaked structure in our calculation. The DOS for the liquid shows fine structure and peaks, not observed in any of the calculations discussed above.

8.2 COMPARISON WITH EXPERIMENTAL RESULTS

Detailed profile of the electronic DOS in bulk condensed matter can be obtained from various experiments, such as photoemission, soft x-ray emission, positron annihilation and Compton scattering etc. However, extracting this information from the exprimentally observed energy distribution of the emitted electrons or the photons is often a difficult task. For example, photoemission can be envisaged as a three-step process consisting of 1) optical excitation of an electron, 2) transport to the surface and 3) escape into the vacuum. It is difficult to estimate the energy lost by the electron during the processes 2) and 3). There is also the problem of separating the surface from

the bulk contributions. Usually one writes the distribution of electrons photoemitted with energy E as

$$I(E,\hbar\omega) = \sum_{if} |\langle f|H|i\rangle|^2 \, \delta(E_f - E_i - \hbar\omega) \, \delta(E - E_f) \qquad (8.2)$$

where $\hbar\omega$ is the photon energy and H is the interaction operator. It is sometimes further assumed that the matrix elements of transition are constant. This yields

$$I(E,\hbar\omega) = C \, \eta(E) \, \eta(E-\hbar\omega) \qquad (8.3)$$

i.e., the energy distribution of the photoemitted electrons is supposed to be proportional to the product of the initial and the final density of states. Eqn. (8.3) has been used by Williams and Norris[138] to compare the energy distribution of the photoemitted electrons in liquid Cu with the theoretically calculated results for the density of states. However, no such experiment has been performed for liquid or amorphous iron. The transition matrix elements may play an important role in determining the energy distribution of the photoemitted electrons. The theory to calculate such matrix elements in case of surface photoemission has been provided by McLean and Haydock.[139]

X-ray emission and absorption experiments offer information regarding the band width. While the emission experiments yield the width of the occupied portion of the valence band, the absorption experiments can be used to extract information regarding the unoccupied part of the band. Also the selection

rules (under the dipole approximation) governing the transitions to and from the core levels make the K emission (valence band→ 1s) and absorption (1s→conduction band) experiments reflect only the p like character of the band, while the L emission (valence band→2p) or absorption (2p→conduction band) experiments show the s and the d character. Many body effects and the lack of accurate knowledge of the transition matrix elements make it difficult to extract information about the magnitude of the density of states from the intensity distribution curves. However, the information about the band width can be obtained. Such experiments on liquid iron have been performed by Garg and Källne[140] and Hague et al.[141] The K emission experiment of Garg and Källne shows no change in the intensity distribution curve from the solid to the liquid. The width of the occupied band remains unaltered and the half-width of the band is found to be (7.5 ± 0.5)eV. The L3 emission (valence band $\longrightarrow 2p_{3/2}$) and absorption ($2p_{3/2} \longrightarrow$ conduction band) experiments on solid and liquid iron by Hague et al bear similar results. The L3 emission of liquid Fe is indistinguishable from the solid. The absorption curves for these two systems are only slightly different, suggesting small modification in the density of unoccupied states of the conduction band. However, this is reported only as a tentative conclusion by Hague et al. No change is observed at the Fermi level in the emission or the absorption curves. The band width from the emission experiment is approximately 10eV.

Positron annihilation and Compton scattering experiments yield information about the momentum distribution $N(\vec{k})$ of the conduction electrons. Theoretically this can be calculated from the spectral function $\rho(\vec{k},E)$, which is the density of states projected onto plane wave states of wave vector $\vec{k}$,

$$N(\vec{k}) = \int_{-\infty}^{E_f} \rho(\vec{k},E)\, dE \qquad (8.4)$$

The data available from positron annihilation experiments are difficult to interpret on account of the many-electron effects involved. The positron-electron interaction results in the polarisation of the background and the response of the interacting electron gas. So far these experiments have not been performed for liquid or amorphous iron. Compton scattering experiments provide reliable data on the momentum distribution of the electrons. Since the photon interacts only weakly with the electrons, the experiment measures effectively the unperturbed momentum distribution. Unfortunately such experiments have not been performed for liquid or amorphous transition metals.

Meyer et al[142] have proposed a method of evaluating N(Ef), the DOS at the Fermi level, in liquid transition metals from the measured structure factors and entropies. Assuming that the theory originally proposed for simple liquid metals by Silbert et al[143] works also for liquid transition metals, they express the total entropy St as a sum of three terms; Sg, the entropy of the ideal gas; Sp, the excess entropy described by the hard sphere

model and Se, the entropy due to electrons. The last term, in the first order in temperature, is given by

$$Se = \pi^2/3\ N(E_f)\ k_B^2\ T \qquad (8.5)$$

Since St is observed and Sg and Sp can be calculated when temperature, the density and the packing fraction are known, Se or N(Ef) can be calculated. However, Sg and Sp sum up to 80% of St. Thus even a few percent error in St will cause a difference in N(Ef) as much as a factor of two or even larger. Therefore the theory is useful for evaluating the total entropy theoretically from the calculated N(Ef), but not for evaluating N(Ef) from the observed total entropy, except perhaps for an order of magnitude estimate of N(Ef). Utilising this idea we calculate the total entropy of liquid iron at 1560°C. We use the value of the packing fraction quoted by Meyer et al.[142] Using the value of N(Ef) obtained in our calulation (30 states/atom/Ryd.) we obtain a value of 11.4 Kb/atom (Kb is the Boltzmann constant) for the total entropy in liquid iron, which compares well with the experimental value of 12 Kb/atom.

8.3 SUMMARY OF RESULTS

The results of the present calculations are summarised as follows:

1. The double-peaked structure of the electronic DOS in bcc iron is found to survive in the amorphous but not in the liquid phase. There is a gradual smoothing of the structure

as one goes from the bcc to the amorphous and then to the liquid state.

2. There is no appreciable change in the band width from one system to another. X-ray emission measurements on solid and liquid iron tend to support this result.
3. There is a small decrease in the DOS at the Fermi level as we go from the amorphous and then to the liquid phase (see Tables 1 and 2).
4. The DOS in the liquid and the amorphous iron is closer to that of the fcc than the bcc iron.
5. In calculating the local density of states, the Recursion method of Haydock, Heine and Kelly is found to be considerably faster than the equation of motion method. However, the results obtained by the two methods are very similar.
6. A study of the dispersion relation of the s and the d states in various clusters reveals that the s states retain their propagating character in the disordered phases, while the d states in these clusters can at best be said to be weakly propagating. However, this does not imply that the contribution of these d states to the electrical conductivity in these systems is small compared to that due to the s states. A tight-binding calculation of resistivity based on the Kubo formula is required to resolve this issue.

IX. APPENDIX

(A-1)

In this section we will derive some results involving vectors and matrices in a nonorthogonal basis, which we have used earlier in the main body of the thesis. For convenience, we will use a notation involving raised and lowered indices and follow the convention of summing over the repeated indices.

a) THE IDENTITY OPERATOR

Let $\{|\phi_\alpha\rangle\}$ form a complete set of nonorthogonal but linearly independent basis vectors in a linear vector space V. Any general vector $|\psi_i\rangle$ in this vector space can be written as a linear combination of $|\phi_\alpha\rangle$'s :

$$|\psi_i\rangle = C_i^{\alpha} |\phi_\alpha\rangle \tag{A.1}$$

If $\{|\psi_i\rangle\}$ form a complete set of orthonormal vectors spanning the same space V, then the identity operator I in this space can be written as

$$I = |\psi_i\rangle\langle\psi_i| \tag{A.2}$$

Using expansion of type (A.1),

$$I = C_i^{\alpha} C_i^{\beta *} |\phi_\alpha\rangle\langle\phi_\beta| \tag{A.3}$$

Let $S_{\alpha\beta}$ represent the elements of the overlap matrix for the basis $\{|\phi_\alpha\rangle\}$, i.e.,

$$\langle \phi_\alpha | \phi_\beta \rangle = S_{\alpha\beta} \qquad (A.4)$$

If the basis vectors $|\phi_\alpha\rangle$ are normalised, then the diagonal elements of S are unity. The elements of the inverse, S^{-1}, of the overlap matrix will be given by

$$(S^{-1})^{\alpha\beta} S_{\beta\gamma} = \delta^\alpha{}_\gamma ,$$

$$S_{\alpha\beta} (S^{-1})^{\beta\gamma} = \delta_\alpha{}^\gamma \qquad (A.5)$$

Taking the inner product of both sides in eqn. (A.1) with $|\phi_\beta\rangle$, we obtain

$$\langle \phi_\beta | \psi_i \rangle = C_i{}^\alpha S_{\beta\alpha} \qquad (A.6)$$

Using (A.5),

$$(S^{-1})^{\gamma\beta} \langle \phi_\beta | \psi_i \rangle = C_i{}^\alpha (S^{-1})^{\gamma\beta} S_{\beta\alpha} = C_i{}^\alpha \delta^\gamma{}_\alpha = C_i{}^\gamma$$

Using this expression for $C_i{}^\gamma$ in (A.3), we have

$$I = (S^{-1})^{\alpha\gamma} \langle \phi_\gamma | \psi_i \rangle \left[(S^{-1})^{\beta\delta} \langle \phi_\delta | \psi_i \rangle \right]^* | \phi_\alpha \rangle \langle \phi_\beta |$$

$$= (S^{-1})^{\alpha\gamma} \langle \phi_\gamma | \psi_i \rangle (S^{-1})^{\beta\delta *} \langle \psi_i | \phi_\delta \rangle | \phi_\alpha \rangle \langle \phi_\beta |$$

Using (A.2), we can write

$$\langle \phi_\gamma | \psi_i \rangle \langle \psi_i | \phi_\delta \rangle = S_{\gamma\delta}$$

Thus

$$I = (S^{-1})^{\alpha\gamma} S_{\gamma\delta} (S^{-1})^{\beta\delta *} |\phi_\alpha\rangle\langle\phi_\beta|$$

$$= \delta^\alpha{}_\delta (S^{-1})^{\delta\beta} |\phi_\alpha\rangle\langle\phi_\beta|$$

$$= |\phi_\alpha\rangle (S^{-1})^{\alpha\beta} \langle\phi_\beta| \qquad (A.7)$$

This is the expression for the identity operator in the nonorthogonal basis $\{|\phi_\alpha\rangle\}$.

For convenience, we sometimes write (A.7) in a slightly different form. To do this we introduce kets with raised indices

$$|\phi^\alpha\rangle = |\phi_\beta\rangle (S^{-1})^{\beta\alpha} \qquad (A.8)$$

The inverse relationship is

$$|\phi_\beta\rangle = |\phi^\alpha\rangle S_{\alpha\beta} \qquad (A.9)$$

The bra corresponding to the ket $|\phi^\alpha\rangle$ will be given by

$$\langle\phi^\alpha| = (S^{-1})^{\alpha\beta} \langle\phi_\beta| \qquad (A.10)$$

and the inverse relationship is given by

$$\langle\phi_\alpha| = S_{\alpha\beta} \langle\phi^\beta| \qquad (A.11)$$

The vectors $|\phi^\alpha\rangle$ and $|\phi_\beta\rangle$ form a biorthogonal set, i.e.,

$$\langle\phi^\alpha|\phi_\beta\rangle = (S^{-1})^{\alpha\gamma}\langle\phi_\gamma|\phi_\beta\rangle = (S^{-1})^{\alpha\gamma} S_{\gamma\beta} = \delta^\alpha{}_\beta \qquad (A.12)$$

and $$\langle\phi_\alpha|\phi^\beta\rangle = \langle\phi_\alpha|\phi_\gamma\rangle (S^{-1})^{\gamma\beta} = \delta_\alpha{}^\beta \qquad (A.13)$$

The matrix elements $(S^{-1})^{\alpha\beta}$ are the inner products of the kets with raised indices. This follows by taking the inner product of both sides of (A.8) with $|\phi^{\gamma}\rangle$:

$$\langle\phi^{\gamma}|\phi^{\alpha}\rangle = \langle\phi^{\gamma}|\phi_{\beta}\rangle(S^{-1})^{\beta\alpha} = \delta^{\gamma}{}_{\beta}(S^{-1})^{\beta\alpha}$$
$$= (S^{-1})^{\gamma\alpha} \qquad (A.14)$$

In terms of the kets and bras with raised indices, the identity operator has the following representation :

$$I = |\phi_{\alpha}\rangle(S^{-1})^{\alpha\beta}\langle\phi_{\beta}| = |\phi^{\beta}\rangle\langle\phi_{\beta}| = |\phi_{\alpha}\rangle\langle\phi^{\alpha}| . \qquad (A.15)$$

b) REPRESENTATIONS OF OPERATORS

The representation of an operator in the basis of the nonorthogonal vectors $\{|\phi_{\alpha}\rangle\}$ is obtained as follows :

$$A = |\phi_{\alpha}\rangle(S^{-1})^{\alpha\beta}\langle\phi_{\beta}|A|\phi_{\gamma}\rangle(S^{-1})^{\gamma\delta}\langle\phi_{\delta}|$$

$$= |\phi_{\alpha}\rangle(S^{-1})^{\alpha\beta}A_{\beta\gamma}(S^{-1})^{\gamma\delta}\langle\phi_{\delta}|$$

$$= |\phi_{\alpha}\rangle A^{\alpha\delta}\langle\phi_{\delta}| , \qquad (A.16)$$

where

$$A_{\beta\gamma} = \langle\phi_{\beta}|A|\phi_{\gamma}\rangle$$

and $$A^{\alpha\delta} = (S^{-1})^{\alpha\beta}A_{\beta\gamma}(S^{-1})^{\gamma\delta} = \langle\phi^{\alpha}|A|\phi^{\delta}\rangle \qquad (A.17)$$

Introducing the matrix elements

$$A^{\alpha}{}_{\delta} = \langle \phi^{\alpha} | A | \phi_{\delta} \rangle \quad , \; A_{\alpha}{}^{\delta} = \langle \phi_{\alpha} | A | \phi^{\delta} \rangle \quad ; \quad (A.18)$$

we can write

$$A = |\phi_{\alpha}\rangle \, A^{\alpha\delta} \langle \phi_{\delta}| = |\phi^{\alpha}\rangle \, A_{\alpha\delta} \langle \phi^{\delta}|$$

$$= |\phi^{\alpha}\rangle \, A_{\alpha}{}^{\delta} \langle \phi_{\delta}| = |\phi_{\alpha}\rangle \, A^{\alpha}{}_{\delta} \langle \phi^{\delta}| \; . \qquad (A.19)$$

The action of an operator A on the ket $|\phi_{\beta}\rangle$ generates a linear combination of $|\phi_{\alpha}\rangle$'s, i.e.,

$$A|\phi_{\beta}\rangle = |\phi_{\alpha}\rangle \langle \phi^{\alpha}| A |\phi_{\beta}\rangle$$

$$= A^{\alpha}{}_{\beta} \, |\phi_{\alpha}\rangle$$

In particular, the Hamiltonian operator, H, acting on $|\phi_{\beta}\rangle$ will yield

$$H|\phi_{\beta}\rangle = H^{\alpha}{}_{\beta} |\phi_{\alpha}\rangle \; .$$

In section (3.1) we used the notation

$$H|\phi_{\beta}\rangle = D_{\alpha\beta} |\phi_{\alpha}\rangle \; .$$

Thus $D_{\alpha\beta} = H^{\alpha}{}_{\beta} = \langle \phi^{\alpha}| H |\phi_{\beta}\rangle$

$$= \langle \phi^{\alpha} | \phi^{\gamma} \rangle \langle \phi_{\gamma}| H |\phi_{\beta}\rangle = (S^{-1})^{\alpha\gamma} H_{\gamma\beta}$$

$$= (S^{-1}H)^{\alpha}{}_{\beta}$$

While $[H^{\alpha}{}_{\beta}]$ or equivalently $[D_{\alpha\beta}]$ represents the Hamiltonian matrix, the elements of this matrix are different from the matrix elements of the Hamiltonian $H_{\alpha\beta}$. This distinction disappears when the basis $\{|\phi_\alpha\rangle\}$ is orthonormal, i.e.,

$$S_{\alpha\beta} = \delta_{\alpha\beta}$$

We note that the Anderson-Bullett scheme discussed in section (3.1) (chapter(3)) directly generates the elements $D_{\alpha\beta}$ or $H^{\alpha}{}_{\beta}$.

c) TRACE OF AN OPERATOR

If $\{|\psi_i\rangle\}$ represents a complete set of orthogonal vectors in V, then for any operator A,

$$\mathrm{Tr}\, A = \langle\psi_i|A|\psi_i\rangle$$

In the nonorthogonal basis $\{|\phi_\alpha\rangle\}$, this takes the following form :

$$\mathrm{Tr}\, A = \langle\psi_i|\phi_\alpha\rangle(S^{-1})^{\alpha\beta}\langle\phi_\beta|A|\phi_\gamma\rangle(S^{-1})^{\gamma\delta}\langle\phi_\delta|\psi_i\rangle$$

Using $\langle\phi_\delta|\psi_i\rangle\langle\psi_i|\phi_\alpha\rangle = S_{\delta\alpha}$

we get

$$\begin{aligned}\mathrm{Tr}\, A &= S_{\delta\alpha}(S^{-1})^{\alpha\beta}\langle\phi_\beta|A|\phi_\gamma\rangle(S^{-1})^{\gamma\delta} \\ &= \langle\phi_\delta|A|\phi_\gamma\rangle(S^{-1})^{\gamma\delta} = (S^{-1})^{\gamma\delta}A_{\delta\gamma} \\ &= A_{\delta\gamma}(S^{-1})^{\gamma\delta}\end{aligned}$$

Thus trA is not the sum of diagonal elements $A_{\alpha\alpha}$. It is given by the sum of the diagonal elements of $(S^{-1}A)$ or (AS^{-1}),

$$Tr\ A = A_{\alpha}{}^{\alpha} = A^{\alpha}{}_{\alpha} . \qquad (A.20)$$

d) PROJECTION OPERATOR

The expression for the projection operator, P, which will project any vector in the space V onto one of its subspace, U, can be obtained in a way similar to that used for the identity operator. If $\{|\xi_i\rangle\}$ forms a complete set of orthonormal vectors in the subspace U, then the projection operator P is given by

$$P = |\xi_i\rangle\langle\xi_i| . \qquad (A.21)$$

If $\{|\phi_\alpha\rangle\}$ forms a complete set of nonorthogonal vectors spanning the subspace U, then following the derivationn for the identity operator, we can write

$$P = |\phi_\alpha\rangle (S^{-1})^{\alpha\beta}\langle\phi_\beta| . \qquad (A.22)$$

e) TIGHT-BINDING(LCAO) EQUATIONS

The tight-binding eigenvalue equations of section (3) can be reexpressed in the present notation. The eigenfunctions $|\Psi_i\rangle$ of the equation

$$H|\Psi_i\rangle = E_i|\Psi_i\rangle \qquad (A.23)$$

can be expanded in the localised basis $\{|\phi_\alpha\rangle\}$, giving

$$|\psi_i\rangle = C_i^{\alpha} |\phi_\alpha\rangle . \qquad (A.24)$$

Substituting (A.24) into (A.23) we obtain

$$C_i^{\alpha} H |\phi_\alpha\rangle = E_i C_i^{\alpha} |\phi_\alpha\rangle . \qquad (A.25)$$

Taking the inner product of both sides with $|\phi_\beta\rangle$, we get

$$C_i^{\alpha} H_{\beta\alpha} = E_i C_i^{\alpha} S_{\beta\alpha} .$$

The homogeneous system of equations

$$(H_{\beta\alpha} - E_i S_{\beta\alpha}) C_i^{\alpha} = 0$$

has nontrivial solutions for C_i^{α} when

$$\det [H_{\beta\alpha} - E_i S_{\beta\alpha}] = 0 . \qquad (A.26)$$

Alternatively one could take the inner product of both sides in (A.25) with $|\phi^\beta\rangle$ to obtain

$$C_i^{\alpha} H^{\beta}{}_{\alpha} = E_i C_i^{\alpha} \delta^{\beta}{}_{\alpha} .$$

Thus the secular equation is

$$\det [H^{\beta}{}_{\alpha} - E_i \delta^{\beta}{}_{\alpha}] = 0 . \qquad (A.27)$$

If $|\psi_i\rangle$'s are expanded in the basis $|\phi^\alpha\rangle$, then the form of the secular equation is

$$\det [H_{\alpha}{}^{\beta} - E_i \delta_{\alpha}{}^{\beta}] = 0 . \qquad (A.28)$$

Thus depending on the matrix elements available, one can decide to solve either of the equations (A.26), (A.27) and (A.28). These equations are related to each other as

$$\det\left[H_{\beta\alpha} - E_i S_{\beta\alpha}\right] = \det\left[S_{\beta\gamma}\left((S^{-1})^{\gamma\delta} H_{\delta\alpha} - E_i \delta^{\gamma}{}_{\alpha}\right)\right]$$

$$= \det\left[S_{\beta\gamma}\right] \det\left[H^{\gamma}{}_{\alpha} - E_i \delta^{\gamma}{}_{\alpha}\right] .$$

Similarly,

$$\det\left[H_{\beta\alpha} - E_i S_{\beta\alpha}\right] = \det\left[H_{\beta}{}^{\gamma} - E_i \delta_{\beta}{}^{\gamma}\right] \det\left[S_{\gamma\alpha}\right] .$$

Thus solving any one of the eqns. (A.26), (A.27) and (A.28) is equivalent to solving the others if

$$\det\left[S_{\alpha\beta}\right] \neq 0 ,$$

which is true if the set $\{|\phi_\alpha\rangle\}$ is linearly independent. For a linearly dependent set

$$\det\left[S_{\alpha\beta}\right] = 0 ,$$

or equivalently, the smallest eigenvalue of $[S_{\alpha\beta}]$ is zero. In that case, the secular determinant (A.26) vanishes for any E_i, and solving (A.27) or (A.28) will no longer yield the eigenvalues of the original Hamiltonian. For near linear dependence of the set $\{|\phi_\alpha\rangle\}$, the smallest eigenvalue of $[S_{\alpha\beta}]$ is only slightly greater than zero. In this case, the almost identically vanishing secular equation will cause a

corresponding loss of accuracy in E_i. Thus it is necessary that the set $\{|\phi_\alpha\rangle\}$ be linearly independent.

(A-2)

THE TOTAL DENSITY OF STATES

In appendix (A-1), we discussed the trace of an operator A in a nonorthogonal basis. In this case the trace is no longer the sum of the diagonal matrix elements of A. This means that in calculating the total or the average density of states, one cannot simply sum over the local density of states in the nonorthogonal basis $\{|\phi_\alpha\rangle\}$. The total density of states is given by

$$\begin{aligned}
\eta(E) &= Tr\,(\rho(E)) \\
&= -\frac{1}{\pi} \lim_{\varepsilon \to 0^+} Tr\, Im\, G(E+i\varepsilon) \\
&= -\frac{1}{\pi} \lim_{\varepsilon \to 0^+} Im\, Tr\, G(E+i\varepsilon) \\
&= -\frac{1}{\pi} \lim_{\varepsilon \to 0^+} Im\left[(S^{-1})^{\gamma\beta} G_{\beta\gamma}(E+i\varepsilon)\right] \\
&= -\frac{1}{\pi} \lim_{\varepsilon \to 0^+} Im\left[(S^{-1})^{\gamma\beta} \langle \phi_\beta | (E+i\varepsilon - H)^{-1} | \phi_\gamma \rangle\right] \qquad (A.29)
\end{aligned}$$

Thus if one works in the basis $\{|\phi_\alpha\rangle\}$, it is necessary to calculate the nondiagonal elements of the Green's function, $G_{\beta\gamma}(E)$, which can be obtained by forming four independent linear combinations of $|\phi_\beta\rangle$ and $|\phi_\gamma\rangle$ (see Haydock, Ref.95, page

250) and calculating the local Green's function for these states. However, the problem can be simplified by working in a mixed basis. This is because (A.29) can be written as

$$\eta(E) = -\frac{1}{\pi} \lim_{\varepsilon \to 0^+} \mathrm{Im} \langle \phi^\gamma | (E + i\varepsilon - H)^{-1} | \phi_\gamma \rangle .$$

Since

$$\langle \phi^\alpha | (E + i\varepsilon - H)^{-1} | \phi_\beta \rangle \langle \phi^\beta | (E + i\varepsilon - H) | \phi_\gamma \rangle = \delta^\alpha{}_\gamma$$

or,

$$\langle \phi^\alpha | (E + i\varepsilon - H)^{-1} | \phi_\beta \rangle \left((E + i\varepsilon)\delta^\beta{}_\gamma - H^\beta{}_\gamma \right) = \delta^\alpha{}_\gamma ,$$

$\langle \phi^\alpha | (E+i\varepsilon - H)^{-1} | \phi_\alpha \rangle$ is the diagonal element of the inverse of the matrix $[(E + i\varepsilon)\delta^\alpha{}_\beta - H^\alpha{}_\beta]$. By using the nonsymmetric recursion method, one can first tridiagonalise the matrix $[H^\alpha{}_\beta]$ and then calculate the diagonal element of the Green's function $G^\alpha{}_\alpha(E)$ in the mixed basis, by expanding this quantity as a continued fraction in the elements of the tridiagonalised matrix. A sum over the imaginary parts of these diagonal elements will then yield the density of states, and no nondiagonal element or inverse overlap matrix need be calculated.

PARAMETERS USED IN THE BAND STRUCTURE CALCULATIONS

a) ANDERSON-BULLETT SCHEME (section 3.1)

The atomic potential and the orbitals obtained by using the Herman-Skillman program are as follows:

1) Atomic Potential,

$$V_\alpha^0(r) = \left(-4.1049\,\frac{e^{-0.26562r}}{r} - 36.6920\,\frac{e^{-2.19758r}}{r}\right) \text{Ryd.}$$

2) 4s Atomic orbital

$$\phi_\alpha(r) = 6.8163\,e^{-21.07538r} - 52.416\,r\,e^{-8.17065r} + 14.665\,r\,e^{-3.83766r} - 0.6466\,r\,e^{-0.77987r}$$

3) 3d Atomic Orbital

$$\phi_\alpha(r) = 20.717\,r^2\,e^{-3.48915r} + 0.57484\,r^2\,e^{-1.49442r}$$

The parameters used in this scheme are:

1) The correction term in the potential (see eqn. (3.37)):

$$\delta V_x = 0.3 \text{ Ryd.}$$

2) Atomic s level: $\epsilon_s = -0.200$ Ryd.

3) Atomic d level: $\epsilon_d = -0.672$ Ryd.

b) EMPIRICAL LCAO SCHEME (section 3.3)

In expression (3.39),

$\alpha_1 = 3.8378$, $\alpha_2 = 7.3796$, $A = -2.7892$.

In expression (3.40),

$$\alpha_3 = 3.3803 .$$

In expressions (3.41)-(3.43),

$C_1 = -77.3713$ Ryd.,

$C_2 = -11.0000$ Ryd.,

$C_3 = -0.2464$ Ryd.,

$H_{ss}(0) = -0.4570$ Ryd.,

$H_{dd}(0) = -0.7083$ Ryd.

X. BIBLIOGRAPHY

1. J. Friedel, Adv. Phys., 3, 446 (1954).

2. L. E. Ballentine, Adv. Chem. Phys., 31, 263 (1975).

3. Mitsuo Shimoji, "Liquid Metals" (Academic Press Inc. (London) LTD. 1977) ch. 5.

4. S. F. Edwards, Proc. Roy. Soc., A267, 518 (1962).

5. M. Lax, Phys. Rev., 85, 621 (1952).

6. J. M. Ziman, Proc. Roy. Soc., 88, 387 (1966).

7. F. Cyrot-Lackmann, J. Physique, 27, 627 (1966).

8. B. L. Gyorffy, Phys. Rev. B, 1, 3290 (1970).

9. M. Watabe, Prog. Theor. Phys., 45, 977 (1971).

10. J. Korringa and R. L. Mills, Phys. Rev. B, 5, 1654 (1972).

11. L. Schwartz and H. Ehrenreich, Ann. Phys., NY 64, 100 (1971).

12. Y. Ishida and F. Yonezawa, Prog. Theor. Phys., 49, 731 (1973).

13. B. Movaghar, D. E. Miller and K. H. Benneman, J. Phys. F: Metal Phys., 4, 687 (1974).

14. M. Watabe, "Liquid Metals 1976: Inst. Phys. Conf. Ser. No. 30" (Bristol and London: The Institute of Physics), 288 (1977).

15. P. W. Anderson and W. L. McMillan, Proc. Int. Sch. Phys. 'Enrico Fermi', 37, 50 (1967).

16. P. Soven, Phys. Rev., 156, 809 (1967).

17. J. J. Olson, Phys. Rev. B, 12, 2908 (1975).

18. K. S. Chang, A. Sher, and K. G. Petzinger, Phys. Rev. B, 12, 5506 (1975).

19. J. Oglesby and P. Lloyd, J. Phys. C: Solid St. Phys., 9,

2879 (1976).

20. E. DeDycker and P. Phariseau, Adv. Phys., 16, 401 (1967).

21. W. John and W. Keller, J. Phys. F: Metal Phys., 7, L233 (1977).

22. P. Blaudeck and R. Lenk, Phys. Stat. Sol. (b), 89, 199 (1978).

23. J. Keller and R. Jones, J. Phys. F: Metal Phys., 1, L33 (1971).

24. J. Keller, J. Fritz and A. Garritz, J. Phys. Paris, 35, C4-379 (1974); "Conference on Disordered Metallic Systems", Sept. 1973, Strassburg.

25. J. Klima, T. C. McGill and J. M. Ziman, Discuss. Faraday Soc., 50, 20 (1970).

26. P. Lloyd, Proc. Phys. Soc., 90, 207 and 217 (1967).

27. D. House and P. V. Smith, J. Phys. F: Metal Phys., 3, 753 (1973).

28. F. Yonezawa and M. Watabe, Phys. Rev. B, 11, 4746 (1975).

29. M. Watabe and F. Yonezawa, Phys. Rev. B, 11, 4753 (1975).

30. L. M. Roth, Phys. Rev. B, 9, 2476 (1974).

31. V. A. Singh and L. M. Roth, Phys. Rev. B, 22, 4089 (1980).

32. S. Asano and F. Yonezawa, J. Phys. F: Metal Phys., 10, 75 (1980).

33. S. N. Khanna and F. Cyrot-Lackmann, Phil. Mag., B38, 197 (1978).

34. S. N. Khanna, F. Cyrot-Lackmann, and M. C. Desjonqueres, J. Phys. F: Metal Phys., 9, 79 (1979).

35. T. Fujiwara, J. Phys. F: Metal Phys., 9, 2011 (1979).

36. T. Fujiwara and Y. Tanabe, J. Phys. F: Metal Phys., 9, L73 (1979).

37. T. Fujiwara, J. Phys. F: Metal Phys., 12, 661 (1982).

38. G. S. Cargill III, "Solid State Physics", Vol. 30, ed. H. Ehrenreich, F. Seitz and D. Turnbull (Academic Press, New York, 975), 227 (1975).

39. J. C. Phillips, Phys. Stat. Sol. (b), 101, 473 (1980).

40. J. D. Bernal, Nature (London), 183, 141 (1959); Nature (London), 185, 68 (1960); Proc. Roy. Soc., Ser. A 280, 299 (1964); "Liquids: Structure, Properties, and Solid Interactions" (T. J. Hugel, ed.), p. 25. Elsevier, Amsterdam, 1965.

41. J. D. Bernal and J. L. Finney, Discuss. Faraday Soc., 43, 62 (1967).

42. J. L. Finney, Proc. Roy. Soc., Ser. A 319, 479 (1970).

43. C. H. Bennett, J. Appl. Phys., 43, 2727 (1972).

44. D. J. Adams and A. J. Matheson, J. Chem. Phys., 56, 1989 (1972).

45. J. F. Sadoc, J. Dixmier, and A. Guinier, J. Non-Cryst. Solids, 12, 46 (1973).

46. T. Ichikawa, Phys. Stat. Solidi (a), 29, 293 (1975).

47. L. von Heimendahl, J. Phys. F: Metal Phys., 5, L141 (1975).

48. J. A. Barker, J. L. Finney, and M. R. Hoare, Nature (London), 257, 120 (1975).

49. R. Yamamoto, H. Matsuoka, and M. Doyama, Phys. Stat. Sol. (a), 45, 305 978).

50. N. Metropolis, A. W. Rosenbluth, M. N. Rosenbluth, A. H. Teller, and E. Teller, J. Chem. Phys., 21, 1087 (1953).

51. W. W. Wood, in "Physics of Simple Fluids" (eds. Temperley, Rowlinson and Rushbrooke, Amsterdam: North-Holland, 1968), p. 115.

52. S. G. Brush, H. L. Sahlin and E. Teller, J. Chem. Phys., 45, 2102 (1966).

53. J. M. Haile, D. Litchinsky, R. Mepherson, C. G. Gray, and K. E. Gubbins, J. Comp. Phys., 21, 227 (1976).

54. A. Rahman, "Neutron Inelastic Scattering", Vienna, IAEA (1968), p. 561.

55. L. Verlet, Phys. Rev., 165, 201 (1968).

56. B. J. Alder, W. G. Hoover and D. A. Young, J. Chem. Phys., 49, 3688 (1968).

57. L. V. Woodcock, Chem. Phys. Lett., 10, 257 (1971).

58. R. A. Johnson, Phys. Rev., 134, A1329 (1964).

59. L. E. Ballentine, Phys. Rev. B, 25, 6089 (1982).

60. Y. Waseda and S. Tamaki, Phil. Mag., 32, 273 (1975).

61. T. Ichikawa, Phys. Stat. Solidi (a), 19, 707 (1973).

62. F. Bloch, Z. Phys., 52, 555 (1929).

63. P.-O. Löwdin, J. Chem. Phys., 18, 365 (1950).

64. W. H. Adams, J. Chem. Phys., 34, 89 (1961); 37, 2009 (1962); Chem. Phys. Lett. 11, 71 and 441 (1971); 12, 295 (1971); Phys. Rev. Lett., 32, 1093 (1974).

65. T. L. Gilbert, in "Molecular Orbitals in Chemistry, Physics and Biology" (P.-O. Lowdin and B. Pullman eds.), p. 405. Academic Press, New York, 1964.

66. P. W. Anderson, Phys. Rev. Lett., 21, 13 (1968); Phys. Rev., 181, 25 (1969); see also J. D. Weeks, P. W. Anderson, and A. G. H. Davidson, J. Chem. Phys., 58, 1388 (1973).

67. B. J. Austin, V. Heine, and L. J. Sham, Phys. Rev., 127, 276 (1962).

68. A. B. Kunz, Phys. Stat. Sol., 36, 301 (1969).

69. H. Schlosser, J. Chem. Phys., 55, 5453, 5459 (1971).

70. E. Huckel, Z. Phys., 70, 204 (1931); 72, 310 (1932); 76, 628 (1932).

71. A. Streitwieser, Jr., "Molecular Orbital Theory for Organic Chemists." Wiley, New York, 1961; M. J. S. Dewar, "The Molecular Orbital Theory of Organic Chemistry." McGraw-Hill, New York, 1969.

72. D. W. Bullett, Phil. Mag., 32, 1063 (1975).

73. D. W. Bullett, Phys. Rev. Lett., Vol. 39, p 664 (1977).

74. J. C. Slater, Phys. Rev., 81, 385 (1951).

75. P. Hohenberg, and W. Kohn, Phys. Rev., B136, 864 (1964); W. Kohn and L. J. Sham, Phys. Rev., A140, 1133 (1965); L. J. Sham and W. Kohn, ibid. 145, 561 (1966).

76. P. A. M. Dirac, Proc. Cambridge Philos. Soc., 26, 376 (1930).

77. J. C. Slater, "Quantum Theory of Molecules and Solids", Vol.

4, McGraw-Hill, New York, 1965.

78. U. von Barth and L. Hedin, J. Phys. C: Solid St. Phys., 5, 1629 (1972).

79. K. S. Singwi, A. Sjolander, M. P. Tosi, and R. H. Land, Phys. Rev. B, 1, 1044 (1970).

80. F. Herman, J. P. Van Dyke, and I. B. Ortenburger, Phys. Rev. Lett., 22, 807 (1969); M. Rasolt and D. J. W. Geldart, Phys. Rev. Lett., 35, 1234 (1975).

81. F. Herman and S. Skillman, 'Atomic Structure Calculations' (Prentice-Hall, Inc., Englewood Cliffs, New Jersey, 1963).

82. J. Callaway and C. S. Wang, Phys. Rev. B, 16, 2095 (1977).

83. J. H. Wood, Phys. Rev., 126, 517 (1962).

84. R. A. Tawil and J. Callaway, Phys. Rev. B, 7, 4242 (1973).

85. R. S. Mulliken, C. A. Rieke, D. Vorloff and H. Orloff, J. Chem. Phys., 17, 1248 (1949).

86. M. P. Barnett and C. A. Coulson, Trans. Roy. Soc. London, 243, 30 and 221 (1951).

87. C. C. J. Roothan, J. Chem. Phys., 19, 1445 (1951); J. Chem. Phys., 24, 947 (1956).

88. C. C. J. Roothan and K. Rudenberg, J. Chem. Phys., 19, 1459 (1951).

89. R. A. Sack, C. C. J. Roothan, and W. Wolos, J. Math. Phys., 8, 1093 (1967).

90. K. Rudenberg, K. O. Ohata, and D. G. Wilson, J. Math. Phys., 7, 539 966).

91. H. H. Jaffe and G. O. Doak, J. Chem. Phys., 21, 196 (1953).

92. R. R. Sharma, Phys. Rev. A, 13, 517 (1976).

93. H. W. Jones, Int. J. Quan. Chem., 28, 709 (1980).

94. I. S. Gradshteyn and I. M. Ryzhik, Table of Integrals, Series and Products (Academic Press, New York, 1965), p. 711.

95. V. Heine, D. W. Bullett, R. Haydck and M. J. Kelly, in "Solid State Physics" (Academic Press, Inc., New York, 1980), eds. H. Ehrenreich, F. Seitz and D. Turnbull, Vol. 35.

96. R. Haydock and M. V. You, Solid St. Comm., 33, 299 (1980).

97. J. D. Joannopoulos and F. Yndurain, Phys. Rev. B, 10, 5164 (1974).

98. R. Haydock, V. Heine, and M. J. Kelly, J. Phys. C: Solid St. Phys., 8, 2591 (1975).

99. A. Mookerjee, Pramana, 5, 118 (1975).

100. E. N. Economou, "Green's Functions in Quantum Physics", Springer Series in Solid-State Science, Vol. 7, ed. M. Cardona, P. Fulde and H.-J. Queisser (Springer-Verlag, Berlin, Heidelberg, 1979).

101. C. Papatriantafillou, E. N. Economou and T. P. Eggarter, Phys. Rev. B, 13, 910 (1976).

102. R. Haydock, V. Heine and M. J. Kelly, J. Phys. C: Solid St. Phys., 5, 2845 (1972).

103. R. Haydock, in "Excitations in Disordered Systems", NATO Advanced Study Institute on Excitations in Disordered Systems (1981: Michigan State University), NATO Advanced Study Institute Series, Series B, Physics; Vol. 78, ed. M. F. Thorpe (Plenum Press, New York, 1982).

104. C. C. Paige, J. Inst. Math. Appl., 10, 373 (1972).

105. R. Haydock and M. J. Kelly, J. Phys. C: Solid St. Phys., 8, L290 (1975).

106. J. H. Wilkinson, "The Algebraic Eigenvalue Problem" (Oxford: Claredon Press, 1965).

107. C. M. M. Nex, Cambridge Recursion Method Library of Computer Programs, available from the secretary, T. C. M. Group, Cavendish Laboratory, Madingly Road, Cambridge, CB3 OH3, England.

108. Ph. Lambin and J.P. Gaspard, Phys. Rev. B, 26, 4356 (1982).

109. R. Alben, M. Blume, H. Krakauer, and L. Schwartz, Phys. Rev.

B, 12, 4090 (1975).

110.
D. Beeman and R. Alben, Adv. Phys., 26, 339 (1977).

111.
D. Weaire and A. R. Williams, J. Phys. C: Solid St. Phys., 10, 1239 (1977).

112.
F. Ducastelle and F. Cyrot-Lackman, J. Phys. Chem. Solids, 31, 1295 (1970).

113.
F. Ducastelle and F. Cyrot-Lackman, J. Phys. Chem. Solids, 32, 285 (1971).

114.
J. P. Gaspard and F. Cyrot-Lackman, J. Phys. C: Solid St. Phys., 6, 3077 (1973).

115.
F. Yndurain and L. M. Falicov, Solid St. Comm., 17, 1545 (1975).

116.
F. Yndurain and J. D. Joannapoulos, Phys. Rev. B, 11, 2957 (1975).

117.
R. C. Kittler and L. M. Falicov, J. Phys. C: Solid St. Phys., 9, 4259 (1976).

118.
R. C. Kittler and L. M. Falicov, Phys. Rev. B, 18, 2506 (1978).

119.
J. D. Joannopoulos and M. L. Cohen, in "Solid State Physics" (Academic Press, Inc., New York, 1976), eds. H. Ehrenreich, F. Seitz and D. Turnbull, Vol. 31.

120.
C. E. T. G. da Silva and B. Koiller, Solid St. Comm., 40, 215 (1981).

121.
H. Aoki, J. Phys. C: Solid St. Phys., 13, 3369 (1980).

122.
T. E. Hull, W. H. Enright, and K. R. Jackson, "User's Giude for DVERK - a subroutine for solving non-stiff ODE's", TR No. 100, Dept. of Computer Sciences, University of Toronto,

Oct., 1976.

123.
K. R. Jackson, W. H. Enright, and T. E. Hull, "A Theoretical Criterion for Comparing Runge-Kutta Formulas", TR No. 101, Dept. of Computer Sciences, University of Toronto, Jan., 1977.

124.
W. B. Gragg, J. Siam Num. Analysis, Series B, 2, 384 (1965).

125.
R. Bulirsch and J. Stoer, Numerical Treatment of Ordinary Differential Equations by Extrapolation Methods, Numer. Math., 8, 1 (1966).

126.
P. A. Fox, "Desub: Integration of a first-order system of ordinary Differential Equations," in "Mathematical Software," ed. J. R. Rice (Academic Press, New York, 1971).

127.
J. Stoer and R. Bulirsch, "Introduction to Numerical Analysis" (Springer-Verlag, New York, 1980), ch. 7.

128.
see article by D. Weaire in Ref. 101, p. 535.

129.
B. Kramer and D. Weaire, J. Phys. C: Solid St. Phys., 11, L5 (1978).

130.
B. Krammer, A. Mackinnon, and D. Weaire, Phys. Rev. B, 23, 6357 (1981).

131.
J. M. Gallagher and R. Haydock, Phil. Mag., 35, 845 (1977).

132.
N. F. Mott, Phil. Mag., 26, 1249 (1972).

133.
O. Dreirach, R. Evans, H.-J. Guntherodt, and H.-U. Kunzi, J. Phys. F: Metal Phys., 2, 709 (1972).

134.
A. ten Bosch and K. H. Bennemann, J. Phys. F: Metal Phys., 5, 1333 (1975).

135.
B. Y. Tong, M. M. Pant, and B. Hede, J. Phys. C: Solid St. Phys., 13, 1221 (1980).

136.
T. Fujiwara and Y. Tanabe, J. Phys. F: Metal Phys., 9, 1085 (1979).

137.
J. C. Slater and G. F. Koster, Phys. Rev., 94, 1498 (1954).

138.
G. P. Williams and C. Norris, J. Phys. F, 4, L175 (1974).

139.
R. K. C. McLean and R. Haydock, J. Phys. C, 10, 1929 (1977).

140.
K. B. Garg and E. Kalline, Phys. Stat. Sol. (b), 70, K121 (1975).

141.
C. F. Hague, in "Liquid Metals 1976", Institute of Physics Conference Series Number 30, eds. R. Evans and D. A. Greenwood (The Institute of Physics, Techno House, Redcliffe Way, Bristol, England).

142.
A. Meyer, M. J. Stott, and W. H. Young, Phil. mag., 33, 381 (1976).

143.
M. Silbert, I. H. Umar, M. Watabe, and W. H. Young, J. Phys. F: Metal Phys., 5, 1262 (1975).